

AFWAL-TR-80-4081
Part II

2
P.S.



AD A094350

**INVESTIGATION OF EMAT BASE SYSTEM FOR
THE DETECTION OF BOLT HOLE TYPE CRACKS
Part II – Reliability Evaluation and System Definition
for Detection of Cracks Under Fasteners by EMATs**

J. F. Martin
P. J. Hodgetts
R. B. Thompson

Rockwell International Corporation
Science Center
1049 Camino Dos Rios
Thousand Oaks, California 91360

July 1980

TECHNICAL REPORT AFWAL-TR-80-4081, Part II

Interim Report (Task IV) for Period 12 April 1979 – 15 September 1979

Approved for public release; distribution unlimited.

DDC FILE COPY

Materials Laboratory
Air Force Wright Aeronautical Laboratories
Air Force Systems Command
Wright-Patterson Air Force Base, Ohio 45433

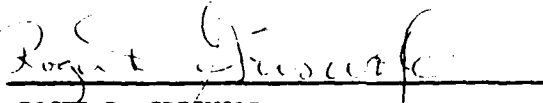
81 2 00 148

NOTICE

When Government drawings, specifications, or other data are used for any purpose other than in connection with a definitely related Government procurement operation, the United States Government thereby incurs no responsibility nor any obligation whatsoever; and the fact that the government may have formulated, furnished, or in any way supplied the said drawings, specifications, or other data, is not to be regarded by implication or otherwise as in any manner licensing the holder or any other person or corporation, or conveying any rights or permission to manufacture use, or sell any patented invention that may in any way be related thereto.

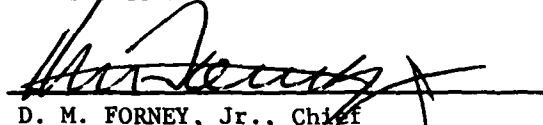
This report has been reviewed by the Office of Public Affairs (ASD/PA) and is releasable to the National Technical Information Service (NTIS). At NTIS, it will be available to the general public, including foreign nations.

This technical report has been reviewed and is approved for publication.



ROGER D. GRISWOLD
Project Engineer

FOR THE COMMANDER



D. M. FORNEY, Jr., Chief
Nondestructive Evaluation Branch
Metals and Ceramics Division

"If your address has changed, if you wish to be removed from our mailing list, or if the addressee is no longer employed by your organization please notify AFWAL/MLLP, W-PAFB, OH 45433 to help us maintain a current mailing list".

Copies of this report should not be returned unless return is required by security considerations, contractual obligations, or notice on a specific document.

UNCLASSIFIED

SECURITY CLASSIFICATION OF THIS PAGE (When Data Entered)

9 Interim rept.
12 Apr-15 Sep 79

19 REPORT DOCUMENTATION PAGE		READ INSTRUCTIONS BEFORE COMPLETING FORM	
18 1. REPORT NUMBER AFWAL-TR-80-4081, Part II	2. GOVT ACCESSION NO. AD-A094350	3. RECIPIENT'S CATALOG NUMBER	
6 4. INVESTIGATION OF EMAT BASE SYSTEM FOR THE DETECTION OF BOLT HOLE TYPE CRACKS. Part II. Reliability Evaluation and System Definition for Detection of Cracks Under Fasteners by EMATs.		5. TYPE OF REPORT & PERIOD COVERED Interim Report (Task IV) 4/12/79 through 9/15/79	
7. AUTHOR(s) J.F. Martin, P.J. Hodgetts, and R.B. Thompson		6. PERFORMING ORG. REPORT NUMBER SC595.65IR	
10		8. CONTRACT OR GRANT NUMBER(s) F33615-74-C-5180 VI DARPA Order - 2828	
9. PERFORMING ORGANIZATION NAME AND ADDRESS Science Center, Rockwell International 1049 Camino Dos Rios Thousand Oaks, California 91360		10. PROGRAM ELEMENT PROJECT, TASK AREA & WORK UNIT NUMBERS 11 7351	
11. CONTROLLING OFFICE NAME AND ADDRESS AFWAL/MLLP Air Force Systems Command Wright-Patterson Air Force Base; Dayton, OH 45433		12. REPORT DATE Jul 1980	
14. MONITORING AGENCY NAME & ADDRESS (if different from Controlling Office)		13. NUMBER OF PAGES 104	
(14) SC595.65IA		15. SECURITY CLASS. (of this report) Unclassified	
16. DISTRIBUTION STATEMENT (of this Report) Approved for public release; distribution unlimited			
17. DISTRIBUTION STATEMENT (of the abstract entered in Block 20, if different from Report)			
18. SUPPLEMENTARY NOTES			
19. KEY WORDS (Continue on reverse side if necessary and identify by block number) Electromagnetic-acoustic transducers; EMAT; cracks under fasteners; ultrasonic testing; wing lap joints; quantitative flaw detection; nondestructive evaluation; nondestructive testing			
20. ABSTRACT (Continue on reverse side if necessary and identify by block number) The detection of laboratory grown fatigue cracks in aircraft wing lap joint fastener holes is demonstrated with EMATs (electromagnetic acoustic transducers). Operating at a 200 kHz central frequency, the EMATs employ acoustic waves in reflection and transmission to measure the presence of both fatigue cracks and loose fasteners. A minicomputer-based data acquisition and analysis system acquires, gates, apodizes and Fourier transforms each received time waveform. The resulting spectra are then			

389749

UNCLASSIFIED

SECURITY CLASSIFICATION OF THIS PAGE(When Data Entered)

(Continued from Block 20):

compared to the spectra of uncracked holes with tight fasteners to determine the presence of a crack or loose fastener. A method for distinguishing the difference between a crack and a loose fastener is demonstrated. A suggested design for a fieldable instrument capable of the same abilities is presented.

A

UNCLASSIFIED

SECURITY CLASSIFICATION OF THIS PAGE(When Data Entered)

FOREWORD

This report describes an in-house effort conducted by personnel of the Science Center, Rockwell International under Project 7351 (DARPA order 2828) of General Order 595, "Interdisciplinary Program for Quantitative Flaw Definition".

The work reported herein was performed during the period 12 April 1979 through 15 September 1979, under the direction of the author, Dr. J. F. Martin. The report was released by the author in January 1980.

This report is Part II of two parts concerned with detection of cracks under fasteners with EMATs (electromagnetic acoustic transducers).

TABLE OF CONTENTS

<u>SECTION</u>	<u>PAGE</u>
I. INTRODUCTION.....	1
II. PROGRAM SUMMARY.....	4
III. SYSTEM REFINEMENT.....	6
1. Probes.....	6
2. Probe Positioning.....	8
3. Signal Processing.....	8
4. Stability Evaluation.....	16
IV. EXPERIMENTS ON UNASSEMBLED MOCKUP.....	17
1. Experimental Technique.....	17
2. Optimization of Gating Window.....	19
V. FABRICATION OF SAMPLES.....	26
1. Actual Wing Section.....	26
2. Wing Section Mock-Up.....	29
3. Fatigued Samples.....	30
VI. MEASUREMENTS IN ORIGINAL TRANSDUCER CONFIGURATION ON ASSEMBLED SAMPLES.....	39
VII. DEVELOPMENT OF ANALYTICAL BASIS FOR PROBE OPTIMIZATION AND CONFIRMING EXPERIMENTS.....	41
1. Theoretical Background.....	41
2. Experimental Determination of Optimum Probe Configuration....	48
VIII. TRANSMISSION EXPERIMENTS.....	52
1. Two-Probe Measurements.....	52
2. Three-Probe Measurements.....	54
IX. REFLECTION EXPERIMENTS, VARIABLE β	64
X. ENGINEERING DRAWINGS, LAYOUTS, SKETCHES, AND SCHEMATICS.....	85
XI. CONCLUSION AND RECOMMENDATIONS.....	93
REFERENCES.....	96

LIST OF ILLUSTRATIONS

<u>Figure</u>		<u>Page</u>
1	Definition of Dimensions of Wing Section Samples Used in This Report. See Table I.....	2
2	Drawing of EMAT Transducers Used. The Flat Copper Strip Was Connected to the Coax Socket through an Impedance-Matching Transformer.....	7
3	Schematic of Experimental Hardware.....	9
4	Photographs of Goniometers Used. (a) Plastic Hand-Holdable Type.....	10
	(b) Brass/Aluminum Type.....	11
5	Drawings of Transducer Configurations. (a) Simple Reflection.....	12
	(b) Two-Probe Transmission.....	13
	(c) Three-Probe Transmission.....	14
6	Gating of Time Waveform. (a) Full Length Received Signal; (b) Hanning Function Used; (c) Resulting Signal for Fourier Analysis.....	18
7	Fourier Analysis of 1 Slotted and 2 Unslotted Holes. (a) Amplitude versus Frequency; (b) Imaginary versus Real for the Frequency Range Indicated in Fig. 7a.....	20
8	Signals from an Unslotted and a Slotted Hole. (a) Unslotted; (b) Slotted; (c) Superposition of (a) and (b).....	21
9	Drawing of Relevant Acoustic Paths. (a) Top View, Paths 1 and 2; (b) Sectional View.....	22
10	Simulated Signals. (a) Signal after Reflection from a Simple Edge, with Irrelevant Time Regions Gated Out; (b) Simulation of the Signal from a Slotted Hole; (c) Simulation of the Signal from an Unslotted Hole.....	24
11	Drawing of Geometry Variation in the Actual Wing Section (Section V - A).....	27
12	Drawing of the Radial Corner Notches and Fatigue Cracks.....	28

LIST OF ILLUSTRATIONS (cont'd)

<u>Figure</u>		<u>Page</u>
13	Drawing of Prefatigue Dimensions of Lower Sections of the Fatigue Samples.....	31
14	Drawing of Final Dimensions of Lower Sections of the Fatigue Samples.....	33
15	(a) Drawing of Upper Sections for the Fatigued Samples and Assembly.....	34
	(b) Drawing of Upper Sections for the Fatigued Samples and Assembly.....	35
16	Photograph of 0.030 in. Fatigue Crack after Treating with Dye Penetrant <u>and</u> Developer.....	36
17	Photograph of 0.100 in. Fatigue Crack after Treating with Dye Penetrant Only.....	37
18	Amplitude versus Frequency for Assembled Sample with 0.100 in. Crack; $\beta = 45^\circ$	40
19	Definition of Variables Used in Theoretical Analysis.	
	(a) Definition of Coordinates.....	43
	(b) Definition of β and the Two Probe Locations.....	44
20	Photograph of EMAT Probe in Use (See Section VII - B).....	49
21	Measurement of $\Delta u_y'$, and $\partial u_y/\partial y$ at $y=0$, for Two Values of β	50
22	Actual Wing Section, Holes 4 through 25. Amplitude versus Frequency for Transducer Configuration 5b (Fig. 5b).....	53
23	Fatigued Samples, Holes 7 through 11. Amplitude versus Frequency for Transducer Configuration 5c (Fig. 5c).	
	(a) 0.100 in. Crack Sample.....	56
	(b) 0.030 in. Crack Sample.....	57
24	Actual Wing Section, Holes 5 through 29. Amplitude versus Frequency for Transducer Configuration 5c (Fig. 5c).	
	(a) Holes 5 through 12.....	58
	(b) Holes 13 through 18.....	59
	(c) Holes 19 through 24.....	60
	(d) Holes 25 through 29.....	61
25	Fatigue Sample with 0.100 in. Crack, Holes 7 through 11, Transducer Configuration 5b, $\beta = 50^\circ$. (a) Amplitude versus Time; (b) Amplitude versus Frequency for 55 to 95 μ s Time Window.....	65

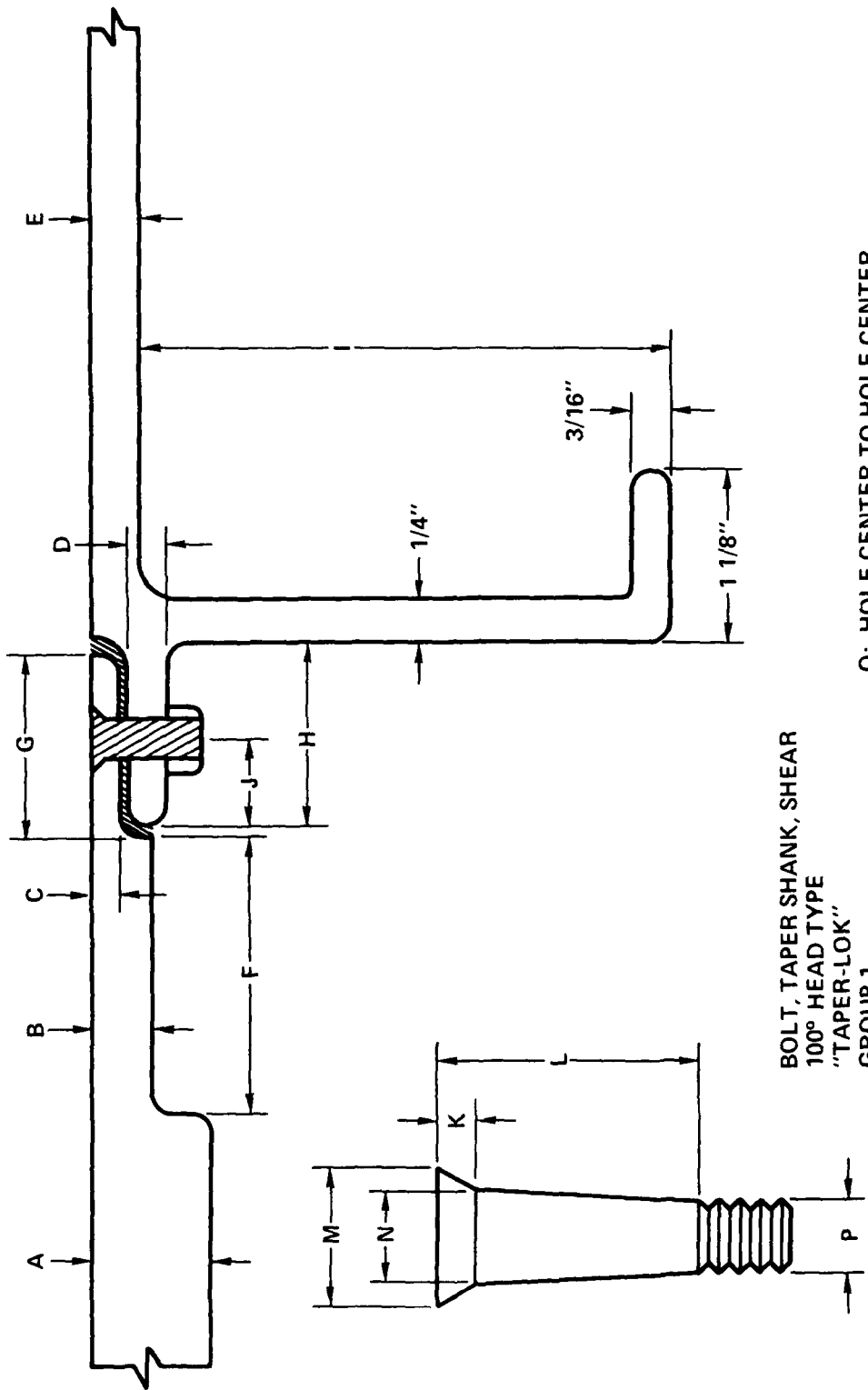
LIST OF ILLUSTRATIONS (cont'd)

<u>Figure</u>	<u>Page</u>
26	66
Fatigued Sample with 0.100 in. Crack, Holes 7 through 11, Transducer Configuration 5b, $\beta = 50^\circ$. Divided Amplitude versus Frequency.....	
27	67
Fatigued Sample with 0.030 in. Crack Holes 7 through 11, Transducer Configuration 5b, $\beta = 50^\circ$. Divided Amplitude versus Frequency.....	
28	70
Mockup Wing Section, Holes 7 through 15, Transducer Configuration 5b, $\beta = 50^\circ$. Divided Amplitude versus Frequency.	
(a) Holes 7 through 11.....	70
(b) Holes 12 through 15.....	71
29	72
Actual Wing Section, Holes 7 through 23, Transducer Configuration 5b, $\beta = 50^\circ$. Divided Amplitude versus Frequency.	
(a) Holes 7 through 11.....	72
(b) Holes 12 through 15.....	73
(c) Holes 16 through 19.....	74
(d) Holes 20 through 23.....	75
30	77
Actual Wing Section, Holes 10, 11, 12, 18, 19, 20, Transducer Configuration 5b, $\beta = 50^\circ$. Real or Imaginary Part versus Frequency.	
(a) Real Part of 18, 19, 20.....	77
(b) Imaginary Part of 18, 19, 20.....	78
(c) Real Part of 10, 11, 12.....	79
(d) Imaginary Part of 10, 11, 12.....	80
31	82
Three Measurements of the Peaks in Figs. 26 through 29.	
(a) Absolute Amplitude of High Peak near 200 kHz for All Holes;	
(b) Absolute Amplitude of High Peak near 200 kHz for Symmetric Peaks Only; (c) Relative Amplitude (See Text for Definition) of Peak near 200 kHz for All Holes.....	82
32	86
Schematic of the Hardware for a Microcomputer Based Instrument Capable of Being Fielded.....	
33	90
Schematic of Instrumentation As It Might Appear in Use.....	

I. INTRODUCTION

A major problem in aircraft maintenance is the detection of cracks growing from fastener holes in wing lap joints. As shown in Fig. 1, the problem is particularly difficult in the lower half of the joint, where direct measurement is obscured by intervening metallic and sealant layers. The former is opaque to all but low frequency eddy currents, whereas the latter has a variable, and often high, attenuation for ultrasonic waves in the MHz frequency range.

The five-month study described herein followed a previous study (1) which demonstrated the feasibility of using horizontally polarized shear ultrasonic waves to detect fatigue cracks growing from fastener holes in the lower half of the joint. In that previous work, the waves were injected into the lap joint region by a couplant free, EMAT (electromagnetic-acoustic transducer) placed on the right hand exposed portion of the lower half of the joint. The energy propagated around the discontinuities, interrogated the fastener region, and returned to a receiving EMAT probe. An analog-based Fourier transform signal processor analyzed the experimental data. Saw slots originating in the fastener holes were successfully detected and the ultrasonic response quantified in terms of slot length. The primary limitations of that study included a high noise level, the lack of an opportunity to study real fatigue cracks in assembled wing joints, and the lack of an opportunity to explore procedures which were adaptable to changes in part geometry.



BOLT, TAPER SHANK, SHEAR
 100° HEAD TYPE
 "TAPER-LOK"
 GROUP 1

Q: HOLE CENTER TO HOLE CENTER

Fig. 1 Definition of Dimensions of Wing Section Samples Used in This Report. See Table I.

The objectives of the present phase were threefold (Ref. 2):

1. to achieve refinement of the system developed in Ref. 1, and to establish procedures to distinguish flaw responses from sample-geometry-determined changes in the ultrasonic response;
2. to prepare, and use in experiments, a minimum of three wing joint specimens, two of which would contain laboratory grown interior layer corner fatigue cracks;
3. to develop a preliminary configuration design of an EMAT system suitable for field inspection of wing lap joints for such cracks.

II. PROGRAM SUMMARY

In order to achieve these objectives, the following program was conducted. First, the previously used apparatus was modified in several ways to improve the quality and reproducibility of the experimental data. These changes in probe design, probe positioning hardware, and signal processing techniques are discussed in Section III.

In order to verify that the new apparatus was functioning properly and represented an improved capability, a series of experiments were performed on the unassembled mock-up sample used in the previous study. The successful results, reported in Section IV, represented a completion of the first half of objective 1.

A set of four, fully assembled samples were then constructed and assembled to evaluate the technique. As described in Section V, two contained 0.030 in. (.076 cm) and 0.100 in. (0.254 cm) corner fatigue cracks in the lower half of the lap joint, grown in a laboratory mechanical testing machine under tension-tension fatigue conditions. These two samples lacked the stiffening rib because of the resulting fabrication savings. A third sample was a section of an actual wing lap joint in which corner EDM notches of the same dimensions had been placed. The fourth was the previously used mock-up, now fully assembled, which contained saw slots of various lengths.

In Section VI-IX, the experimental results obtained on these samples are reported. It was found that the 0.100 in (0.254 cm) fatigue crack and

radial EDM notches were reliably detected using several different techniques, completing the performance of objective 2. The 0.030 in. (0.076 cm) fatigue crack was also detected, but with lower reliability. Further work is needed for this size of flaw before reduction to practice can be seriously contemplated. In addition, a technique was also defined which allowed the same procedure to be applied to samples of different geometry. This represents a partial attainment of the second half of objective 1. However, some more work is required before a completely unambiguous technique for differentiating flaws from geometrical responses is attained. Finally, beyond the initial objectives, a technique is reported for identifying loose fasteners.

Based on these results, a preliminary configuration design and inspection procedure have been prepared, completing the performance of objective 3. These are reported in Section X. In Section XI, a future program to reduce this technique to practice, using the cited configuration and procedure, is presented.

III. SYSTEM REFINEMENT

The system was first refined to improve the quality and reproducibility of the experimental data. Included therein were three major changes. First, the central operating frequency was lowered from 250 kHz to 200 kHz. This placed the operating point further below that point at which higher order modes of the lap joint plate would propagate and produce interfering signals (see Appendix of Ref. 1). It also was designed to place the interference null, used in the previous study for flaw detection and sizing, at the center of the transducer passband rather than at its edge (for the geometry of the original mock-up sample). Second, an improved positioning apparatus was constructed to allow higher quality data to be attained at multiple angles. This was needed for studies aimed at separating flaw from geometric responses. Finally, a digital signal processing system was developed which eliminated the previously observed fluctuations in system outputs, produced a higher signal-to-noise ratio through signal averaging, and allowed much greater flexibility in data analysis. Details are given below.

1. Probes

Based on observations made in the previous phase (1), a new central operating frequency of 200 kHz was chosen. Four EMATs (electromagnetic-acoustic transducers) were fabricated (Fig. 2) to generate or receive ultrasonic horizontally polarized shear waves in aluminum, propagating at a grazing angle to the surface. These were implemented as one transmitter and three

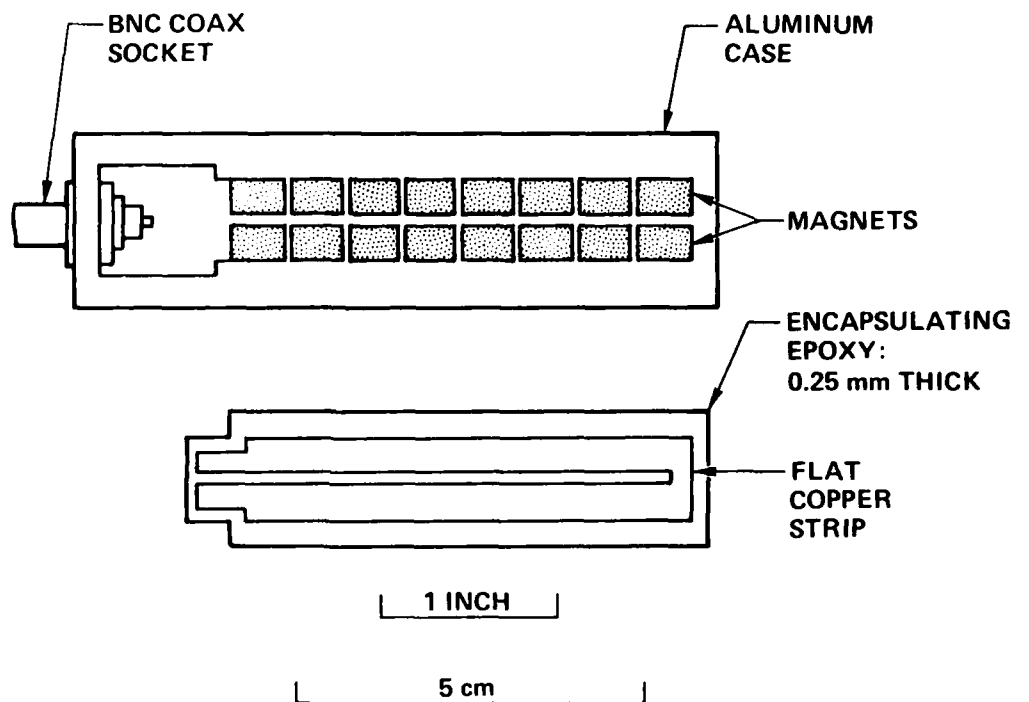


Fig. 2 Drawing of EMAT Transducers Used. The Flat Copper Strip Was Connected to the Coax Socket through an Impedance-Matching Transformer.

receivers. Also constructed and adjusted for operation at 200 kHz were two analog electronic circuits: one for creating a 5-cycle tone burst to drive the transmitter and one for amplifying the signal from one receiver. The input signal to the transmitter was the output of a pulser-function generator combination (see Fig. 3 for system schematic). The output of the receiver amplifier was connected directly to the Biomation 8100 wave form digitizer. As shown in Fig. 3 and discussed in C below, this instrument was interfaced to the minicomputer, which was used to control data taking and to perform all of the waveform analysis.

2. Probe Positioning

Two new goniometers were constructed, one of plastic (Fig. 4a) and one of brass/aluminum (Fig. 4b). These were used to accurately and repeatably position the probes with respect to the fastener holes and lap joint. The brass device was designed for more precise control of the angles ($\pm 17\text{mr}$) and positions ($\pm 0.5\text{mm}$) of the EMATs. The plastic device was used as a prototype of a hand-held fixture such as might be used in the field.

3. Signal Processing

Using these goniometers, three transmitter-receiver configurations were employed in the program (Fig. 5). The ultrasonic results from each of these varied as a function of angles α , β , and γ and are described later in detail. Data was analyzed on a digital signal processing system consisting of a Data General S200 minicomputer-Biomation 8100 combination operating under

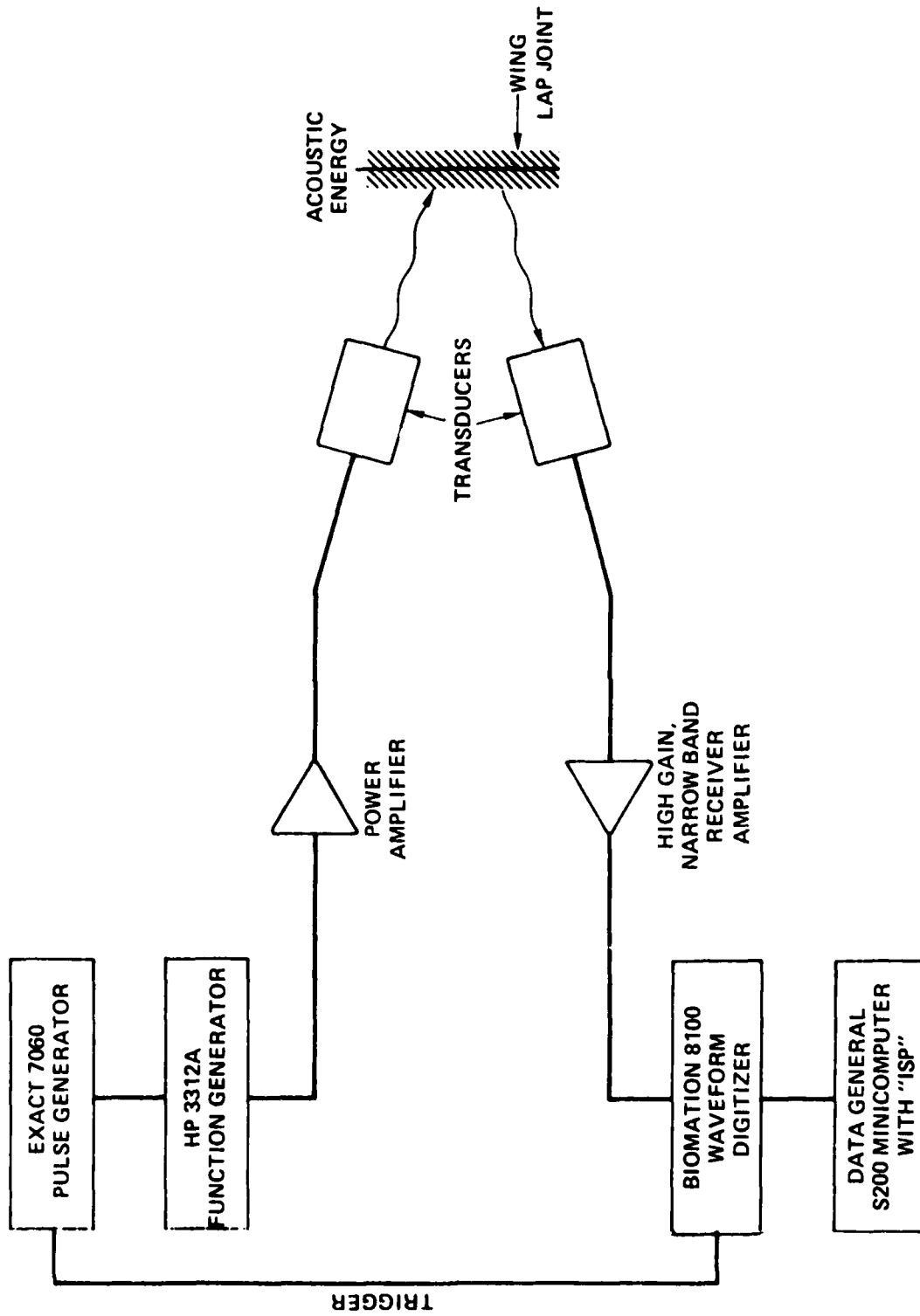


Fig. 3 Schematic of Experimental Hardware.

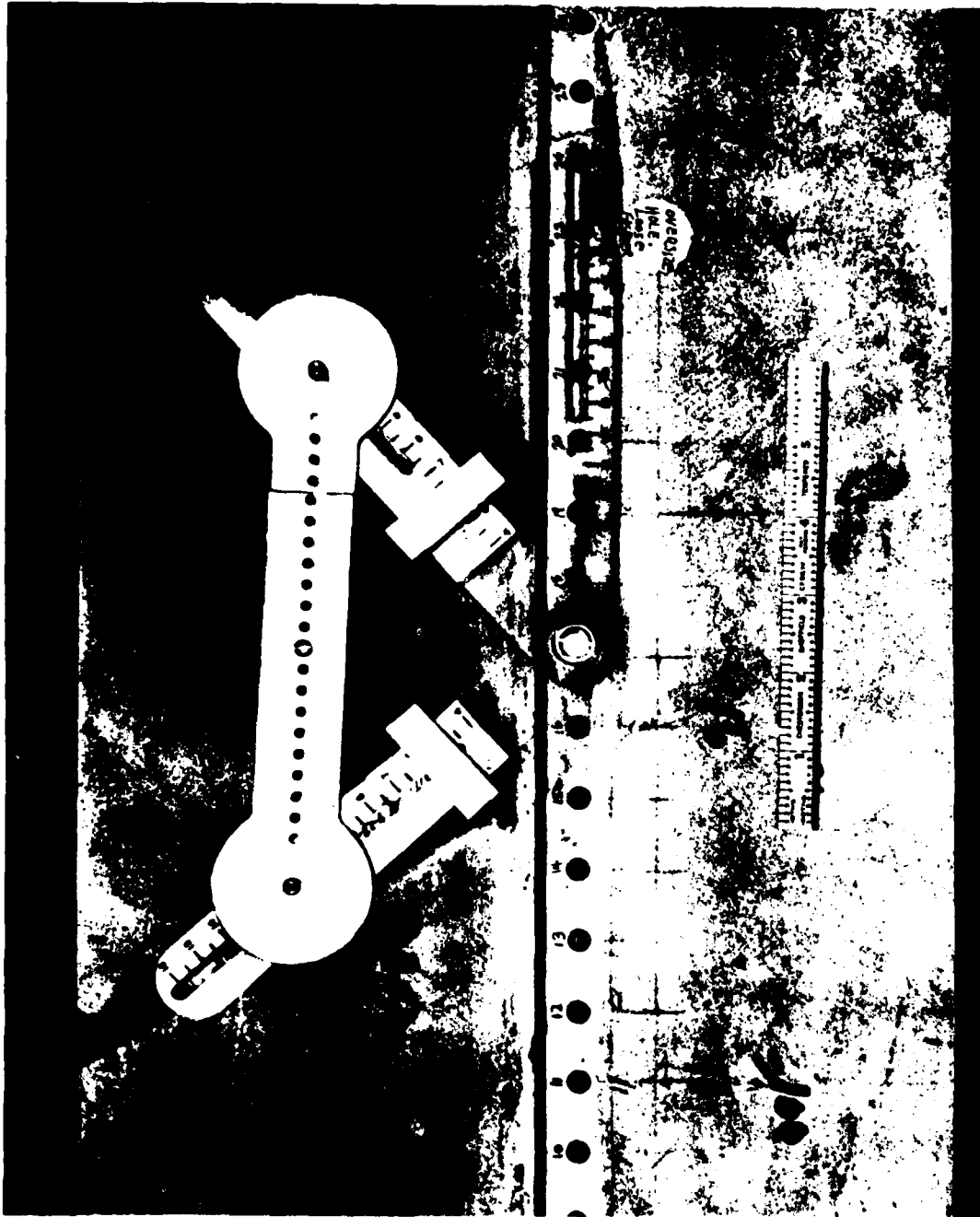


Fig. 4 Photographs of Goniometers Used.
(a) Plastic Hand-Holdable Type.



Fig. 4 Photographs of Goniometers Used.
(b) Brass/Aluminum Type.

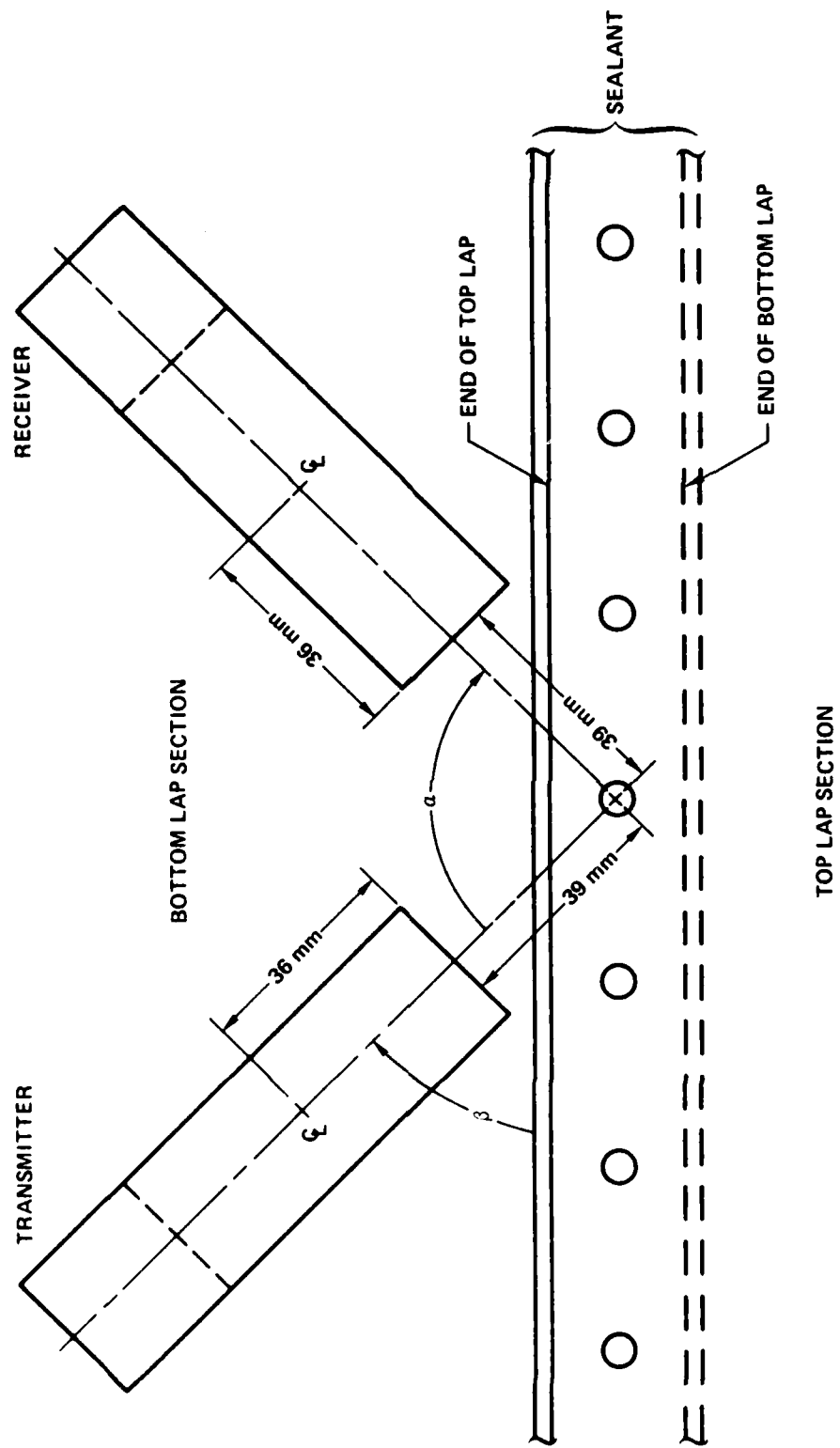


Fig. 5 Drawings of Transducer Configurations.
 (a) Simple Reflection.

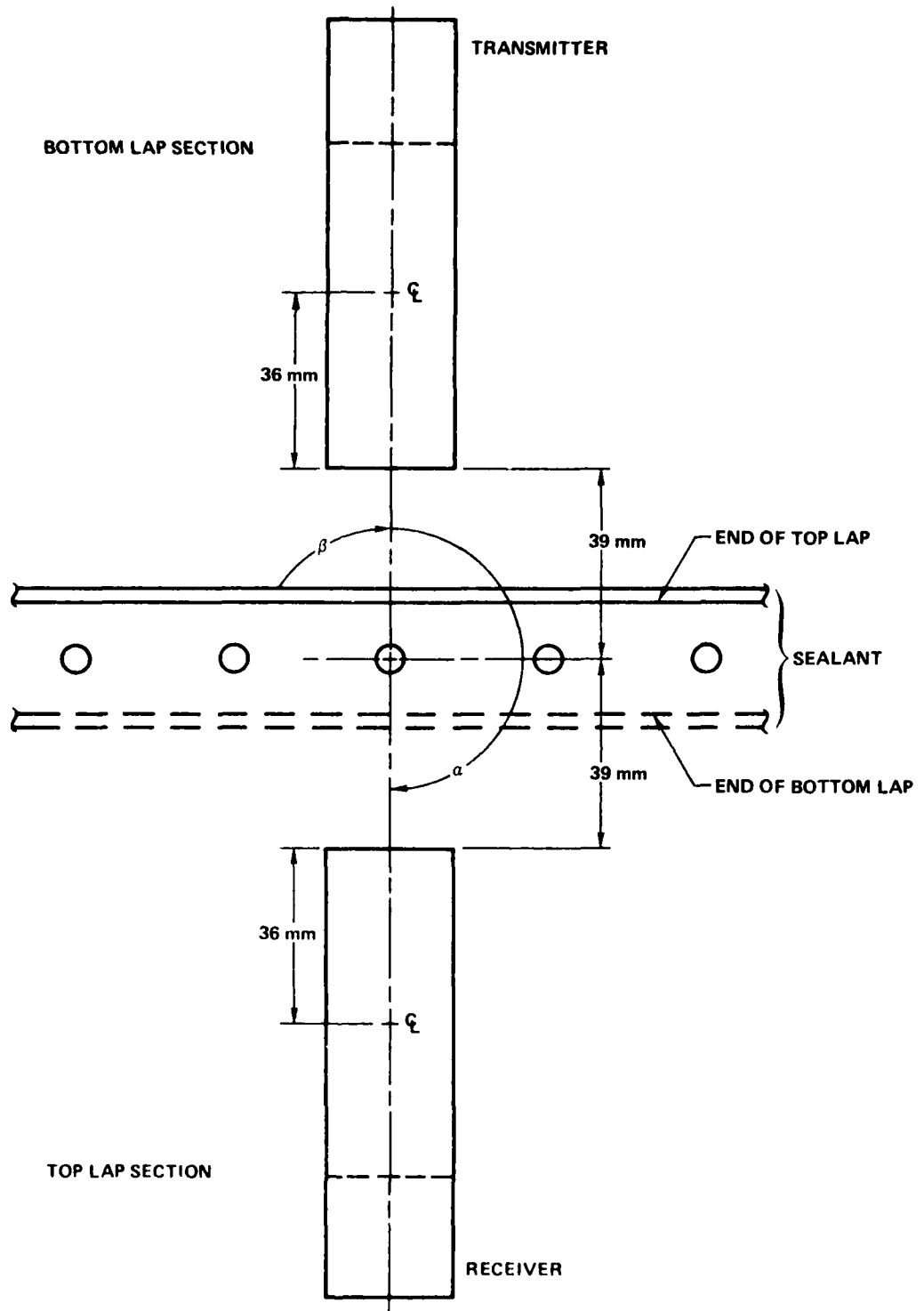


Fig. 5 Drawings of Transducer Configurations.
 (b) Two-Probe Transmission.

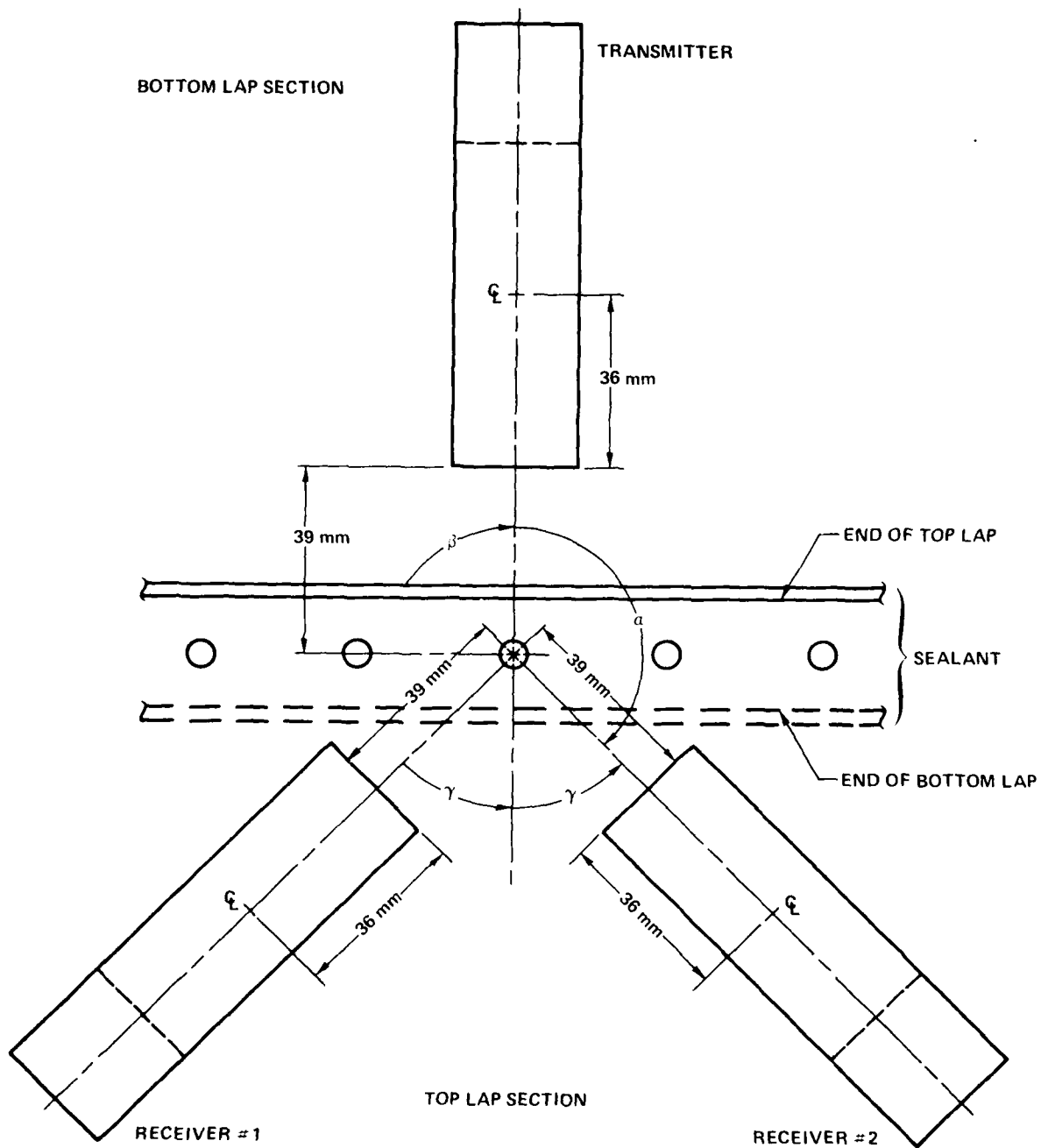


Fig. 5 Drawings of Transducer Configurations.
 (c) Three-Probe Transmission.

the control of the Interpretive signal Processing (ISP) Program. This system was created at the Science Center and is unique in the field of NDE. Both the S200 and the 8100 are commercially available separately. ISP is a large multitasking program which runs on the S200 under the command of an external terminal. It is tailored for flexible data collection and signal processing applications and capable of over 40 distinct operations including several for graphics. It was designed and developed at the Science Center and is constantly being upgraded for new NDE applications.

In these experiments, the Biomation 8100 waveform digitizer was triggered by a sync pulse from the 7060 generator, after being armed by a signal from ISP. For each waveform an array of 1024 samples was acquired in the 8100 with a sample interval of 0.2 μ s. This array was transferred to the S200 and added to a special buffer by ISP. After 100 such acquisitions, data taking was complete and the buffer was divided by 100 to yield an average waveform. This average waveform had a factor of 10 less random electronic noise than any single waveform; non-coherent r.f. noise was reduced even further. In this way, the noise-sensitivity was greatly improved over that of the previous study.

At this point, ISP allowed any of several different directions to be taken in the analysis of that signal. Those operations pertinent to this report are:

- a. storage on disk
- b. plotting on a storage CRT (Tektronix 4006 terminal),
- c. a Fourier transform, or its inverse,

- d. subtraction from another waveform, and
- e. division by another waveform.

Because of the flexibility of ISP, these operations could be applied in any order necessary for data analysis.

4. Stability Evaluation

During the experiment, checks were made to verify stable operation of the electronics. The gain was constant to within $\pm 10\%$ over the five-month period, as was the shape of the characteristic frequency spectrum of generated acoustic energy. No large deviations from an established norm were observed which could not be accounted for by an accidental lift off of a transducer from the part, or similar simple mechanisms. In fact, after the initial set-up in April and May of 1979, the only electronic problem was caused by a spurious ground loop between the cases of the transmitter and receiver EMATs. It was eliminated by insulating the aluminum posts of the EMAT cases from the metal goniometer.

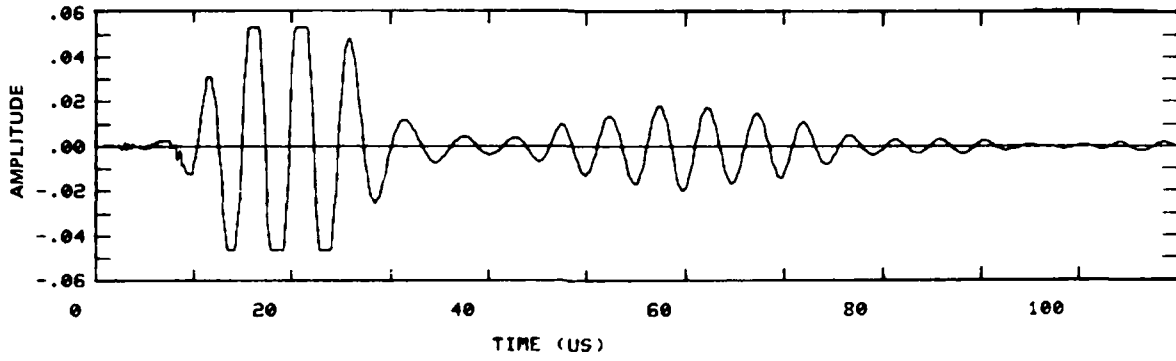
IV. EXPERIMENTS ON UNASSEMBLED MOCK-UP

In order to verify that the new apparatus was functioning properly, the previously reported experiments were performed on the original mock-up, in the unassembled condition. These results can then be compared to those reported in (1) to establish the amount of improvement realized.

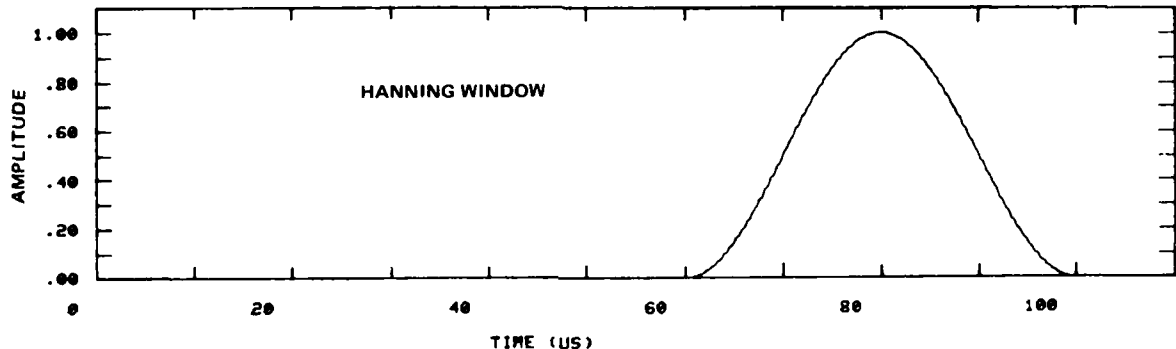
1. Experimental Technique

The transducer configuration used was that shown in Fig. 5a with $\beta = 45^\circ$, $\alpha = 90^\circ$. Fig. 6 shows the time waveforms received in this configuration from an unslotted hole. The previously described signal processing algorithm requires gating out that portion of the waveform containing the flaw information.

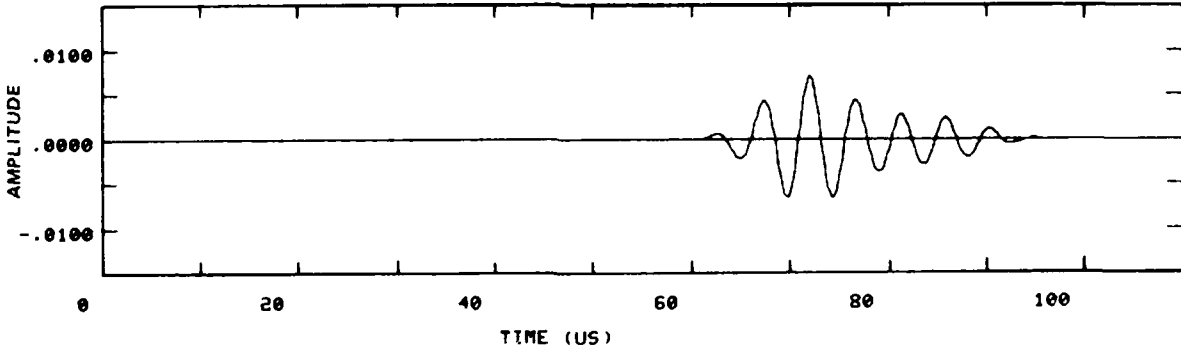
In this work, a Hanning window (Ref. 3) was used to eliminate spurious spikes in the subsequent Fourier analysis. In Fig. 6a, the entire waveform is shown. The clipped signal centered near 20 μs is the result of rf leakage from the transmitter to the receiver. In effect, the receiver acts as a radio antenna. This leakage has been found to be quite useful since it provides a measure of the true zero of time for measurement of acoustic delays. The signal centered near 60 μs is the reflection from the first step encountered in the wing lap joint. This merges with the reflection from the extreme plate edge, which is centered at approximately 80 μsec . At 110 μsec , the reflection from the end of the stiffening rib is just beginning. Fig. 6b shows the Hanning apodization function used to gate out all but the flaw information. Fig. 6c is the product of the waveforms shown in Figs. 6a and 6b. Note the 4x change of scale in going from Fig. 6a to Fig. 6c.



(a)



(b)



(c)

Fig. 6 Gating of Time Waveform. (a) Full Length Received Signal; (b) Hanning Function Used; (c) Resulting Signal for Fourier Analysis.

The transform of the signal in Fig. 6c was then digitally computed using a very fast assembly language routine developed here. (A 1000 point transform takes about 1 second.) Fig. 7 shows the results for holes 10, 11, and 12 in both amplitude versus frequency (7a), and complex impedance (7b), plots. The frequency spectra do not have exactly the same shape as those in Ref. 1 due to the new transducers and new operating frequency, the apodization used in this work, and the greater accuracy inherent in a computed transform as opposed to the crude analog transform of the previous work. Nevertheless, the data exhibit similar characteristics: an interference effect which is different in a slotted hole (#11, 0.220 inches long) from that in non-slotted holes (#10 and #12). It was found in this work that the depth and location of the interference dip or dips depended strongly on the exact location of the time window used for the Fourier transform. For this reason, an investigation was carried out to confirm the interference model proposed in the previous study and to determine from a physical understanding what time window should be used. The results are discussed in Section B.

2. Optimization of Gating Window

Figs. 8a and 8b show two time waveforms: one for hole #8, a hole with a large slot (0.150 in.), and one for hole #13, an unslotted hole. In Fig. 8c, these are superposed. Notice the near-similarity at 60 μ s is altered drastically near 90 μ s, although by 115 μ s the waveforms are very similar again. Fig. 9a shows the two reflection paths proposed in the model of Ref. 1; the first is from the complex region where the thickness changes and the

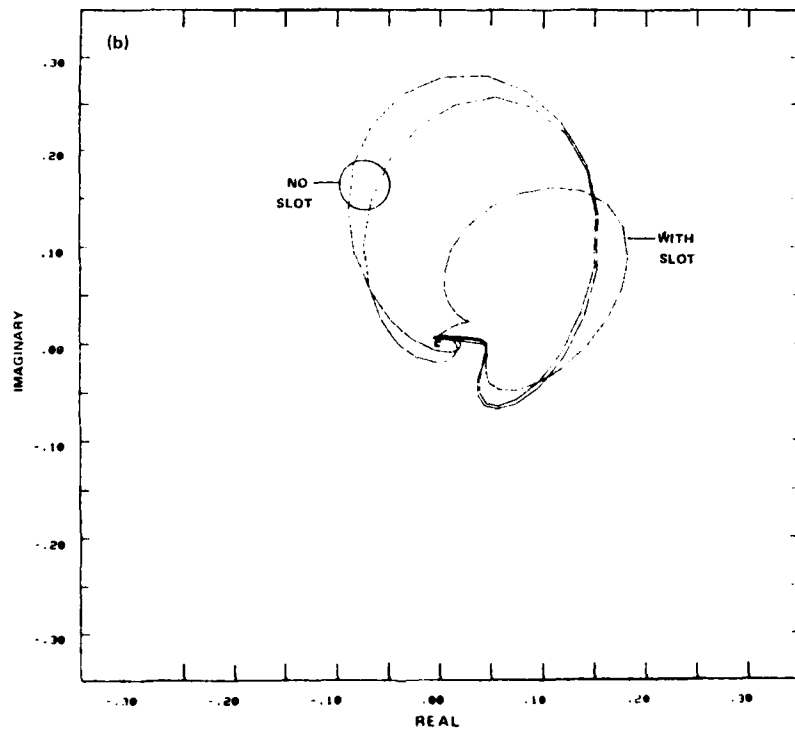
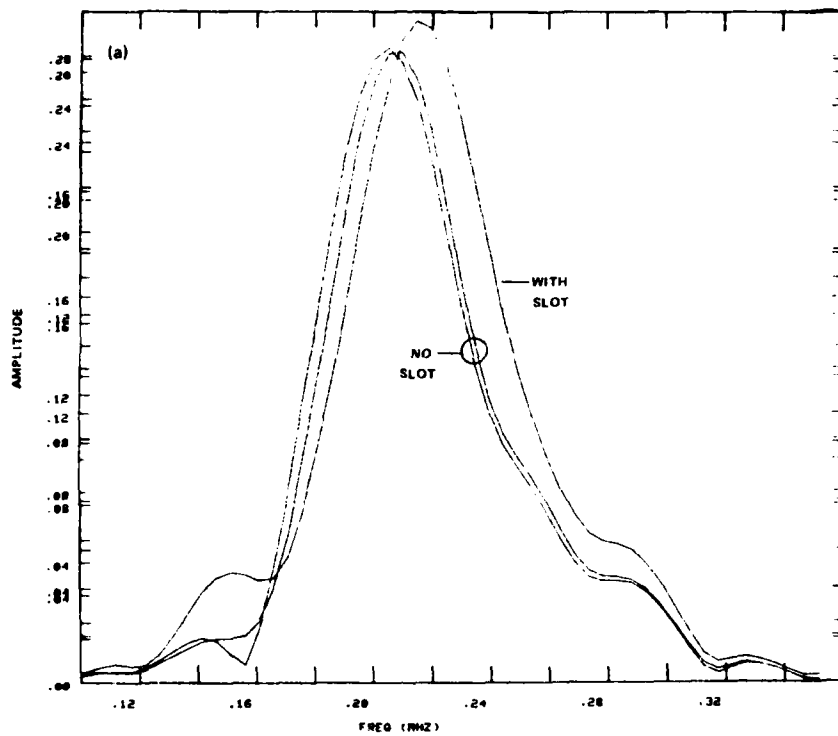


Fig. 7 Fourier Analysis of 1 Slotted and 2 Unslotted Holes.
 (a) Amplitude versus Frequency; (b) Imaginary versus Real
 for the Frequency Range Indicated in Fig. 7a.

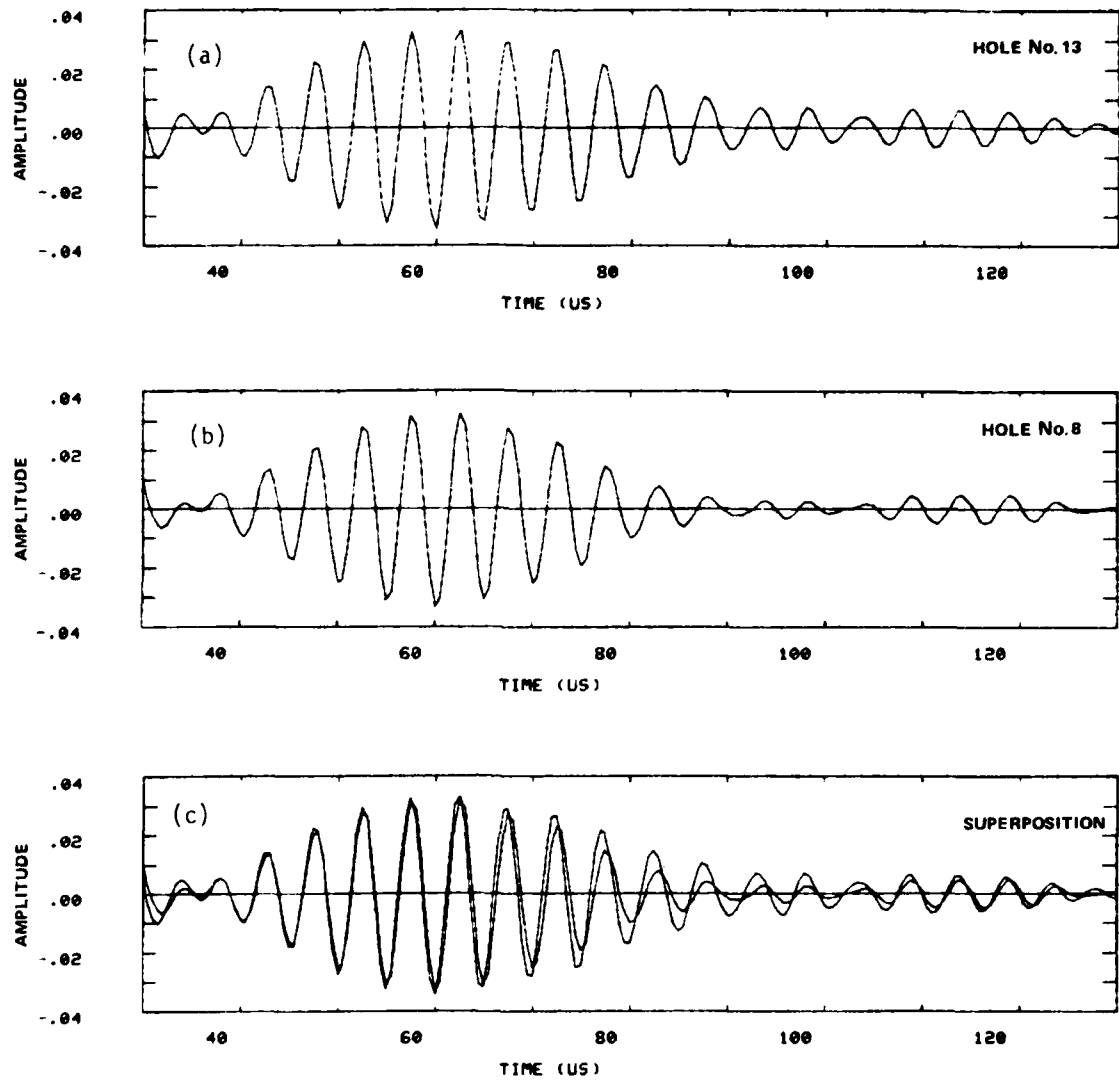


Fig. 8 Signals from an Unslotted and a Slotted Hole.
 (a) Unslotted; (b) Slotted; (c) Superposition
 of (a) and (b).

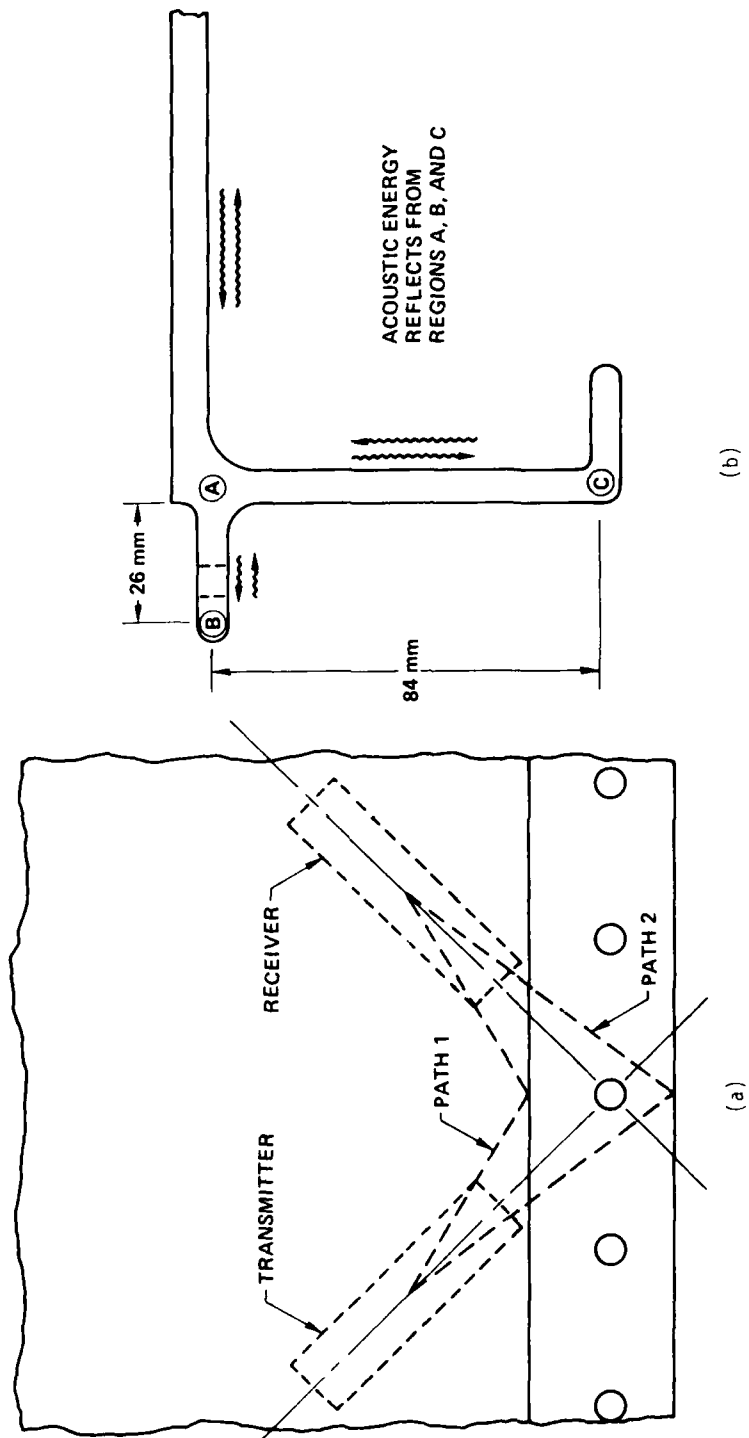


Fig. 9 Drawing of Relevant Acoustic Paths. (a) Top View, Paths 1 and 2; (b) Sectional View.

stiffening rib connects, and the second is from the extreme edge of the sample. Since the time difference between paths 1 and 2 is only one-quarter of the length of the signal in path 1 or path 2 individually, one would not expect the signals from the two paths to be resolved in time. In principle, there is also a reflection from the fastener itself but this is very small in amplitude compared to the signals from paths 1 and 2 and would not be distinguishable in Fig. 8

A simple interpretation of Fig. 8 in terms of Fig. 9 is that the acoustic signal in hole #13 has a large component from path 1, a smaller component from path 2, and a much smaller signal which is a reflection from the end of the rib (see Fig. 9b). However, the signal from hole #8 (Fig. 8a) has almost no component added in from path 2 due to the barrier presented by the slot. Its amplitude in the 80-100 μ s region is therefore smaller. Depending on the exact geometry of the transmitter and receiver transducers, the signals from the two paths could interfere destructively instead of constructively as is the case here. The locations of the interference null used in crack detection and sizing could also shift. The speed of sound for a shear wave in aluminum is 3.05 mm/ μ s. From Fig. 9b, one can estimate that the reflection from path 2 will take $(26 \times 2 \times \cos 45^\circ / 3.05)$ μ s, or 12.1 μ s longer than path 1. The reflection from the rib should take $(84 \times 2 / 3.05)$ μ s, or 55.1 μ s longer than path 1.

A test of this interpretation of Fig. 8c is to attempt to simulate it with a signal which is a reflection from simple clean edge. Fig. 10a shows such a signal, obtained by bouncing the acoustic energy at a 45° angle to the

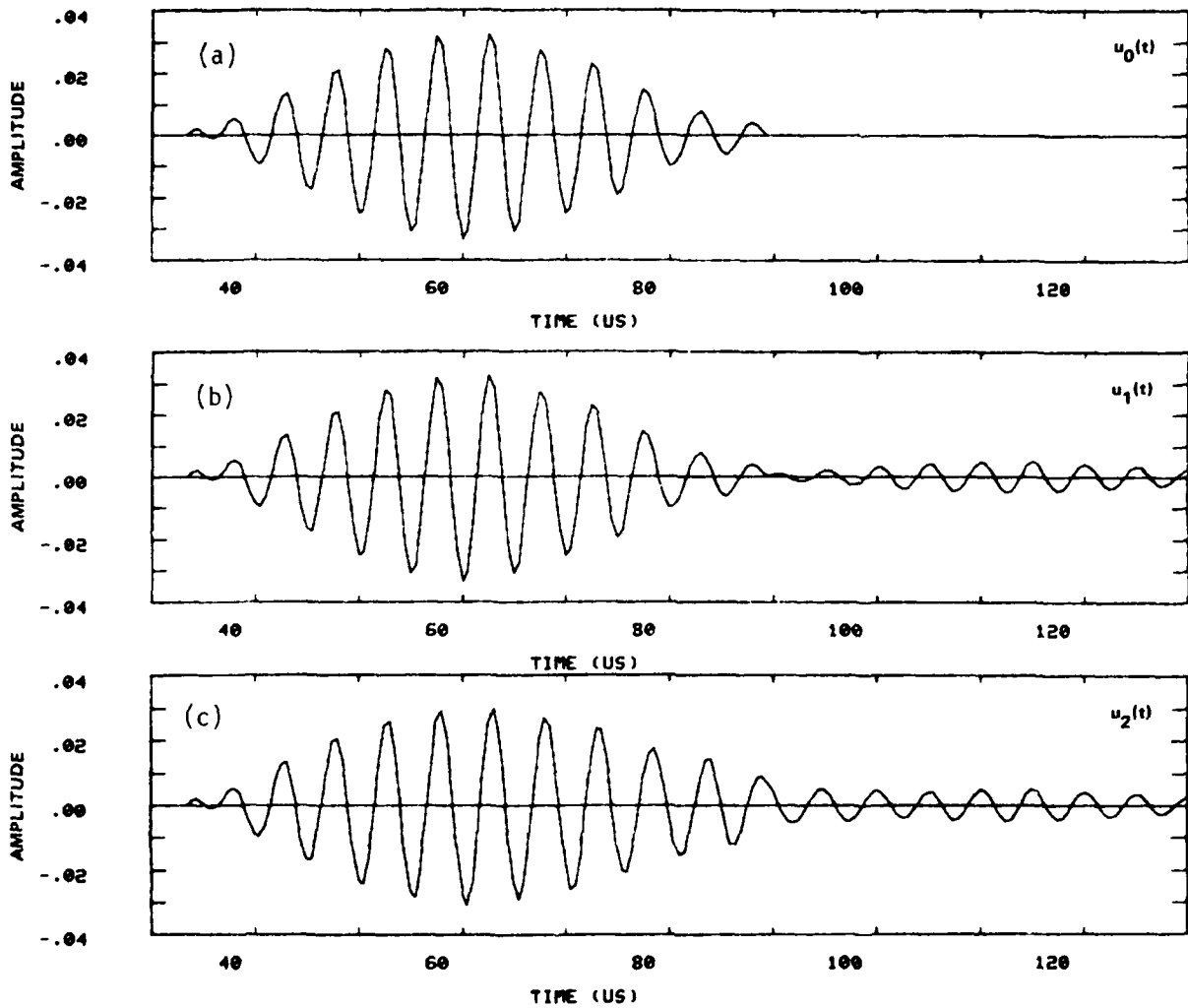


Fig. 10 Simulated Signals. (a) Signal after Reflection from a Simple Edge, with Irrelevant Time Regions Gated Out; (b) Simulation of the Signal from a Slotted Hole; (c) Simulation of the Signal from an Unslotted Hole.

edge of the mock-up opposite to the lap joint, where there is no complex geometry. To produce a successful simulation of the waveforms in Fig. 8a, the following exact summation was required:

$$u_1(t) = u_0(t) + 0.15 u_0(t - 52.5 \mu s) \quad (1a)$$

$$u_2(t) = u_1(t) + 0.30 u_0(t - 11.5 \mu s) \quad (1b)$$

where $u_0(t)$ is the waveform of Fig. 10a.

The results, $u_1(t)$ and $u_2(t)$ are shown in Figs. 10b and 10c. The first signal, u_1 , is intended to simulate the response from the slotted hole #8. The function u_0 represents the signal from path 1, and $0.15 u_0(t-52.5 \mu\text{sec})$ represents the delayed signal from the stiffener. However, no signal is included from the back edge of the plate, path 2, since this is assumed to be blocked by the slot. The function u_2 simulates the signals for the unslotted hole #13, which includes both u_1 and a contribution, $0.30 u_0(t-11.5 \mu\text{sec})$, representing the back edge reflection (path 2). Comparison of Figs. 8 and 10 shows excellent agreement, suggesting that the interpretation is correct. The window position shown in Fig. 6b is optimized to include the two paths of interest. The empirical values of $11.5 \mu s$ for path 2 and $52.5 \mu s$ for the rib reflection are satisfactorily close to the estimated values of $12.1 \mu s$ and $55.1 \mu s$. The multiplying coefficients are also very reasonable and support the simple interpretation advanced above.

V. FABRICATION OF SAMPLES

Four samples were utilized in experiments reported here and are described below in detail. A large fraction of the fabrication effort was performed at another division of Rockwell, the North American Aircraft Division (NAAD), for reasons of efficiency and the availability of machine shop time and particular machines needed. Fig. 1 and Table I provide the dimensions of all samples used. The fasteners and nuts were obtained directly from Voishan, Inc.

1. Actual Wing Section

This is the actual wing section provided for the previous study (1) in which a saw slot had been introduced at one of the fastener holes (#19). To aid in comparison of EDM notches with fatigue cracks this sample was disassembled and two more flaws were created. These were radial corner EDM notches about 0.010" in width. One was 0.100" long and was placed at hole #11 in a region of changing geometry (see Fig. 11). The other was 0.030" long and was placed at hole #16 in a region of fairly constant geometry. Fig. 12a shows a cross-sectional view of the notch geometry. Furthermore, in re-assembling this section, the fastener in hole 4 was omitted and hole #23 was drilled slightly oversize. This was done to provide examples of loose fasteners. The re-assembly was done in the manner described in Section C for fatigued samples.

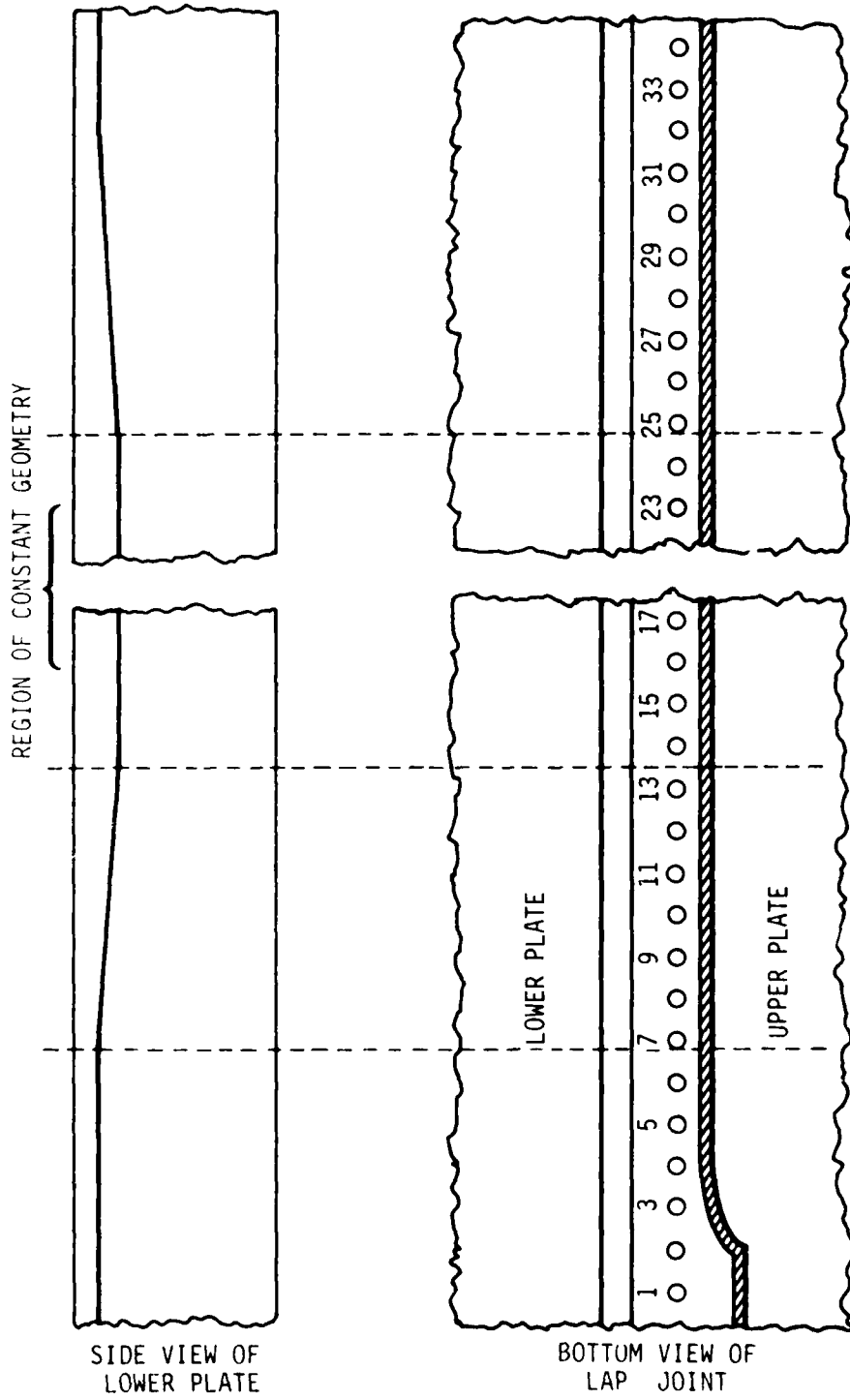
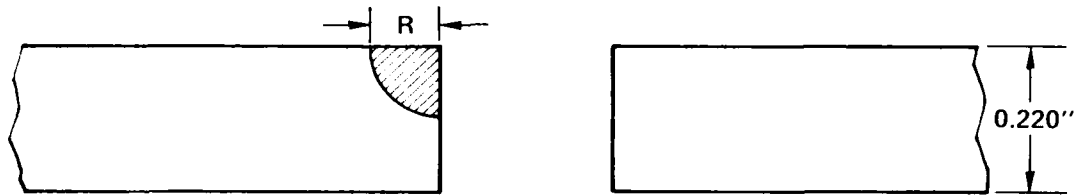
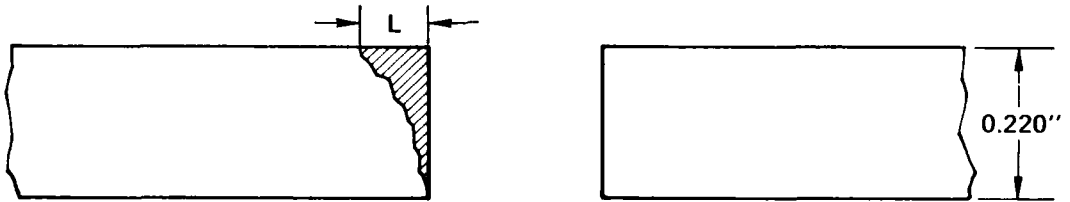


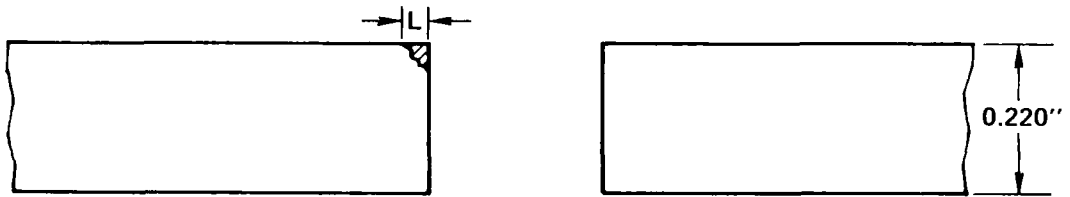
Fig. 11 Drawing of Geometry Variation in the Actual Wing Section (Section V - A).



a) CORNER EDM NOTCH
 $R = 0.100''$, $0.030''$



b) 100 mil FATIGUE CRACK
 ACTUAL $L = 0.110'' \pm 0.010''$



c) 30 mil FATIGUE CRACK
 ACTUAL $L = 0.035'' \pm 0.010''$

Fig. 12 Drawing of the Radial Corner Notches and Fatigue Cracks.

TABLE I

Dimensions in Inches for Values Shown in Figure 1. (Nominal)

	Actual Wing Section	Mock-Up Wing Section	Fatigued Samples
A	0.260	0.688	0.700
B	0.260	0.438	0.438
C	0.195	0.218	0.218
D	0.200	0.218	0.218
E	0.270-0.425	0.281	0.281
F	N.A.	1.96	1.96
G	1.58	1.063	1.063
H	1.68	1.125	N.A.
I	3.04	3.20	N.A.
J	0.450	0.500	0.500
Bolt #	TLB-3-5 SPS	TLI-5-9 VS	TLH1-4-8 VS
K	0.048	0.070	0.063
L	0.312	0.560	0.500
M	0.270	0.455	0.385
N	0.200	0.330	0.265
P	0.186	0.307	0.246
Q	0.87 - 1.15	1.25	1.25

(N.A. means not applicable)

2. Wing Section Mock-up

The lower half of this sample was the full geometry aluminum mock-up fabricated for the previous study with five saw slots of various lengths. A mating upper half was constructed and tapered holes were drilled in each half

to admit the special fasteners. A number of experiments were performed before assembly and were reported in Section IV. The assembly was made in the manner described in Section C below. The actual assembly of this specimen was delayed until after initial studies had been performed on the fatigued samples described next.

3. Fatigued Samples

The work statement for this contract (2) required two samples with simulated induced service fatigue cracks at the fastener holes. Consultation with Dr. O. Buck of the Science Center yielded a plan for creating such fatigue cracks. The full fabrication of these samples involved over ten separate steps. It took three months and cost approximately \$6,000 per sample. In the opinion of the authors of this report, those figures are the minimum which could possibly be expected of any similar future fabrication.

The drawings necessary for fabrication are reproduced in Figs. 13 through 15. First, material was obtained for both the upper and lower sections of the joint for each specimen to be fatigued. The lower sections had to be wide enough (see Fig. 13) to provide an area on each end where the MTS load-cycling machines could connect. The first machining steps, shown in Fig. 13, provided a narrowed region with a pilot hole and an EDM notch which would start a fatigue crack under cycling (the "pre-fatigue shape"). In addition, two spacer pieces of aluminum were constructed for each end of each lower section to provide a fit to the MTS grips. These parts and the section ends were allodyned and bonded together before being drilled to accept the

WING JOINT - LOWER SECTION - PREFATIGUE DIMENSIONS
 MATERIAL 7075-T6Al SCALE 1/2 OR AS NOTED

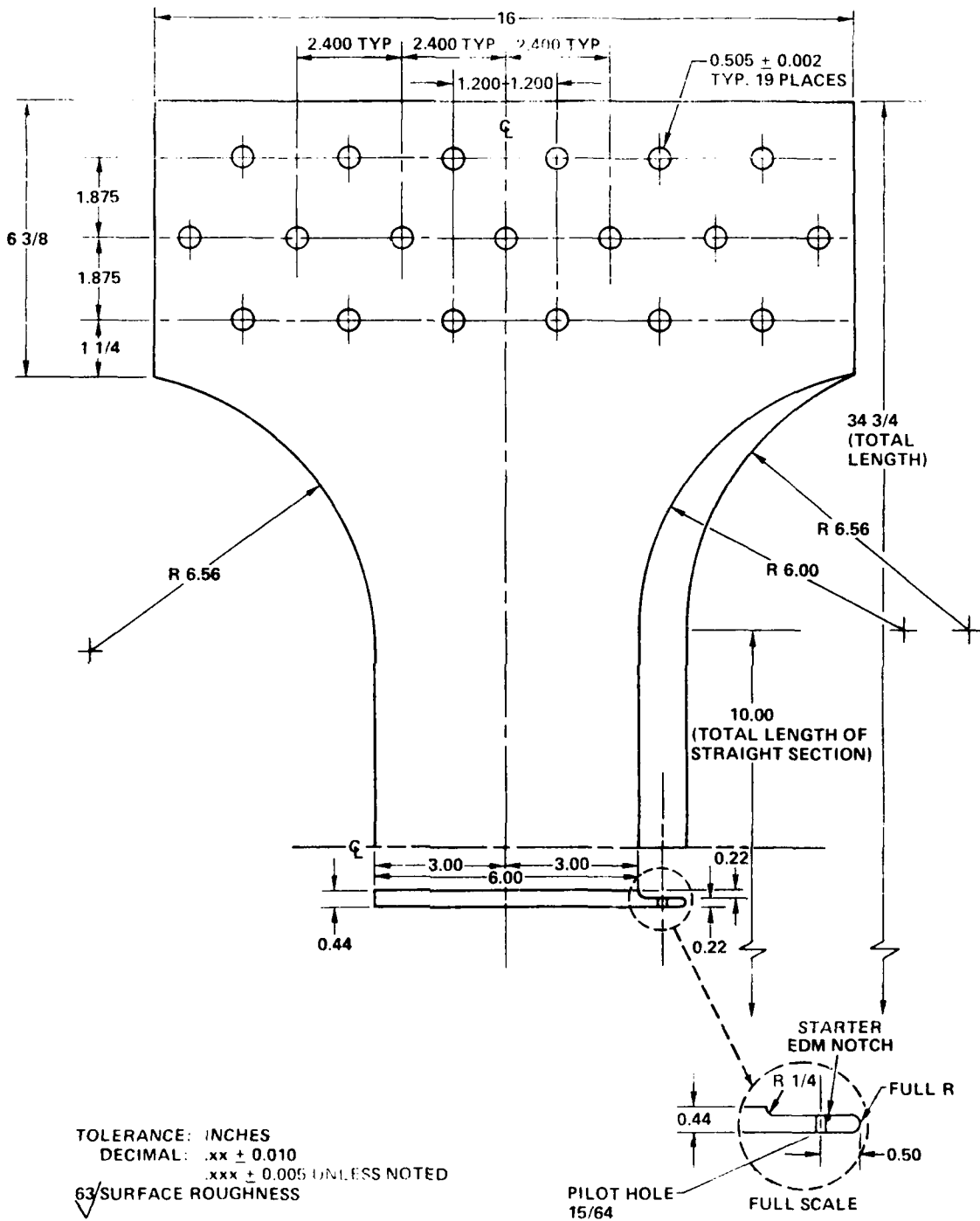


Fig. 13 Drawing of Prefatigue Dimensions of Lower Sections of the Fatigue Samples.

grip bolts. The fatigue cycling was performed over a range of 5 to 50 thousand pounds of tension with a 0.5 Hz cycle rate. Crack initiation required 7600 cycles on one specimen and 11,200 cycles on the other. The cracks could be easily measured under 50,000 pounds of tension. They were allowed to grow long enough that drilling the final taper hole would leave them near the nominal dimensions of 0.030 inch and 0.100 inch (0.076 cm and 0.254 cm). After the correct crack length was reached, the lower sections underwent the finish machining shown in Fig. 14. The upper sections were constructed as shown in Fig. 15a. The tapered holes were drilled by bolting the upper and lower sections together at each end and drilling them at the same time.

Two methods of confirming the length of the fatigue cracks after final drilling were used. They were etched and viewed under a microscope directly, and then they were treated with a fluorescent penetrant and viewed under a microscope again. A photograph of the 0.030" crack is shown in Fig. 16; the 0.100" crack is shown in Fig. 17. The blotchy nature of the 0.030" crack is due to the aqueous developer which was necessary in order to get an image of it. Figs. 12b and 12c show an estimation of the cross-sectional area of these cracks based on the observations made under the microscope. Of course, details of the crack edge within the sample could not be verified without a destructive examination.

Finally, assembly of both samples was performed using the VOI-SHAN TAPERLOCK Installation Specification as a guide. The fasteners were tightened to 125 in-lbs. The sealant was allowed to cure two weeks at room temperature before the measurements reported in later sections were made. Fig. 15b shows the assembly drawing.

WING JOINT - LOWER SECTION - FINAL DIMENSIONS
 SCALE: FULL $\frac{63}{100}$ SURFACE ROUGHNESS
 TOLERANCE, INCHES, DECIMAL $.xx \pm .010$
 $.xxx \pm .005$

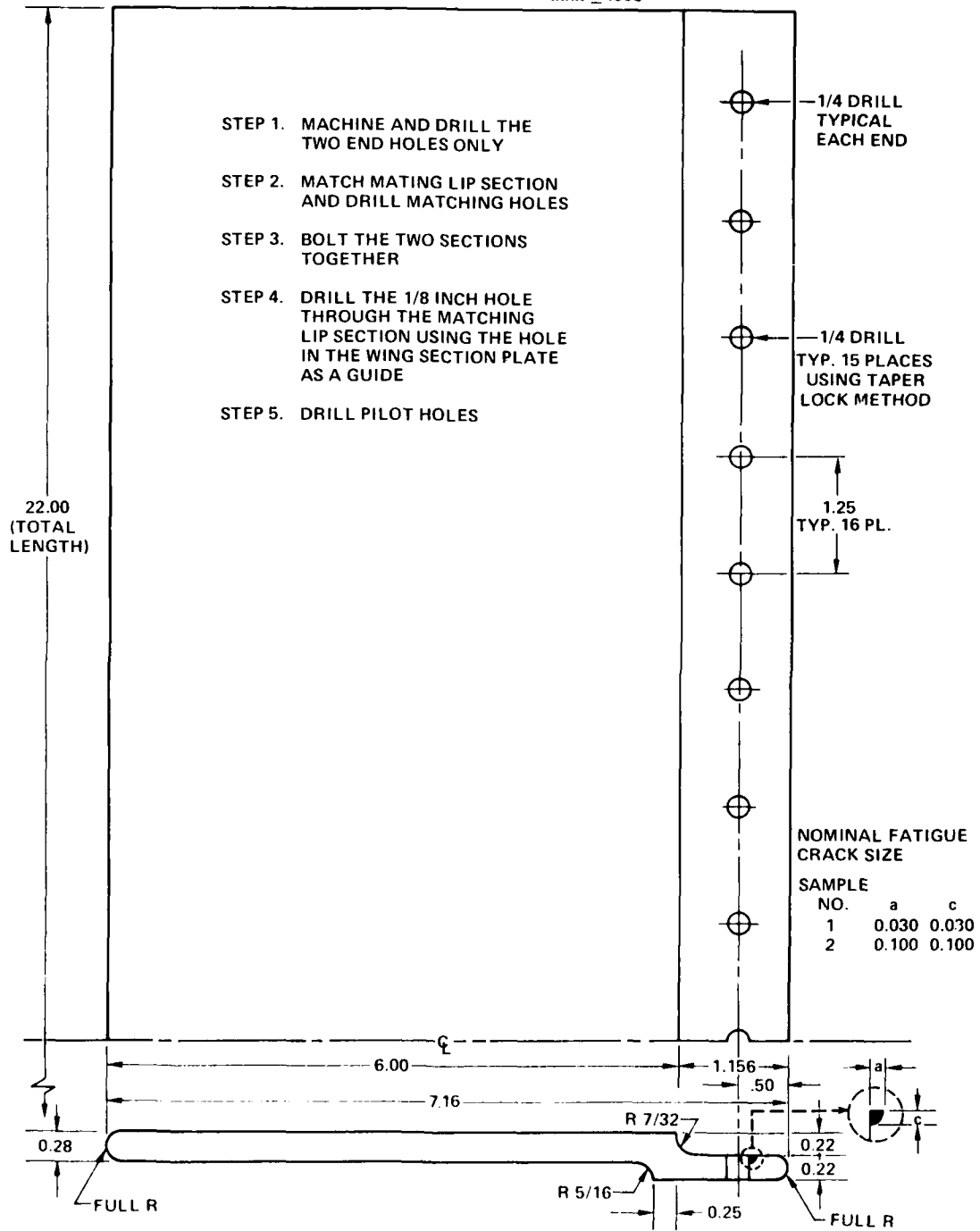


Fig. 14 Drawing of Final Dimensions of Lower Sections of the Fatigue Samples.

WING JOINT - UPPER SECTION
 MATERIAL 7075-T6A1 2 REQUIRED
 FINISH 63

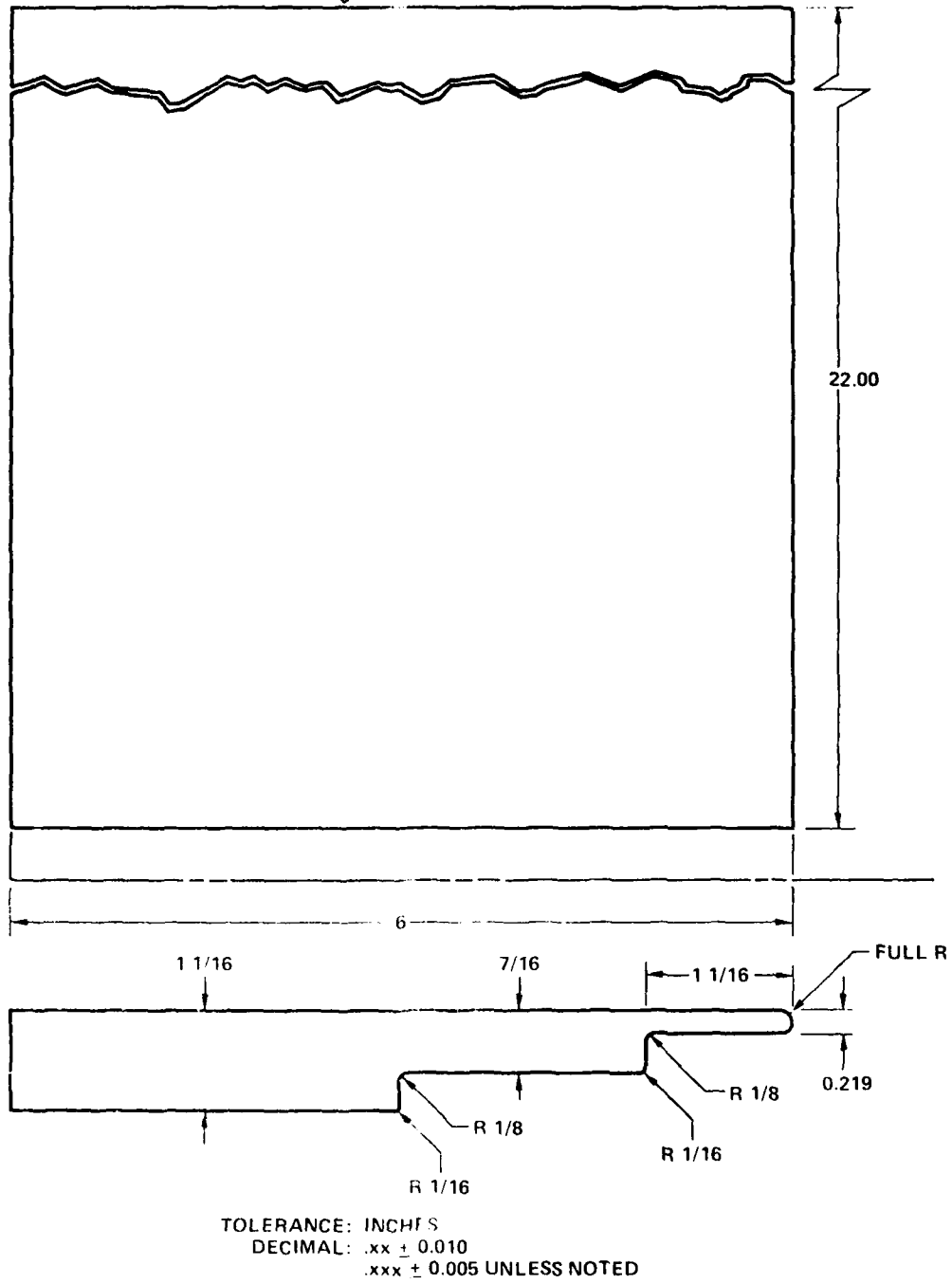
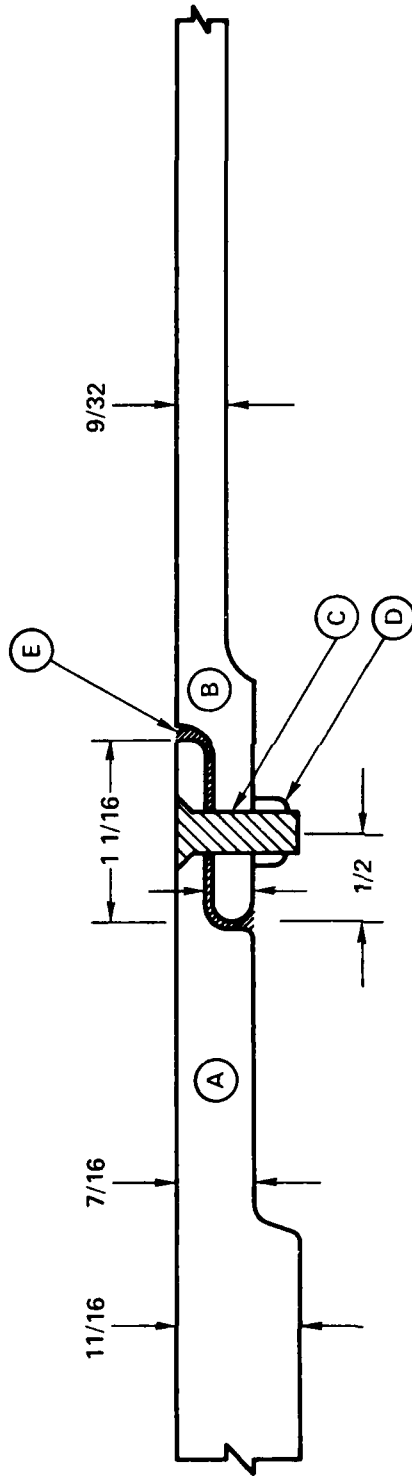


Fig. 15 (a) Drawing of Upper Sections for the Fatigued Samples and Assembly.

ASSEMBLY DRAWING C5A WING LAP - JOINT - FATIGUED SPECIMENS

SCALE: FULL DIMENSIONS - REFERENCE ONLY - TWO REQUIRED



NOTES:

- (A) MAKE FROM "WING SECTION MATE" DRAWING (2 REQUIRED)
- (B) MAKE FROM "WING SECTION PLATE" DRAWING
- (C) VSI TAPER LOK FASTENER TL-H-100-4-X-X OR TL-V-100-4-X-X INSTALL PER BRILES PROCESS SPECIFICATION BPS 148
- (D) VSI TAPER LOK NUT TLN-1010-CPD1-4 OR SS HEX NUTS 1/4-28
- (E) PREPARE FAYING SURFACE WITH MIL-S-8802-B2 SEALANT PRIOR TO ASSEMBLY

Fig. 15 (b) Drawing of Upper Sections for the Fatigued Samples and Assembly.



Fig. 16 Photograph of 0.030 in. Fatigue Crack after Treating with
Dye Penetrant and Developer.

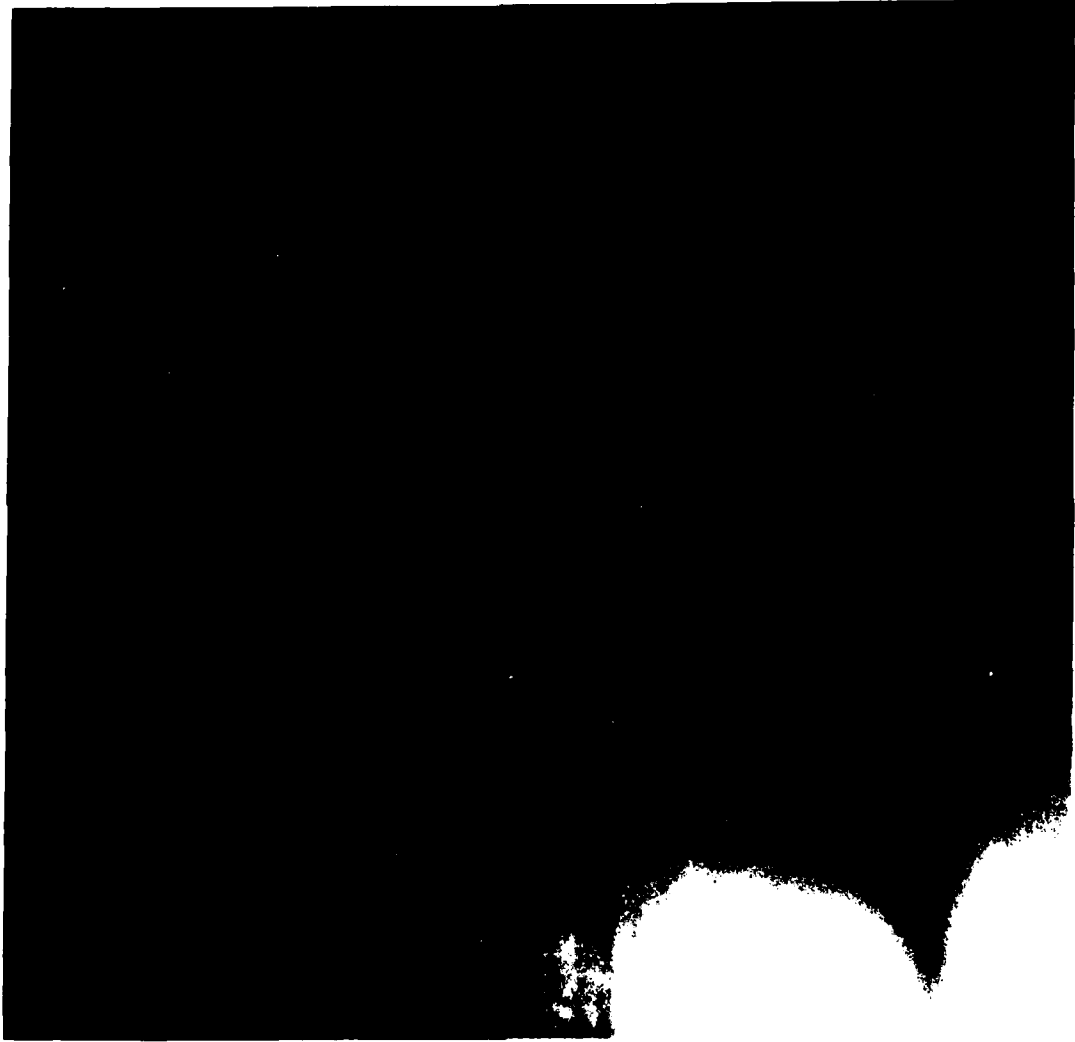


Fig. 17 Photograph of 0.100 in. Fatigue Crack after Treating with Dye Penetrant Only.

The absence of the stiffening rib from these samples was motivated by the excessive cost involved and a much greater risk of failure when placing a fatigue crack in the desired location. It is justifiable since from the studies in Sections IV it is known that the rib reflection occurs well after the time window of interest.

VI. MEASUREMENTS IN ORIGINAL TRANSDUCER CONFIGURATION ON ASSEMBLED SAMPLES

After assembly of the fatigued specimens a crucial experiment was performed on the sample with the nominal 0.100" fatigue crack. The transducer configuration was that shown in Fig. 5a with $\beta = 45^\circ$. This is the same configuration as that used successfully in Ref. 1 and Section IV of this report. The results are shown in Fig. 18 with the curves scaled to be of approximately the same peak height for the purpose of comparison. The spectra in Fig. 18 show only a very small systematic difference between hole 9, the hole with a 0.100" fatigue crack, and the other holes. This difference did not appear large enough to serve as a reliable estimate for the presence of a crack, and indicated that this transducer configuration might not be satisfactory for success in the field on fully assembled wing lap joints.

The ability to find a fatigue crack of this length in an assembled specimen of uniform geometry is a minimum standard of performance which must be achieved in any transducer configuration. Since the configuration which worked well for the unassembled mock-up did not generalize to the fully assembled structure, an optimization procedure was sought. Ideally, this should be based on an examination of the mechanisms of the interaction of acoustic energy with the fastener hole in much greater detail for this complex geometry. As described in the following section, it was found that some recent developments in acoustic theory (4) could be applied to this problem to provide a framework for understanding the dependence of the flaw's reflection coefficient on the angle of the incoming acoustic beam.

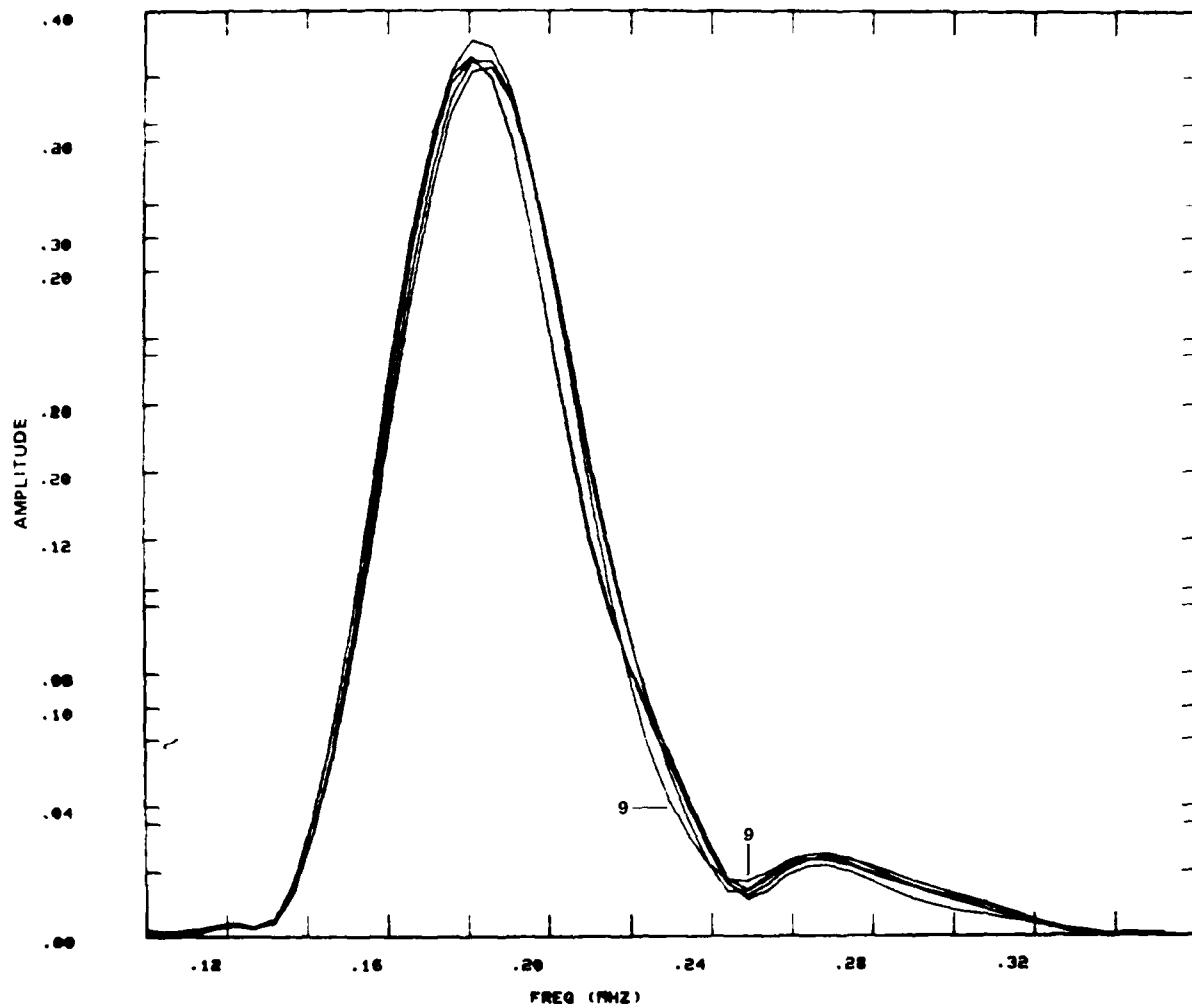


Fig. 18 Amplitude versus Frequency for Assembled Sample with 0.100 in. Crack; $\beta = 45^\circ$.

VII. DEVELOPMENT OF ANALYTICAL BASIS FOR PROBE
OPTIMIZATION AND CONFIRMING EXPERIMENTS

1. Theoretical Background

The basic approach used here is the scattering theory work in Ref. 4. It applies to the SH acoustic waves employed in this report. The central concept is an expression for the reflection coefficient for scattering of an acoustic beam from a void in a material. Suppose Γ is the signal propagated between a transmitter and a receiver in the absence of a void. Then, if a void is present, this will change by an amount $\delta\Gamma$ given by

$$\delta\Gamma = \frac{i\omega}{4P} \int_{\text{surface}} \underline{T}_{u'} \cdot \underline{R}_T \cdot \hat{n} \, ds \quad (2)$$

where the presubscript refers to the transducer used to generate the elastic fields and the post prime indicates that the void is assumed to be present. Thus $\underline{T}_{u'}$ is the material displacement at the surface of the void when it is illuminated by the transmitting transducer driven by a power P , \hat{n} is a unit vector normal to the surface of the void, and \underline{R}_T is the material stress that would be produced at the mathematical location of the void surface if the void was absent and the region was illuminated by an electrical power P applied to the receiving transducer. Similarly, \underline{R}_u , which will be used in the following discussion, is the material displacement at the mathematical surface of the void with the void absent, as illuminated by the receiving transducer.

For the case of a crack such as that shown in Fig. 19a, Eq. (2) can be simplified and placed in a form containing direct measureables. To do so, it can be noted that, for a crack, the integrations on the left and right surfaces of the crack differ only in the sign of \hat{n} . Consequently, Eq. (2) can be simplified into the form

$$\delta\Gamma = \frac{i\omega}{4p} \int_{\text{surface}} \underline{T_{\Delta u'}} \cdot \underline{R_T} \cdot \hat{n} \, ds, \quad (3)$$

(y = + ε)

where ϵ is small with respect to the radius of the fastener hole and the quantity $\underline{T_{\Delta u'}}$ is defined by

$$T_{\Delta u_y'} \equiv T_{u_y'}(y = + \epsilon) - T_{u_y'}(y = - \epsilon). \quad (4)$$

$T_{\Delta u_y'}$ can be physically interpreted as the opening of the crack induced by the applied stress field. Fig. 19b shows an experimental definition of $T_{\Delta u_y'}$. In order to further simplify Eq. (6), it is desirable to relate $\underline{T_{\Delta u'}}$ to the applied load. This can be done by noting that, when the crack is small with respect to the ultrasonic wavelength, the crack opening is given by

$$T_{\Delta u_y'}(x,z) = K(x,z) T_{T_{yy}}(x=a) \quad (5)$$

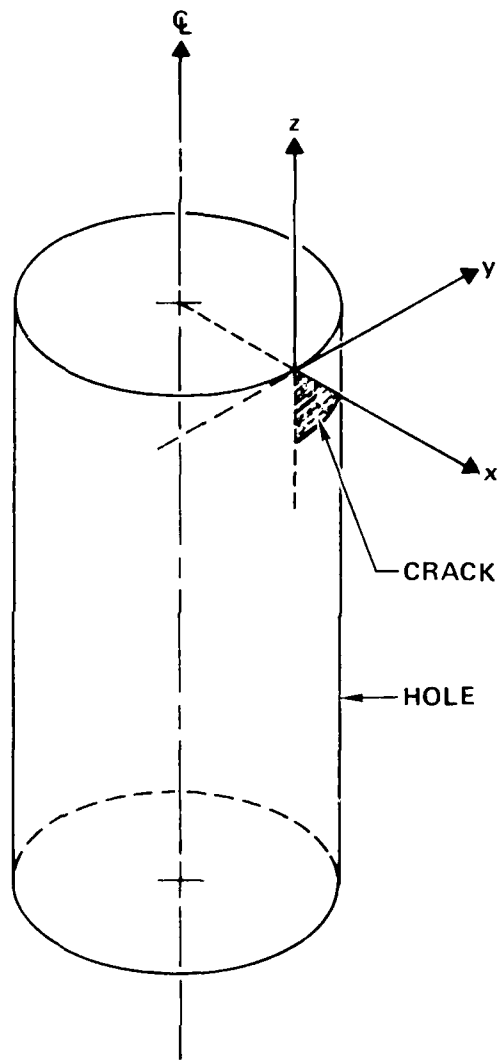


Fig. 19 Definition of Variables Used in Theoretical Analysis.
(a) Definition of Coordinates.

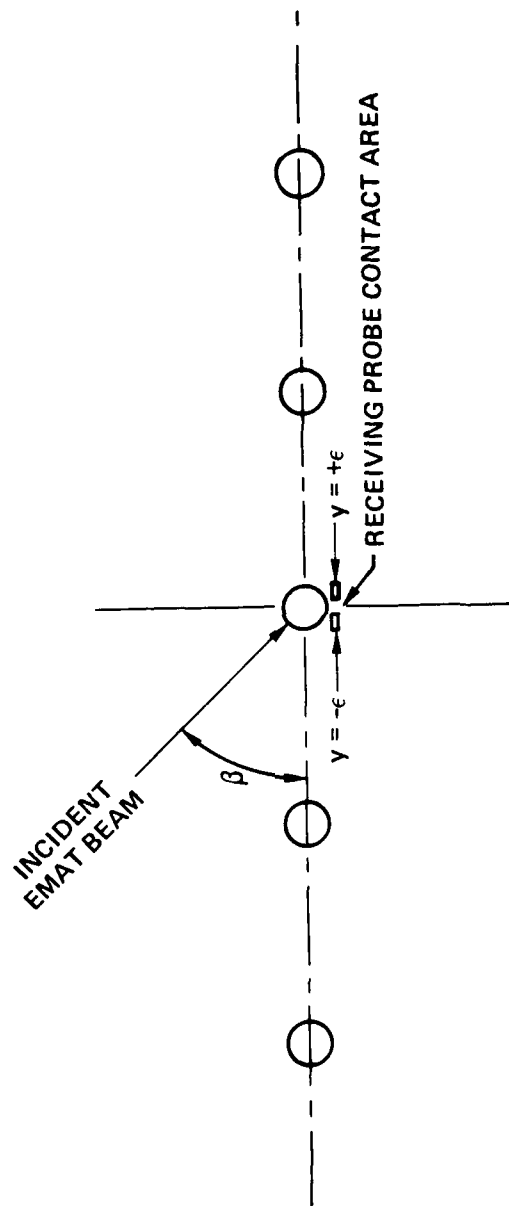


Fig. 19 Definition of Variables Used in Theoretical Analysis.
 (b) Definition of β and the Two Probe Locations.

where the factor K can be determined from static elasticity solutions and is a function of crack length. This is known as the quasi-static approximation. Substitution of Eq. (5) into Eq. (2) yields the result

$$\delta\Gamma \approx \frac{i\omega}{4P} T_{yy}(x=a)^R T_{yy}(x=a) \int_{\text{surface}} dx dz K(x,z) \quad (6)$$

(y=ε+)

From this result, it is clear that a given crack will produce the maximum change in the ultrasonic signal when the transducer positions are chosen to be symmetric with respect to the lap joint and at such an angle that a maximum stress is produced in an uncracked hole at the potential crack location. The strength of the crack indication will be given by the integral of K.

To express the quantities T_{yy} in terms of physical measurements, additional analysis is required. This was stimulated by consultation performed as a part of this program by Prof. B.A. Auld, of Stanford University, who suggested that a sound practical approach would be to find the solution for the scattering of an SH wave from a cylindrical void in an unbounded medium and then to reduce it to the case of a plate in order to determine T. Here the hole is considered to be part of the initial geometry, and the "void" defined in Eq. (2) is the crack growing from the cylindrical hole. For small cracks, u' is derived from T using a quasi-static scattering approximation and Eq. (2) could then be used to find the change in scattering.

This procedure was performed as follows. The stress matrix equation for a material is

$$\underline{\mathbf{T}} = \underline{\mathbf{C}} \cdot \underline{\mathbf{S}} \quad (7)$$

where $\underline{\mathbf{C}}$ is the elastic stiffness coefficient matrix relating $\underline{\mathbf{S}}$, the material strain to $\underline{\mathbf{T}}$, the stress. This equation represents six individual linear equations, which in a homogeneous medium are (Reference 5).

$$T_{xx} = C_{11}S_{xx} + C_{12}S_{yy} + C_{12}S_{zz} \quad (8a)$$

$$T_{yy} = C_{12}S_{xx} + C_{11}S_{yy} + C_{12}S_{zz} \quad (8b)$$

$$T_{zz} = C_{12}S_{xx} + C_{12}S_{yy} + C_{11}S_{zz} \quad (8c)$$

$$T_{xy} = C_{44}S_{xy} \quad (8d)$$

$$T_{xz} = C_{44}S_{xz} \quad (8e)$$

$$T_{yz} = C_{44}S_{yz} \quad (8f)$$

Fig. 19a defines the rectilinear coordinate space used. Remembering that the vector u describes the particle displacement at a particular point, S_{xx} is the gradient of the x component of u in the x direction. T_{xx} is the stress component in the x direction acting on the x face of the infinitesimal volume

element the deformation of which is described by S . Similar definitions apply to the other T_{ij} and S_{ij} terms.

In this work, the aluminum plate is thin with respect to the acoustic wavelength. Therefore, to a very good approximation, all T_{iz} terms are zero. Further, since the crack is near the cylinder surface, it is safe to approximate T_{xx} and T_{xy} by zero. Equations (8a) and (8c) then yield

$$S_{xx} = S_{zz} \quad (9a)$$

which simplifies Eq. (8b) to the form

$$T_{yy} = C_{11}S_{yy} + C_{12}(S_{xx} + S_{zz}) = C_{11} \frac{\partial u_y}{\partial y} + 2C_{12} \frac{\partial u_x}{\partial x} \quad (9b)$$

In practice, $C_{12}/C_{11} \sim 0.5$ and $(\partial u_x/\partial x)/(\partial u_y/\partial y) = 0.3$. Therefore, to a first approximation, the second term in Eq. (9) can be dropped and combination with Eq. (5) yields the result

$$\Delta u_y' = K(x,z) \frac{\partial u_y}{\partial y} \quad (x=a). \quad (10)$$

According to the theory, K should be the same no matter what direction the acoustic wave arrives from; hence a test of this line of analysis is to measure $\Delta u_y'$ and $\frac{\partial u_y}{\partial y}$ for two different values of β (see Fig. 19b) and see if the proportionality constant is in fact the same. The next section reveals the results of this test.

2. Experimental Determination of Optimum Probe Configuration

In order to verify this analysis, a set of measurements were made, using a special EMAT probe to measure both u_y and \dot{u}_y . It was necessary for the area of contact to be quite small; Fig. 19b shows the approximate size of the contact area of the probe with the aluminum plate near the hole. Figure 20 is a photograph of the actual probe. It consisted of a 1" x 0.030" x 18" thin plate of mild steel, magnetically attached to the receiver EMAT. It provided a nearly ideal means of converting the surface displacements in a very small region (caused by the entering acoustic beam) into SH waves which could travel down to and be detected by the attached EMAT. At the low frequencies of this work, pressure contact was adequate to couple the shear energy from the plate into the probe.

Fig. 21 shows the measurement of $\Delta u'_y$ as a function of time for two different values of β , and the corresponding plots of $\partial u_y / \partial y$. Notice that as expected they are all sinusoidal with a period equal to that of the acoustic field (5 μ sec). Taking the amplitudes of these plots, the following table can be obtained:

Table II

	$\beta = 45^\circ$	$\beta = 70^\circ$
$\frac{\partial u}{\partial y} \Big _{y=0}$	1.15 ± 0.17	6.0 ± 1.0
$\Delta u'_y$	7.0 ± 0.7	39.0 ± 0.4
Resulting constant of proportionality	6.1 ± 1.2	6.5 ± 1.3

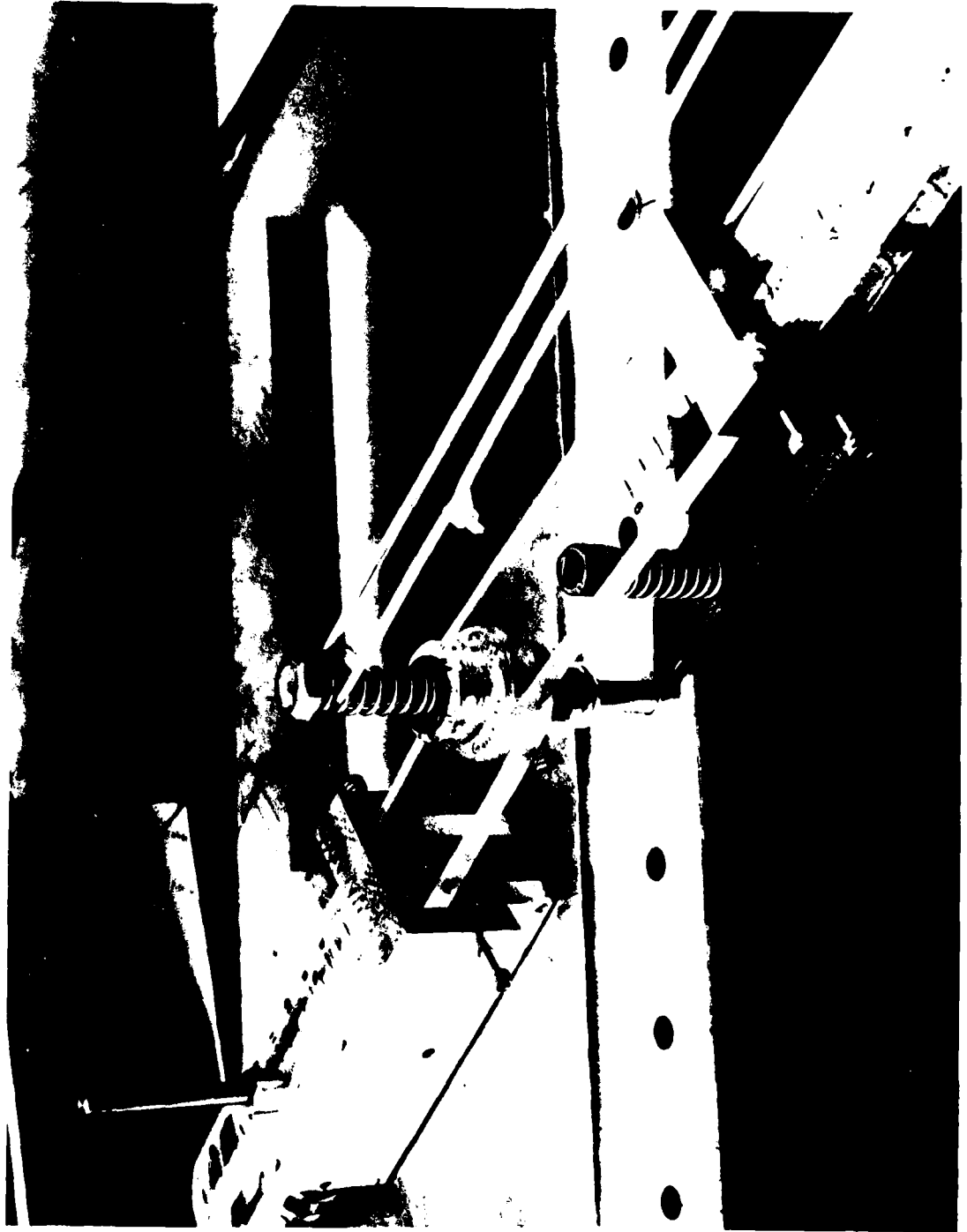


Fig. 20 Photograph of EMAT Probe in Use (See Section VII - B).

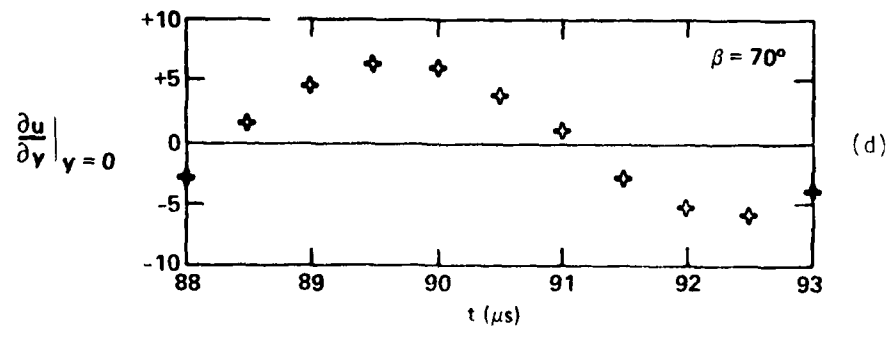
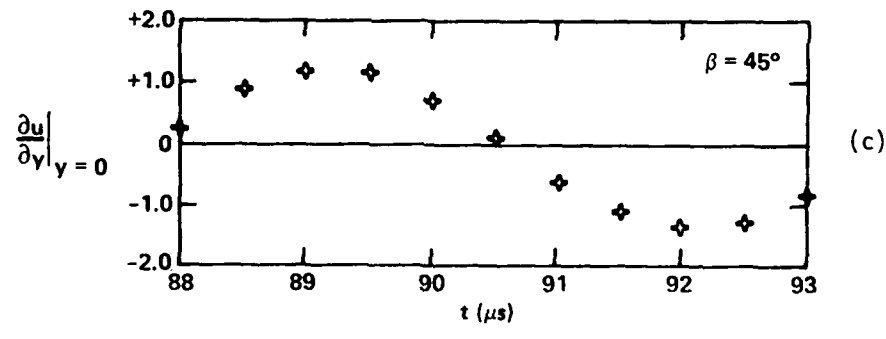
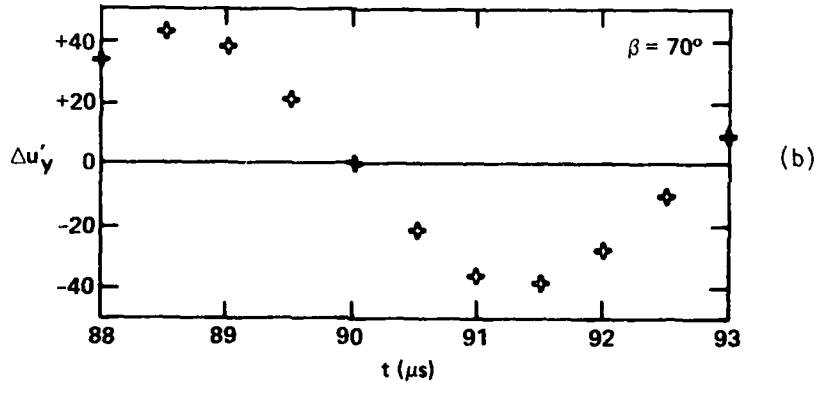
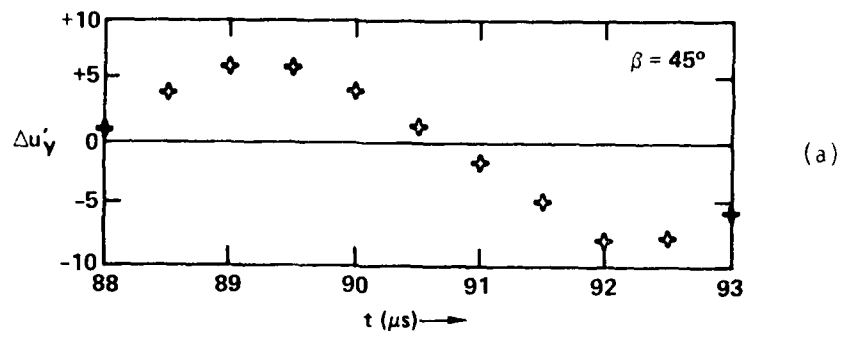


Fig. 21 Measurement of $\Delta u'_y$, and $\partial u / \partial y$ at $y = 0$, for Two Values of β .

The errors shown for $\partial u/\partial y$ and $\Delta u'_y$ are estimates of all errors involved in measuring these values. According to Eq. (10), the resulting constants of proportionality should be identical for the same crack for the two different values of β . They agree to well within the estimated measurement errors, thus confirming the analysis. Ideally, in order to maximize $\delta\Gamma$, it would be necessary to measure u' and u over a large enough range of x , y , and β to calculate the surface integral in Eq. (2). The amount of effort involved was estimated to be much larger than could be justified within the scope of this contract. Hence the approximate form presented in Eq. (6) was used as a guideline.

The practical implications for this work included an increased understanding of acoustic field behavior in the crack region, and the realization that angles of incidence different from the previously studied case of $\beta = 45^\circ$ could yield a better differentiation of the cracked hole.

Armed with this knowledge, two more configurations were employed (Fig. 5b, 5c) to yield useful results; these are reported in the following sections.

VIII. TRANSMISSION EXPERIMENTS

1. Two-Probe Measurements

Exploratory experiments were performed using the transducer configurations shown in Fig. 5b. Two facts were observed. The first was that, although particular values of α and β could be found which would detect a cracked hole in a fixed geometry, these values changed from one geometry to another in a pattern which was not predictable. The second observation was that the acoustic energy transferred through the wing lap joint in the simplest configuration, $\alpha = 180^\circ$, $\beta = 90^\circ$, was a strong function of whether the fastener was loose or tight. Fig. 22 illustrates this, using the Fourier transformed data in a time window which includes just the wing lap joint.

The data shown in Fig. 22 was obtained on the actual wing section described in Section V-A and illustrated in Fig. 11. At holes 23 (a loose fastener) and 4 (a missing fastener), less than half the acoustic energy was transmitted across the lap joint and the interference notch at 0.21 MHz for the tight fastener holes is not present. Hole 5, directly next to hole 4, also seems to be somewhat affected. Notice that the effect of a loose fastener in this configuration was much larger than the effect of any notch or slot (holes 11, 16, 19) and was not as strongly influenced by the geometrical variations in this sample (recall Fig. 11). This technique was used on the mockup wing section (see Section V-B) where some fasteners were also loosened with equally good results. Thus it appears that the transducer configuration

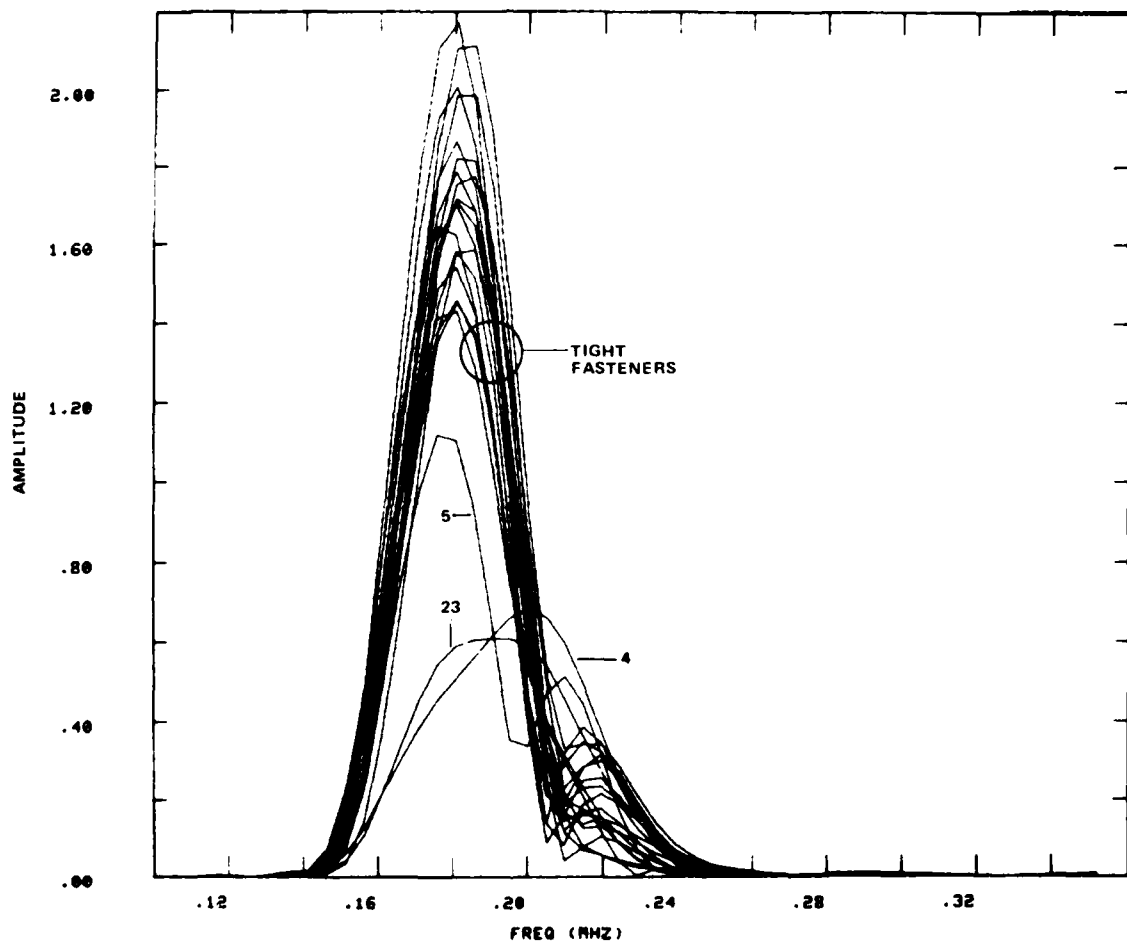


Fig. 22 Actual Wing Section, Holes 4 through 25. Amplitude versus Frequency for Transducer Configuration 5b (Fig. 5b).

of Fig. 5b, simple transmission, would be likely to yield a capability for discovering loose fasteners in a large variety of wing lap geometries. Since for a loose fastener the amount of acoustic energy transmitted is strongly damped and the interference notch is eliminated, the signature for a loose fastener should be correspondingly easy to recognize.

2. Three-Probe Measurements

A second set of exploratory experiments employed the transducer configuration shown in Fig. 5c. This was motivated by the need to find a configuration which would be less sensitive to the geometry of the wing lap joint than those previously studied. Motivated partly by the analysis of the previous section, the signal from one of the two receiver transducers was subtracted from the other and the frequency spectrum of the result found.

It might initially be thought that this difference would vanish for a crack normal to the plate edge by symmetry. However, close examination shows that for shear waves, the two receiver positions are not equivalent since the transducer polarization defines a preferred direction. Moreover, it can be intuitively argued that the degree of this difference is a measure of crack size.

In order to obtain a reproducible spectrum, extreme care was necessary in the alignment of the receiver signals. This is because the difference signal is generally quite small, and it is sensitive to any errors in transducer positioning as well as to the presence of a crack. In general,

features in frequency space would not repeat from one data collection to another unless the signal alignment was better than 0.05 μ s (1% of the period). This tolerance was met using a simple loop feature of ISP to replot the signals from each transducer until the correct mechanical location was secured. Fig. 23a exhibits the results for the 0.100 in (0.254 cm) fatigue crack. The cracked hole is #9 and displays a significantly different signature from the other non-cracked holes.

The signature appears as a significantly depressed spectrum, as if constructive interference is occurring over the whole frequency range as well as at 200 kHz. Fig. 23b displays four more uncracked holes, as well as the hole with the 0.030 inch (0.076 cm) fatigue crack. The two holes with cracks are the only ones in Fig. 23 with spectra which are depressed at 200 KHz. Figs. 24a through 24d show the results of this same technique when applied to the actual wing section described in Section V-A. There, the hole with a 0.100" EDM notch is depressed near 200 KHz. Using an amplitude criterion to provide the basis for an accept/reject decision for these three samples, the following results can be obtained. First, require the amplitude at 200 KHz to be greater than 0.02 millivolts in order for the hole to be accepted (Criterion #1). This yields 0 false rejects out of 8 possibles and 0 false accepts out of 2 possibles for the two fatigued samples (Fig. 23). For the actual wing section (Fig. 24), it yields 0 false rejects out of 22 possible and 2 false accepts (hole 16 with a 0.030" EDM notch and hole 19 with a 0.100" saw slot) out of 3 possibles. A more stringent criterion (Criterion #2) requiring that the amplitude between 200 KHz and 220 KHz be greater than

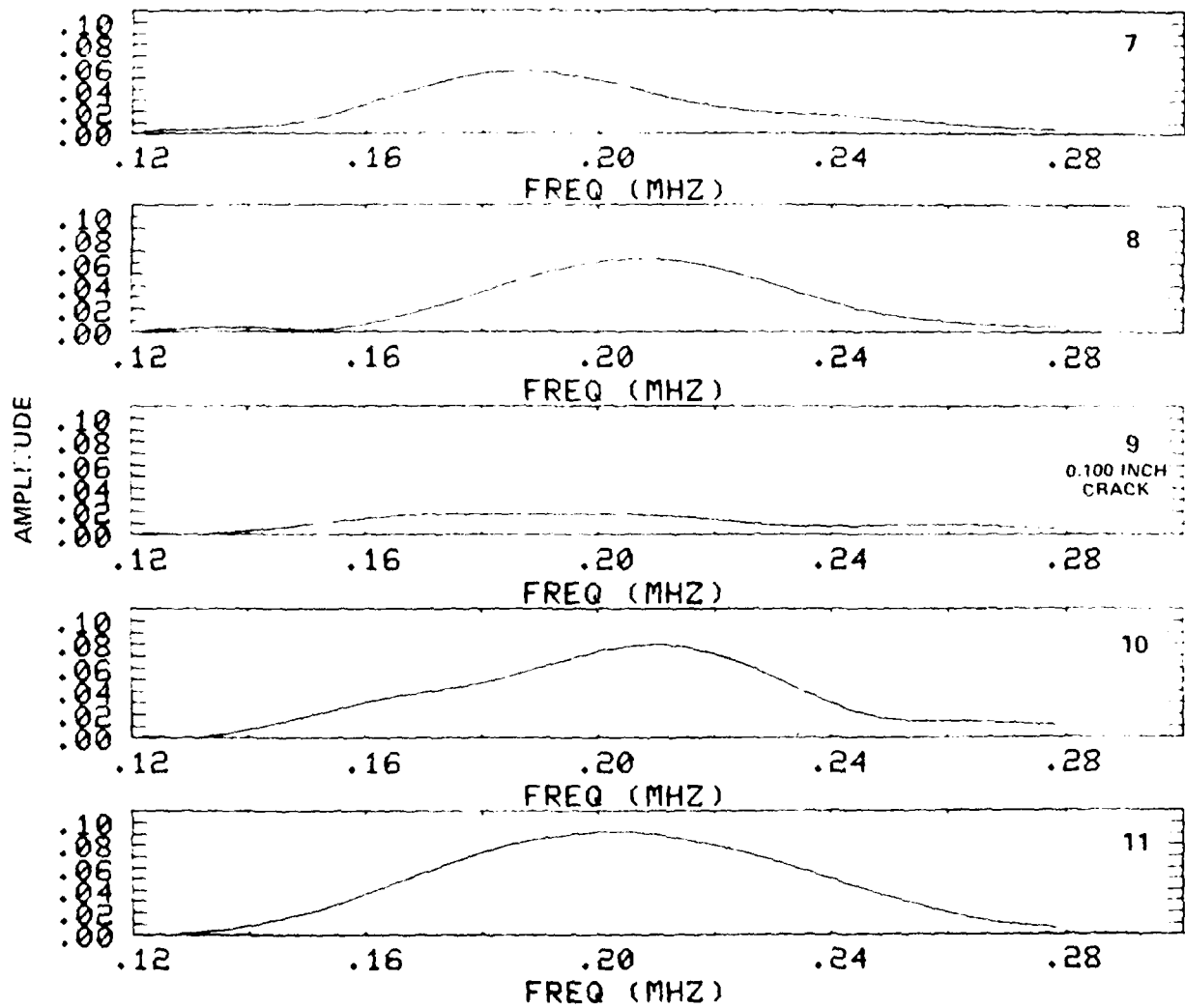


Fig. 23 Fatigued Samples, Holes 7 through 11. Amplitude versus Frequency for Transducer Configuration 5c (Fig. 5c).
 (a) 0.100 in. Crack Sample.

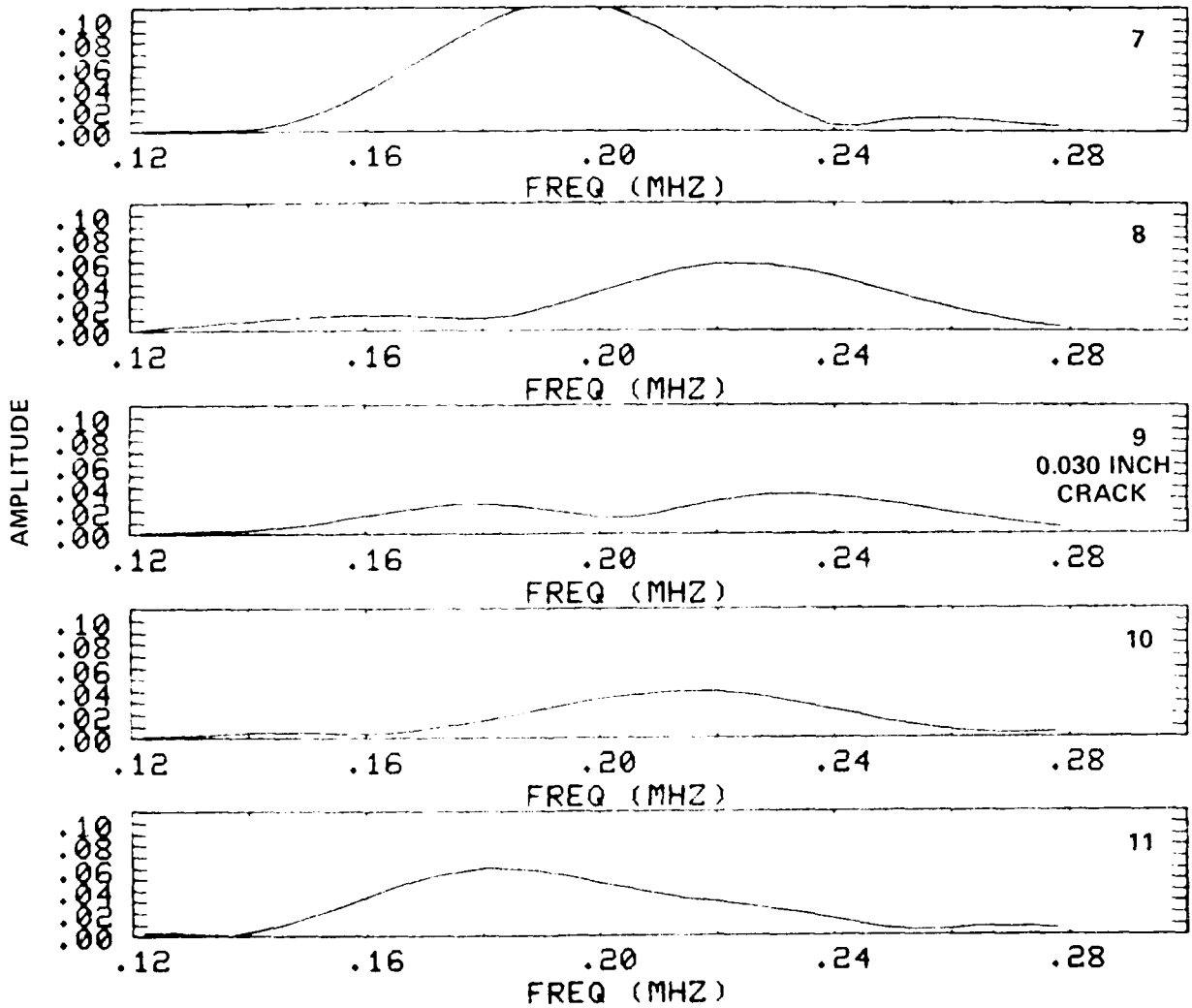


Fig. 23 Fatigued Samples, Holes 7 through 11. Amplitude versus Frequency for Transducer Configuration 5c (Fig. 5c).
 (b) 0.030 in. Crack Sample.

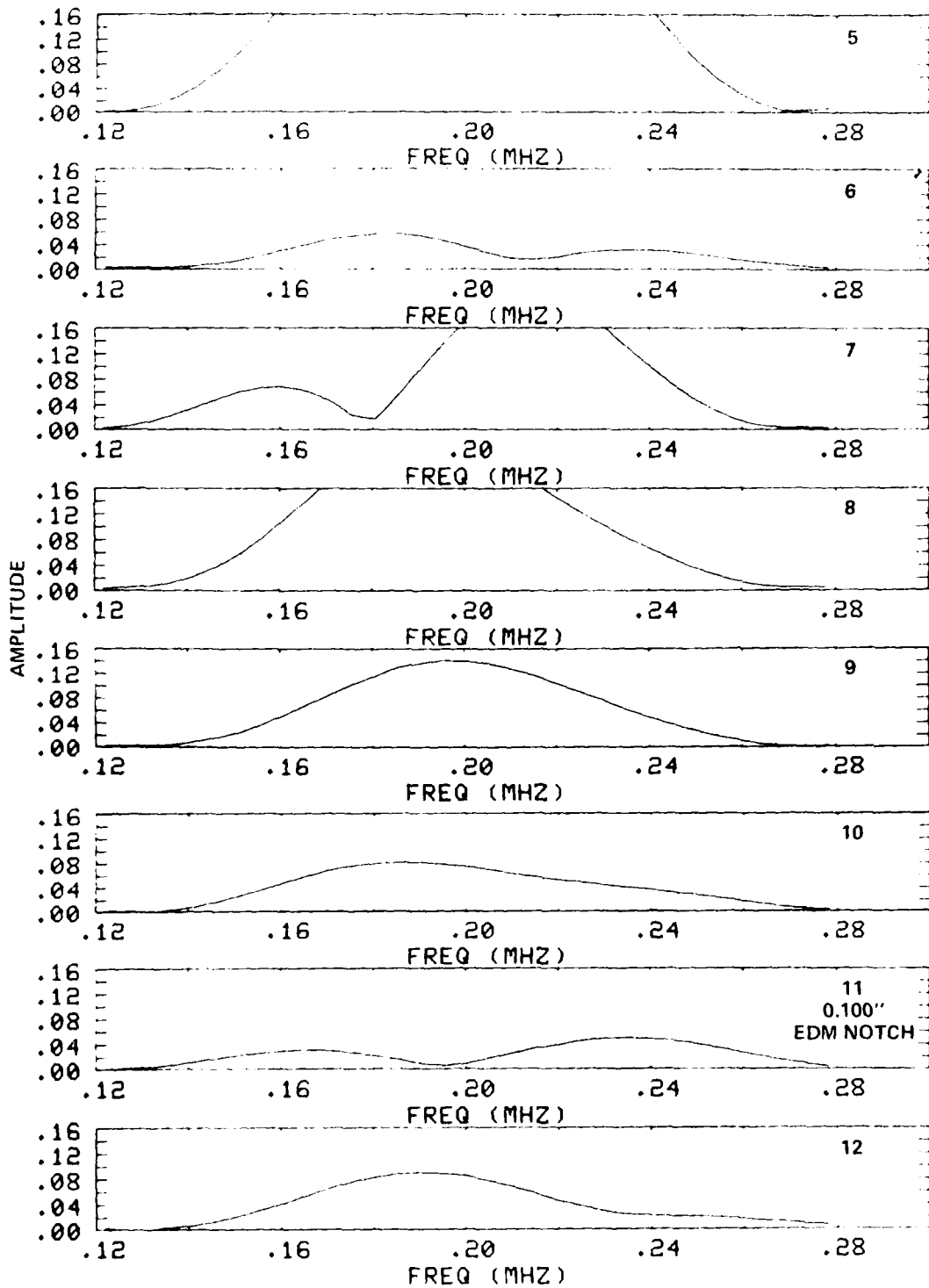


Fig. 24 Actual Wing Section, Holes 5 through 29. Amplitude versus Frequency for Transducer Configuration 5c (Fig. 5c).
 (a) Holes 5 through 12.

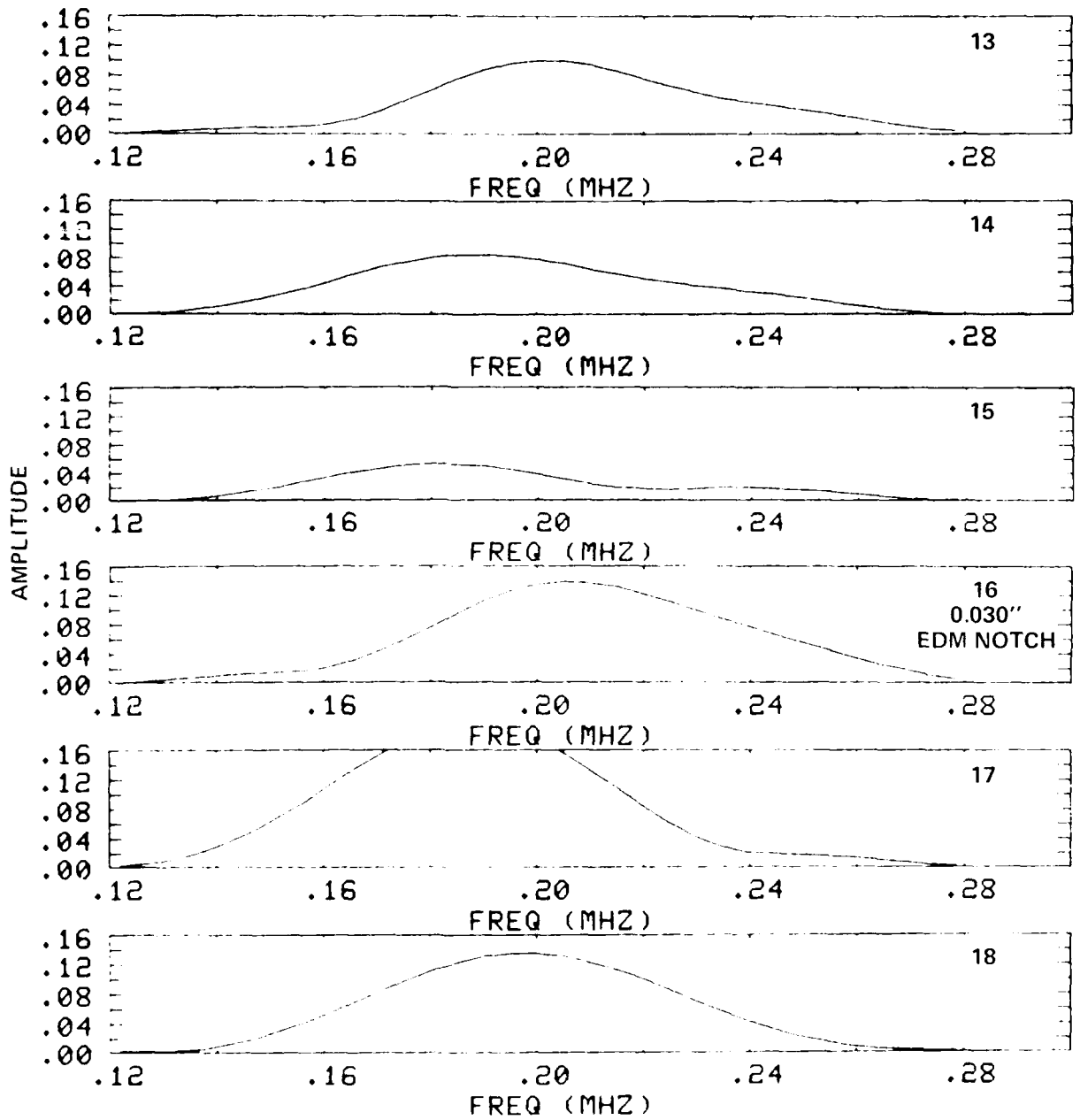


Fig. 24 Actual Wing Section, Holes 5 through 29. Amplitude versus Frequency for Transducer Configuration 5c (Fig. 5c).
 (b) Holes 13 through 18.

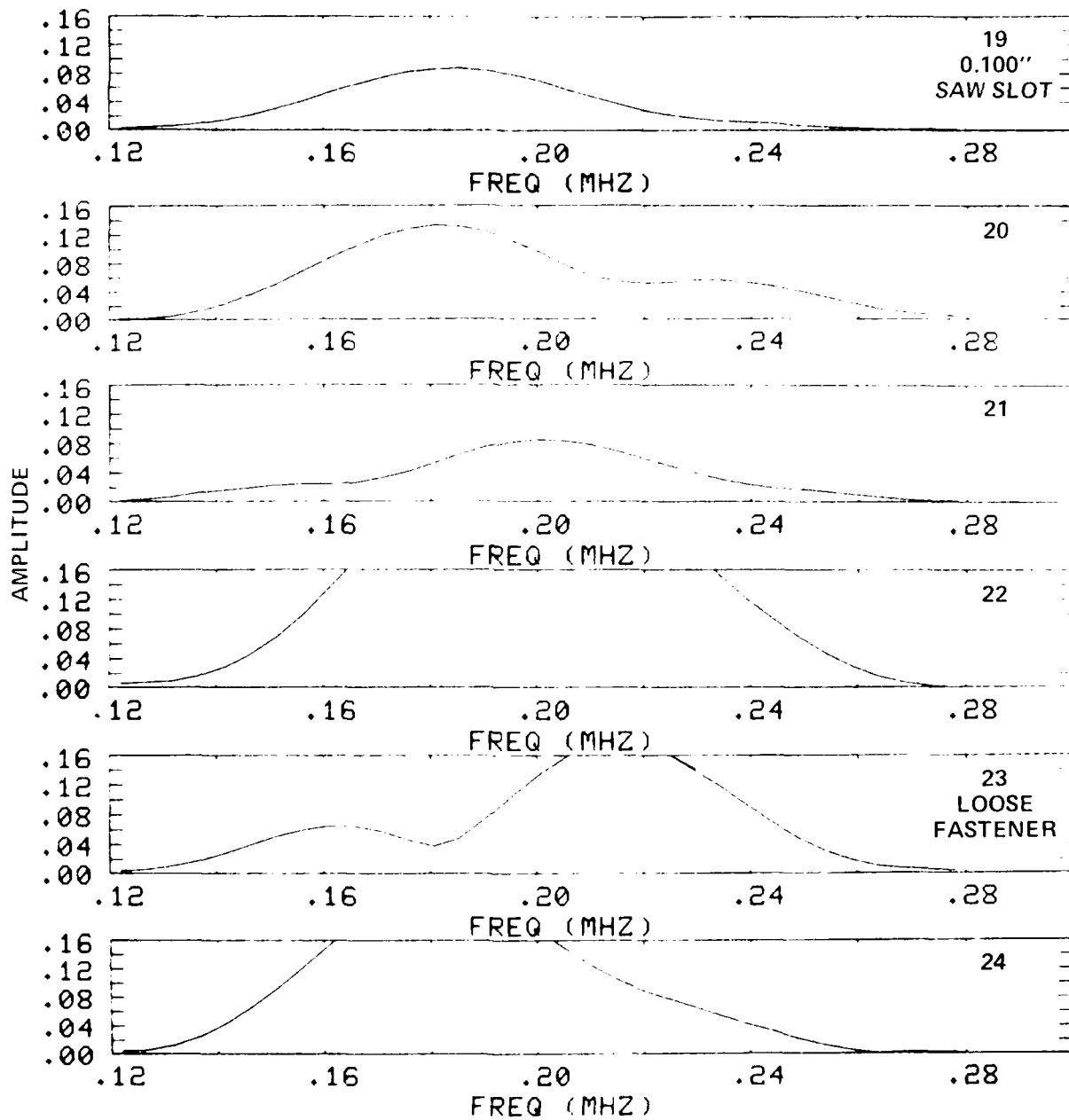


Fig. 24 Actual Wing Section, Holes 5 through 29. Amplitude versus Frequency for Transducer Configuration 5c (Fig. 5c).
 (c) Holes 19 through 24.

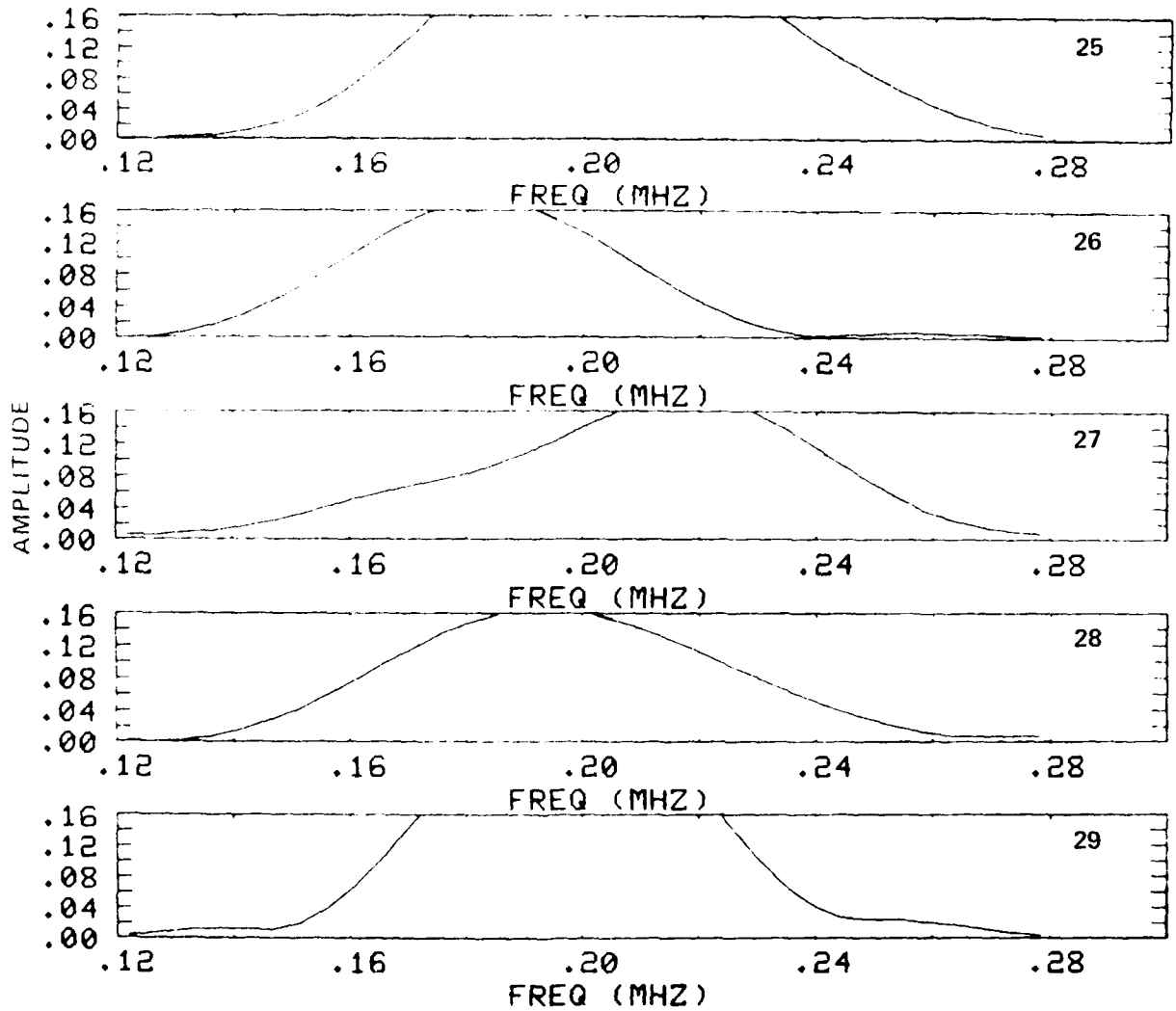


Fig. 24 Actual Wing Section, Holes 5 through 29. Amplitude versus Frequency for Transducer Configuration 5c (Fig. 5c).
 (d) Holes 25 through 29.

0.04 mv, gives fewer false accepts, but more false rejects. Applying this criterion to the fatigued samples there are 3 false rejects out of 8 possibles and 0 false accepts out of 2 possible. Applying the same criterion to the actual wing sample, there are 2 false rejects (#6, #15) out of 22 possibles and 1 false accept (#16) out of 3 possible. Of course, if the criterion were to be varied as a function of geometry, better results would be obtained. The point to remember here is that the same criterion applied with the same transducer configuration gave mostly correct results regardless of the geometrical variation of the sample.

Finally, transducer configuration 5c was tried on the aluminum mockup with the saw slots (Section V-B). It was discovered that the technique would not work on this sample due to the fact that the fraction of transmitted acoustic energy was three times smaller than in the other samples. The resulting signal to noise ratio was too small and the noise destroyed the capability of this configuration to find the saw slots. The short length of time left in the contract did not permit any investigation of the reasons for the loss of transmission in this sample. Therefore the efficacy of this method and this transducer configuration must be left as an open question. It is possible that each geometry has its own particular signature for non-cracked holes and that that signature would have to be established before cracked holes could be identified. Nevertheless, the success that this configuration exhibited with the range of geometrical variation in the first three samples is striking, and it may be the most likely starting point for future investigations.

A final comment is that the configuration 5c is probably sensitive to the quality of the seal at the fastener hole being interrogated. This should be kept in mind when assessing the usefulness of this configuration.

IX. REFLECTION EXPERIMENTS, VARIABLE β

The analysis in Section VIII prompted another set of exploratory experiments, using the configuration of Fig. 5a but varying β , keeping α fixed at 90° . The very encouraging result for the 0.100 in (0.254 cm) fatigue crack was that, at $\beta = 50^\circ$, a difference even in the time waveforms could be observed. Fig. 25a shows signals from five different fastener locations for this sample. The plots are over a very narrow time window, centered on a value corresponding roughly to the center of the fastener hole. The cracked hole (#9) is marked with dashes and it stands out nicely from the rest. Fig. 25b shows the Fourier transforms of these signals over a 40 μ s window centered at 75 μ s. Hole 9 does not have as deep an interference notch as the other four fastener locations.

A straight-forward, and fieldable, method of quantifying this effect is to average the frequency spectra from the uncracked holes in that sample and divide by this average. This operation was performed on data from both specimens with fatigue cracks. Fig. 26 shows the results for the specimen with a 0.100 in (0.254 cm) crack and Fig. 27 shows the results for the 0.030 in (0.076 cm) crack. Holes 7, 8, 10, and 11 in each sample are not cracked; thus the statistical sample for this geometry consists of 10 holes, 8 of which are uncracked and serve as a measure of the range of systematic variation or noise.

In each of these figures, the normalization leads to a display which would have a constant value of unity if all holes were identical. The

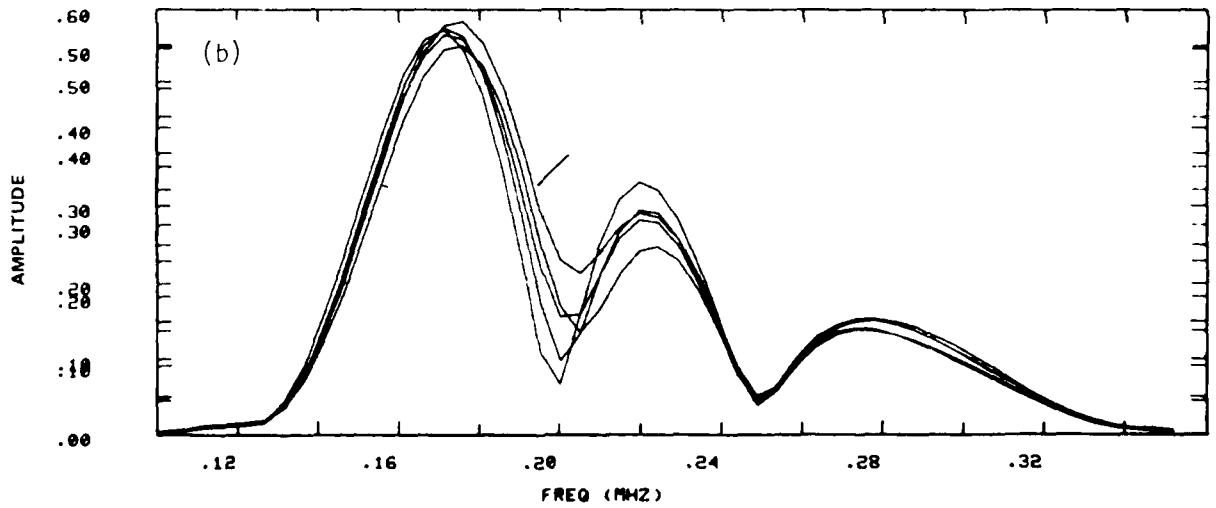
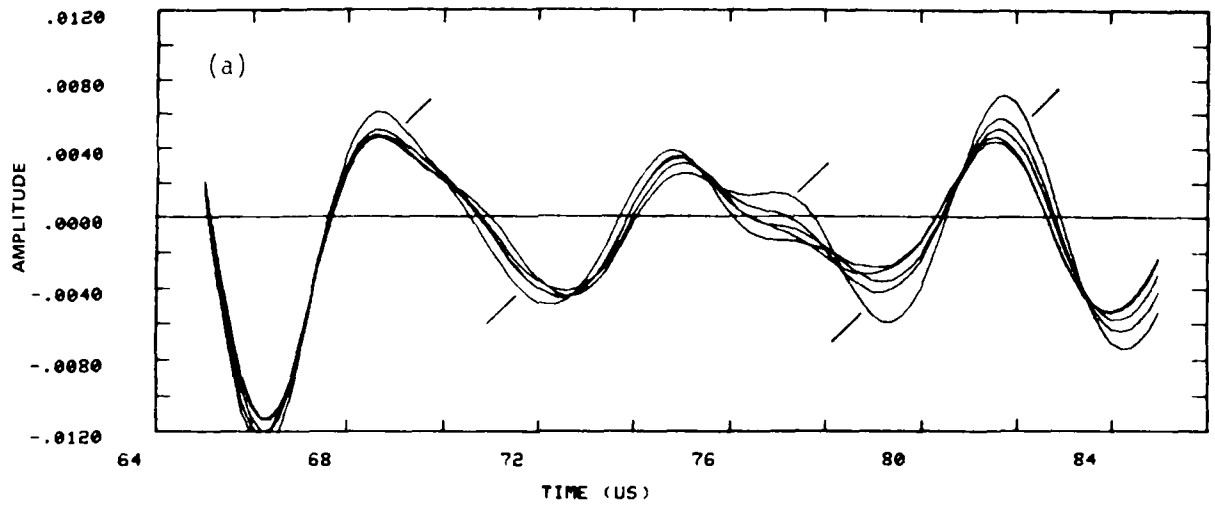


Fig. 25 Fatigue Sample with 0.100 in. Crack, Holes 7 through 11, Transducer Configuration 5b, $\beta = 50^\circ$. (a) Amplitude versus Time; (b) Amplitude versus Frequency for 55 to 95 μ s Time Window.

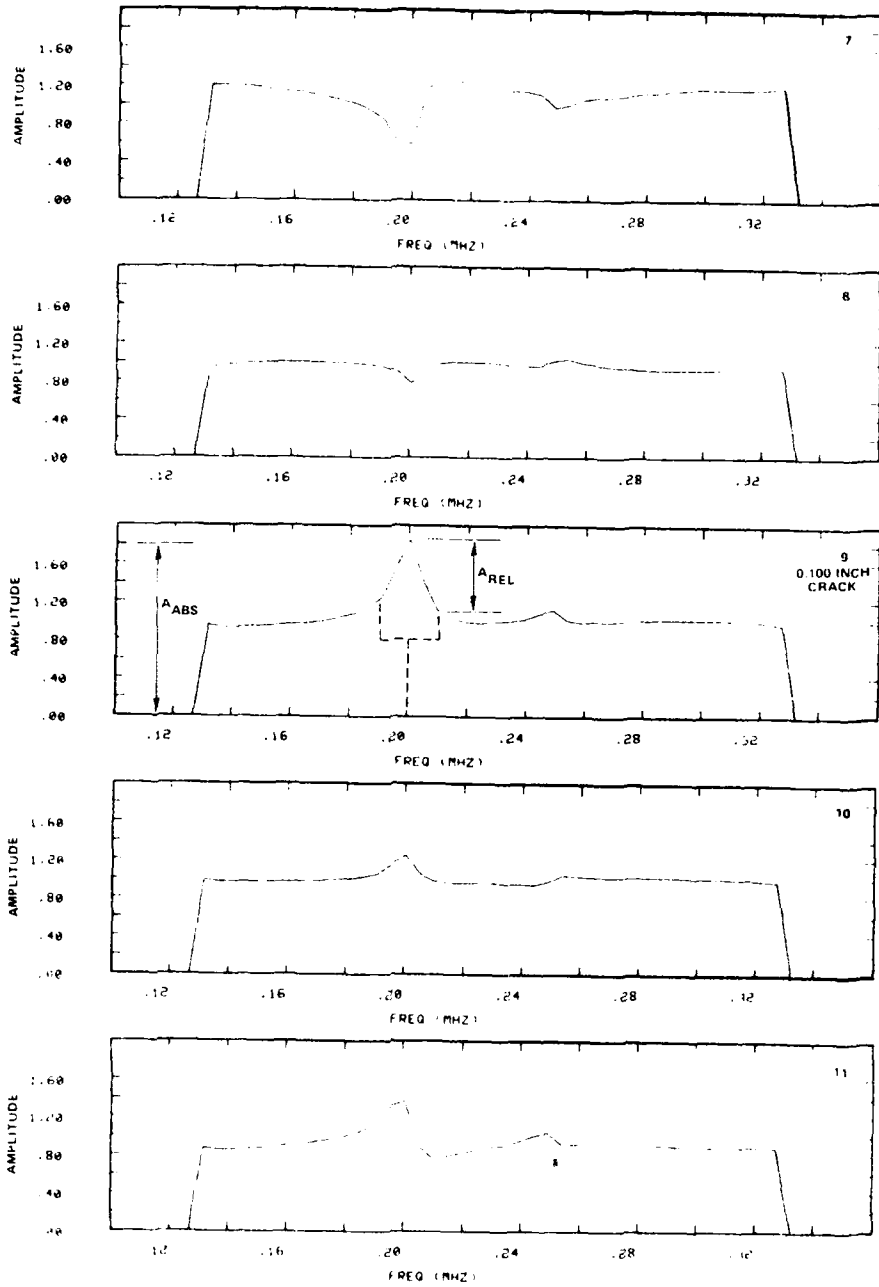


Fig. 2F Fatigued Sample with 0.100 in. Crack, Holes 7 through 11, Transducer Configuration 5b, $\beta = 50^\circ$. Divided Amplitude versus Frequency.

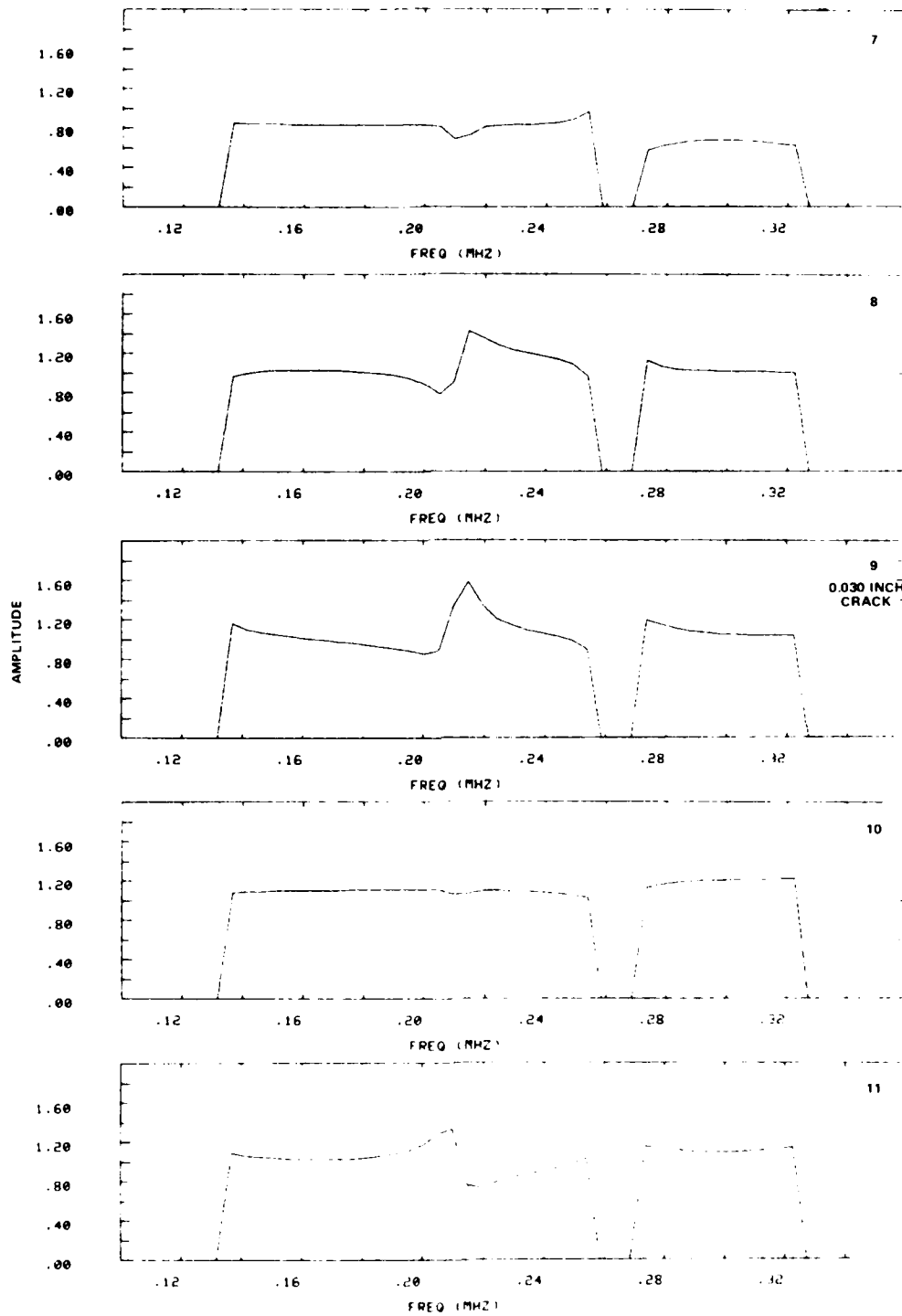


Fig. 27 Fatigued Sample with 0.030 in. Crack Holes 7 through 11, Transducer Configuration 5b, $\beta = 50^\circ$. Divided Amplitude versus Frequency.

destruction of a null, such as was shown in Fig. 25, is indicated by a peak in the normalized plot for that hole. For the 0.100 in. fatigue crack sample data shown in Fig. 26, such a large peak occurs at hole #9, which was in fact the cracked hole. Lesser peaks occur in the plots for holes #10 and #11. These presumably are a result of a lack of reproducibility in the sample preparation and/or measurement technique. To a degree, they can be differentiated from true signals by shape criteria, e.g., note the skewing of the peak for hole #11. Beyond this, they represent the sensitivity limit of the system.

Similar results for a 0.030 inch hole are shown in Fig. 27. There again, the cracked hole #9 is indicated by a peak occurring at about 0.2 MHz. The peak is of course smaller in magnitude now, somewhat asymmetric, and is comparable in peak value to the structure in holes #8 and #11. Again, it appears that it could be distinguished by the size and shape of the peak.

It will also be noted that all of the plots vanish at around 0.26 MHz. This is an artifact of the measurement resulting from an automatic zeroing of the ratio when the denominator falls below a minimum level and should be ignored.

Note also that, since most of the energy is reflected, this method should be less sensitive to variations in sealant properties or fastener tightness than the transmission method. Variations in these parameters produce large fluctuations in the relatively small amount of transmitted signal, but produce only small changes in the reflected energy.

These results clearly show that fatigue cracks can be detected by the EMAT technique. The signal from the 0.100 in. hole is well above the noise level set by variations in nominally identical holes and/or measurement error. The signal from the 0.030 in. hole is comparable to the noise but may be enhanced by signal processing based on the shape of the signal peak. It is next necessary to establish how such a procedure is sensitive to systematic variations in the sample geometry.

Fig. 28 shows the results for the aluminum mockup (which is only slightly different in geometry), where again each spectrum has been divided by the average of the spectra for the unslotted holes, #7, 9, 10, 12, 13, and 14. In Fig. 28 one can recognize the 3 slotted holes, #8, #11, and #15 from the distinctive symmetric peak near 170 kHz. The amplitude of the peak also increases monotonically with the slot lengths which, after being drilled out for the tapered fasteners, were 155 mils, 220 mils, and 70 mils respectively for holes 8, 11, and 15. Note that other peaks do occur, but not with the same form shown by the slotted holes. Also it should be pointed out that the shape of the flaw peak is fatter in Fig. 28 than in Figs. 26 and 27. This may occur because the slots in the mock-up were made by a saw, and have much greater width and area than the radial fatigue cracks of the same length.

Fig. 29 shows the results of the application of this configuration ($5a$, $\alpha = 90^\circ$, $\beta = 50^\circ$) to the actual wing section shown in Fig. 11. In this situation, where the geometry is changing and generally much different from the other three samples, the spectrum for each fastener was divided by the average of the spectra of its four nearest neighbors. This was a simple way

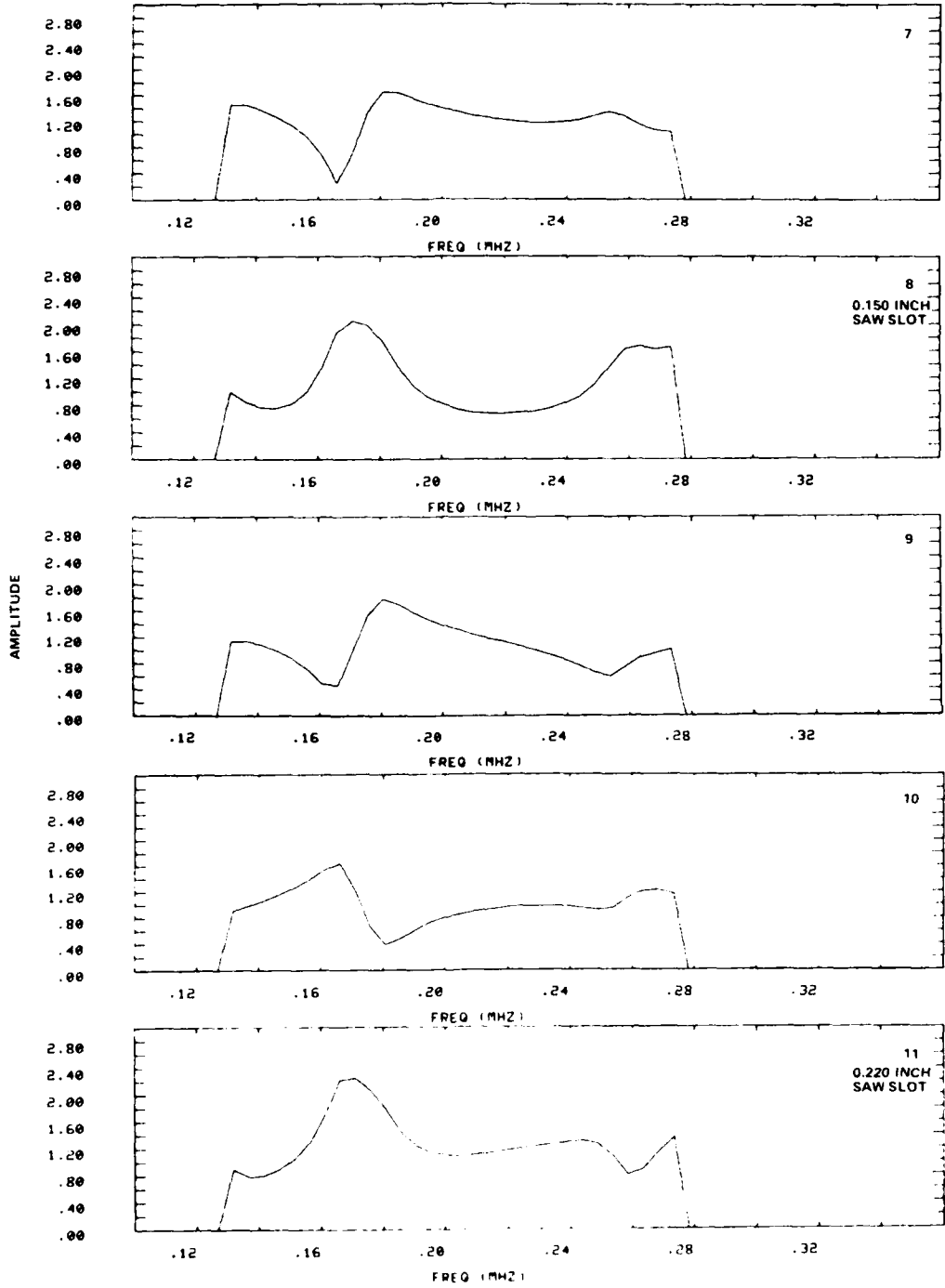


Fig. 28 Mockup Wing Section, Holes 7 through 15, Transducer Configuration 5b, $\alpha = 50^\circ$. Divided Amplitude versus Frequency. (a) Holes 7 through 11.

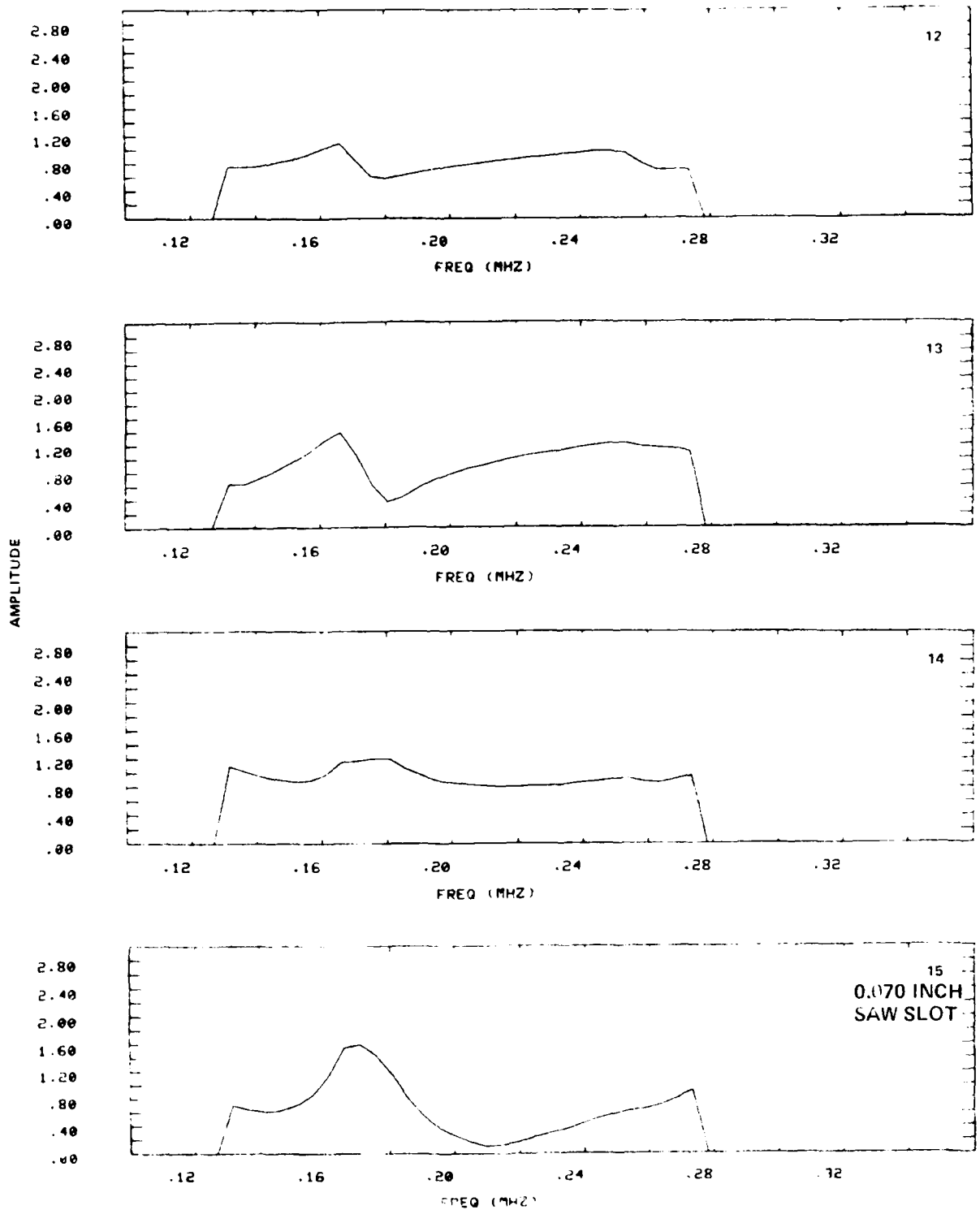


Fig. 28 Mockup Wing Section, Holes 7 through 15, Transducer Configuration 5b, $\alpha = 50^\circ$. Divided Amplitude versus Frequency. (b) Holes 12 through 15.

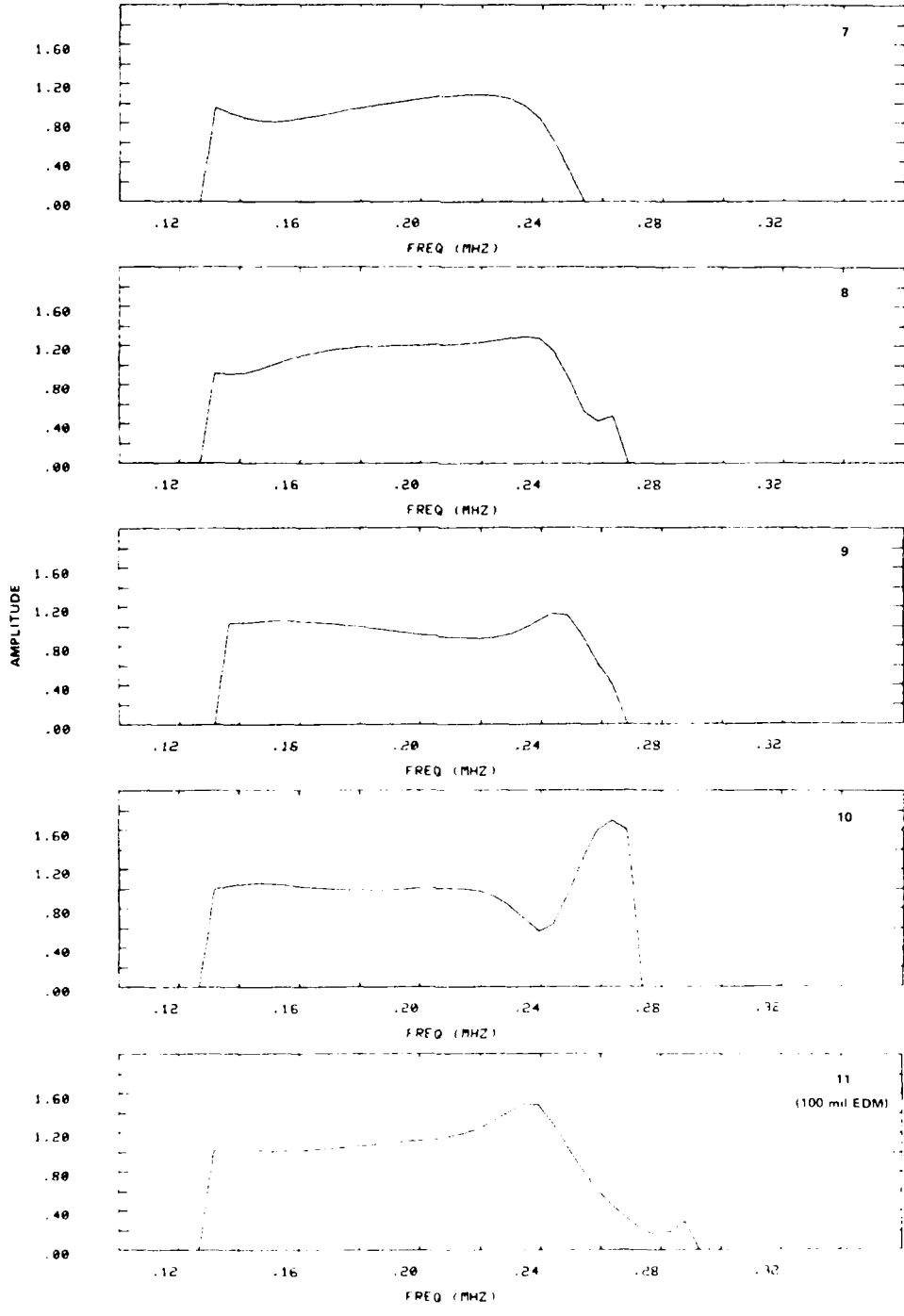


Fig. 29 Actual Wing Section, Holes 7 through 23, Transducer Configuration 5b, $\beta = 50^\circ$. Divided Amplitude versus Frequency. (a) Holes 7 through 11.

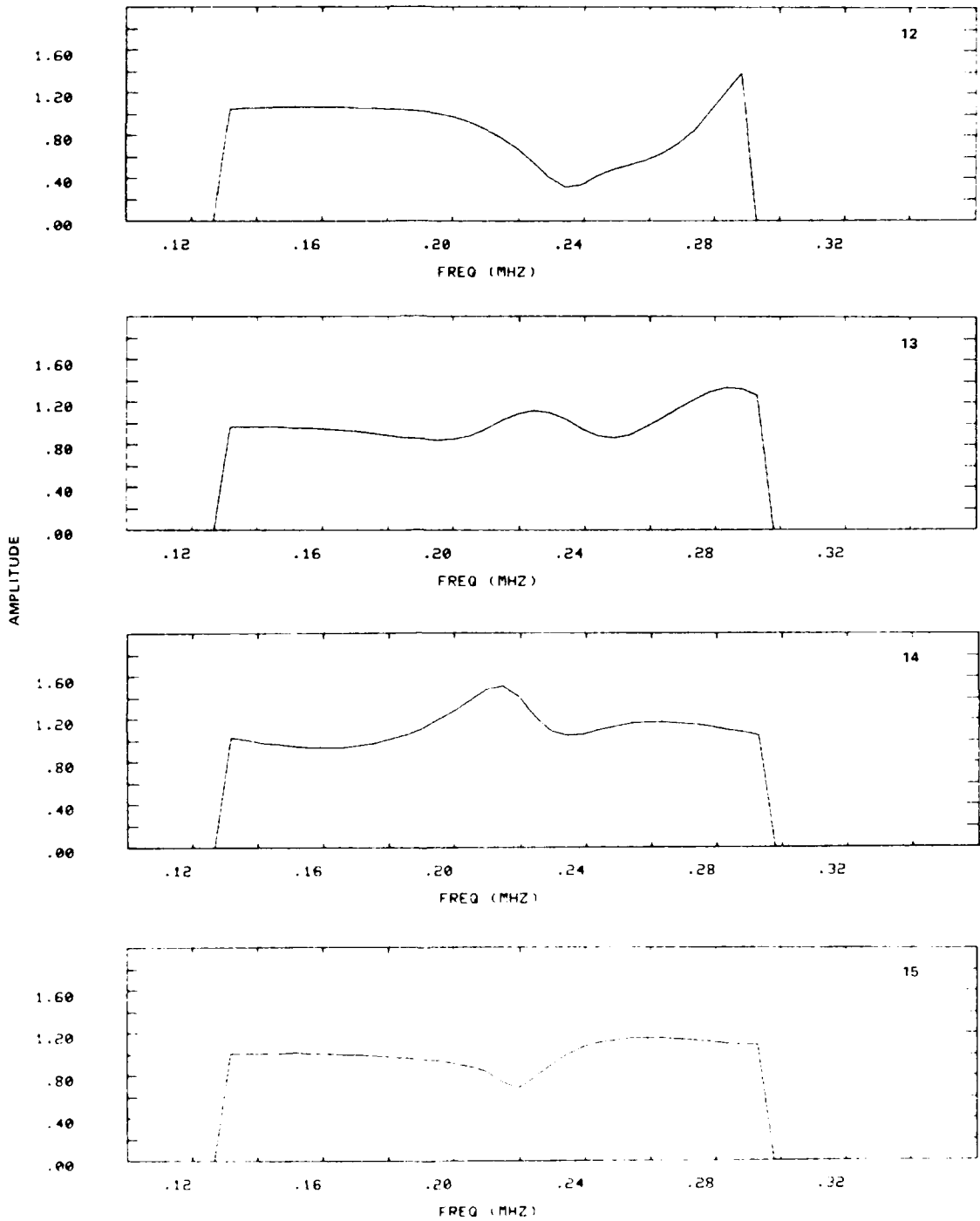


Fig. 29 Actual Wing Section, Holes 7 through 23, Transducer Configuration 5b, $\alpha = 50^\circ$. Divided Amplitude versus Frequency. (b) Holes 12 through 15.

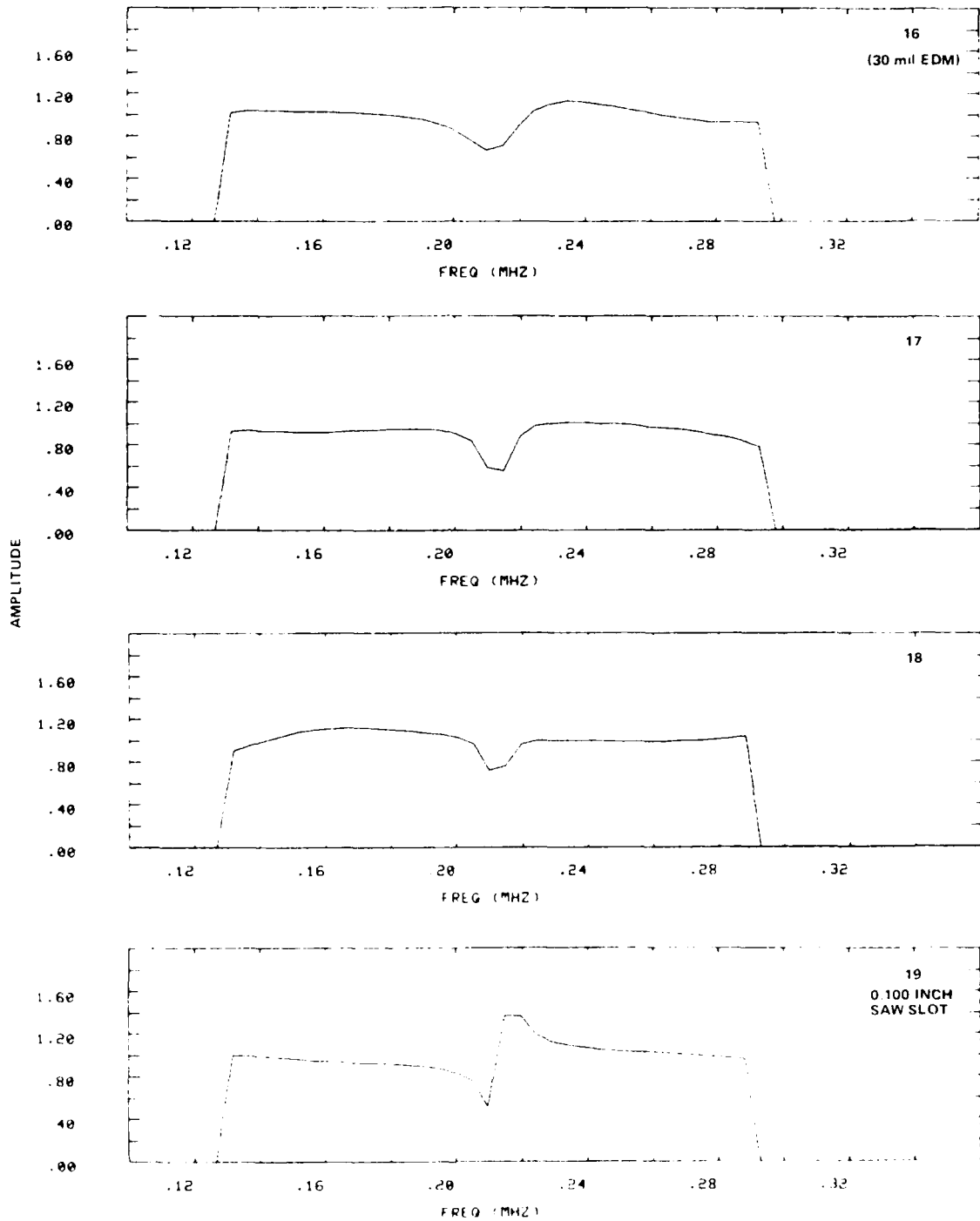


Fig. 29 Actual Wing Section, Holes 7 through 23, Transducer Configuration 5b, $\beta = 50^\circ$. Divided Amplitude versus Frequency. (c) Holes 16 through 19.

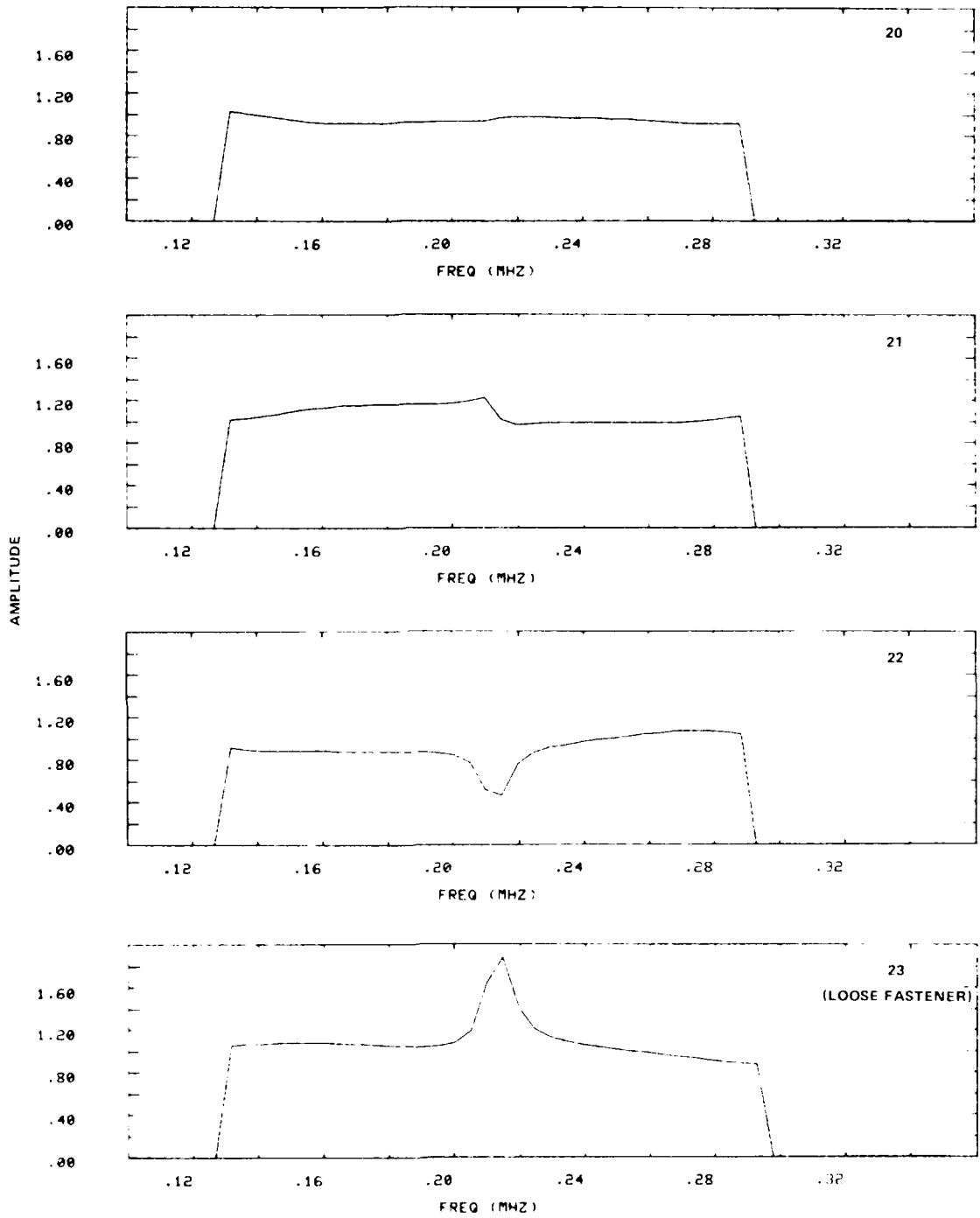


Fig. 29 Actual Wing Section, Holes 7 through 23, Transducer Configuration 5b, $\beta = 50^\circ$. Divided Amplitude versus Frequency. (d) Holes 20 through 23.

to approximate what an uncracked hole in each position should look like. As might be expected, this met with more limited success. On the positive side, most of the holes do not show a large isolated peak. Hole #11 (with a 100 mil EDM corner notch) does have a high, isolated peak similar to those of Fig. 28 even though it is located in a region of varying geometry; and hole # 23 has a sharp clean peak due to its loose fastener. Although these two look similar in their reflection characteristics, these can be differentiated by their transmission properties as was discussed in Section VIII. However, hole 16 (with a 30 mil EDM corner notch) does not show a peak, hole 19 (with a 100 mil saw slot) shows a sharply defined but very asymmetric and low peak, and hole 14 (with no known crack, slot, notch or fastener problem) shows a very convincing isolated peak - i.e., it would be a false reject.

This limited success is partly due to the changing geometry over the length employed; partly it may be because not all available information has been used. Only half the information available in a Fourier transformed spectrum is being shown in any of the plots of amplitude versus frequency: the phase information as a function of frequency has been ignored. Figs. 30a and b show the real and imaginary parts, separately, of the Fourier transforms of the signal for holes 18, 19, and 20 of this sample. Note that holes 18 and 20 are much more like each other than like hole #19. Similar comments apply, in Fig. 30c and 30d, to the real and imaginary parts of the Fourier transforms of holes 10 and 12 compared to hole 11. This kind of comparison could be relatively easily quantified by using a least-squares fit method in a fashion analogous to the division method used above. However, there was not sufficient time to implement and test it in this effort.

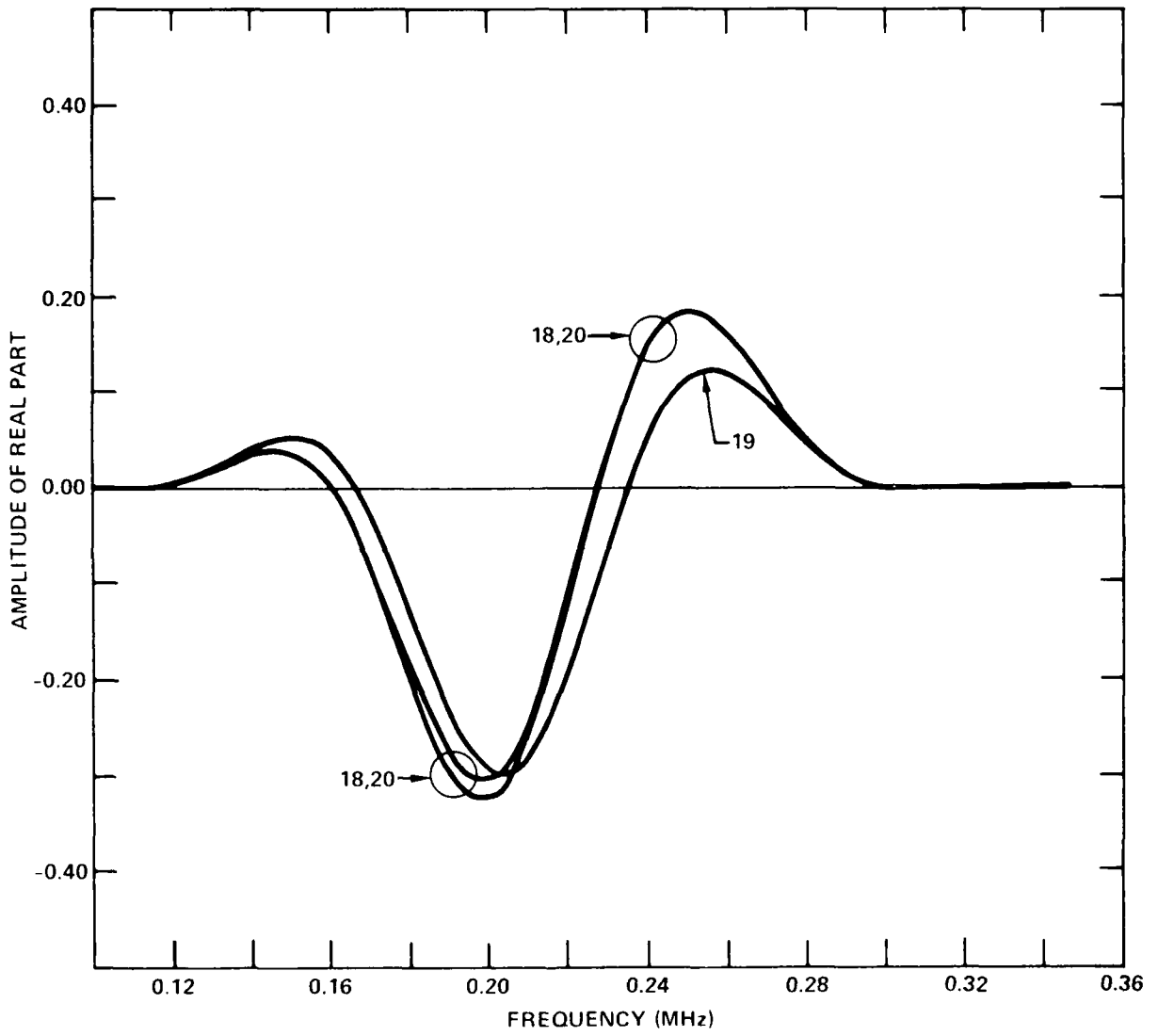


Fig. 30 Actual Wing Section, Holes 10, 11, 12, 18, 19, 20, Transducer Configuration 5b, $\alpha = 50^\circ$. Real or Imaginary Part versus Frequency. (a) Real Part of 18, 19, 20.

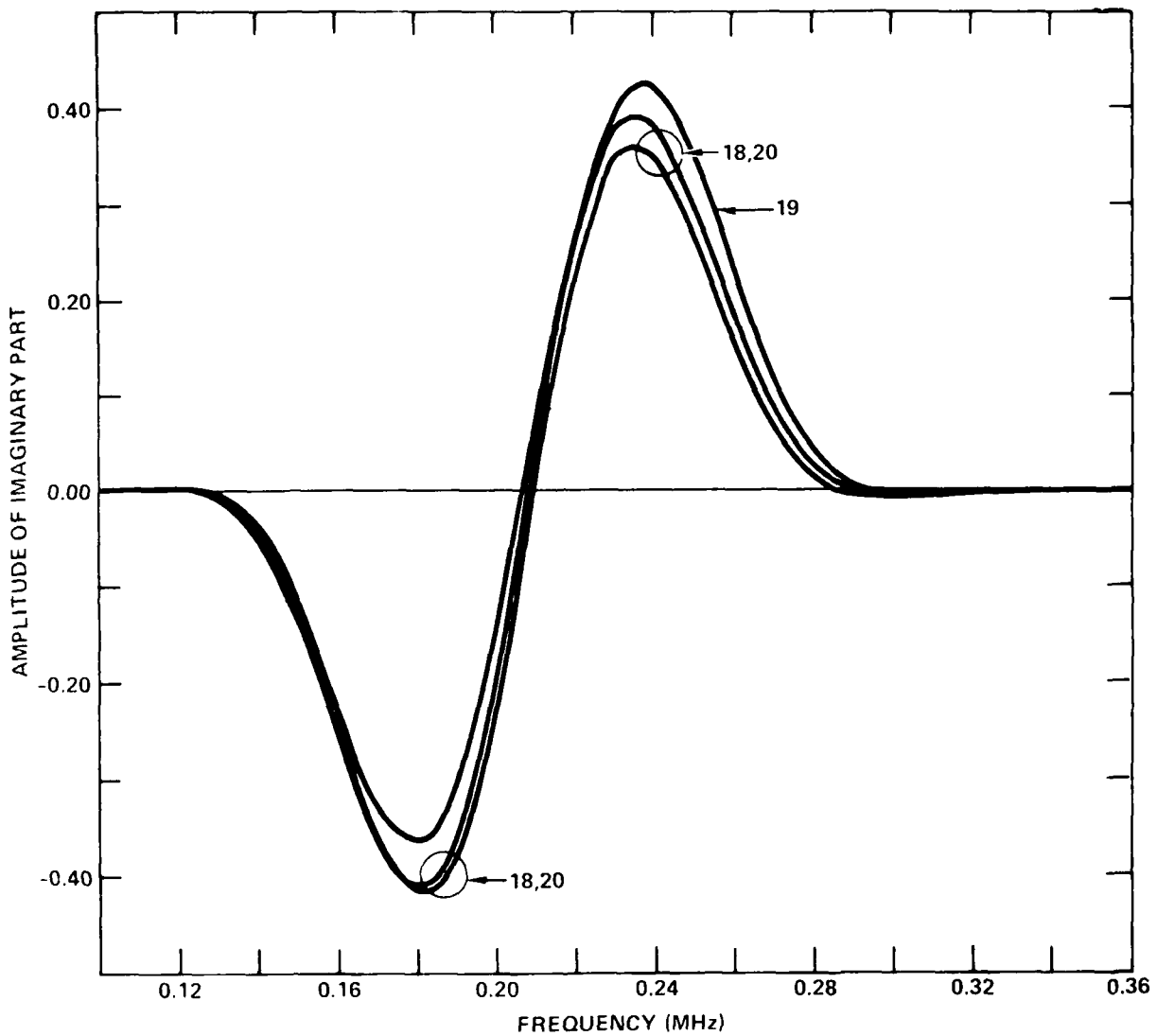


Fig. 30 Actual Wing Section, Holes 10, 11, 12, 18, 19, 20, Transducer Configuration 5b, $R = 50^\circ$. Real or Imaginary Part versus Frequency. (b) Imaginary Part of 18, 19, 20.

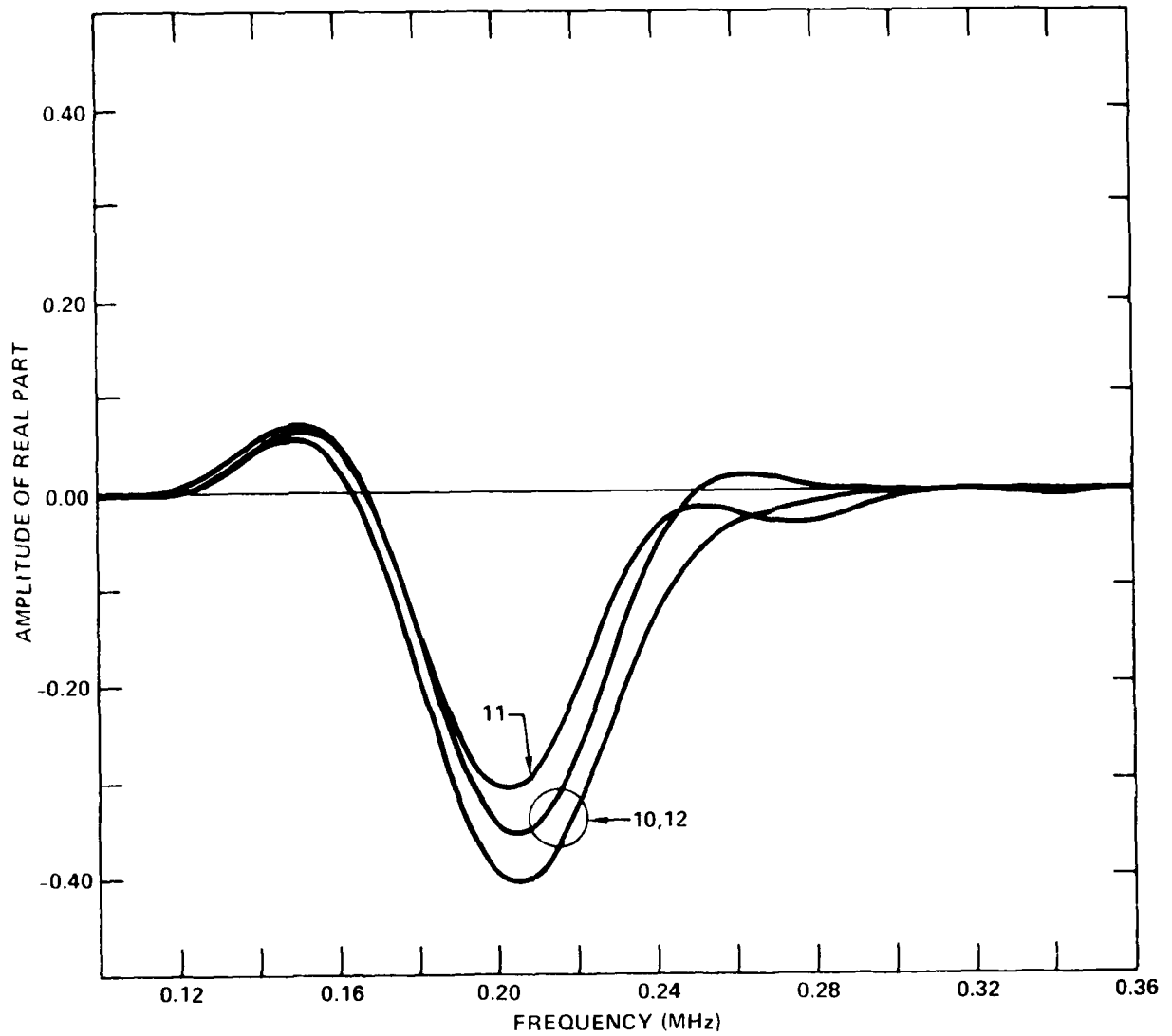


Fig. 30 Actual Wing Section, Holes 10, 11, 12, 18, 19, 20, Transducer Configuration 5b, $\beta = 50^\circ$. Real or Imaginary Part versus Frequency. (c) Real Part of 10, 11, 12.

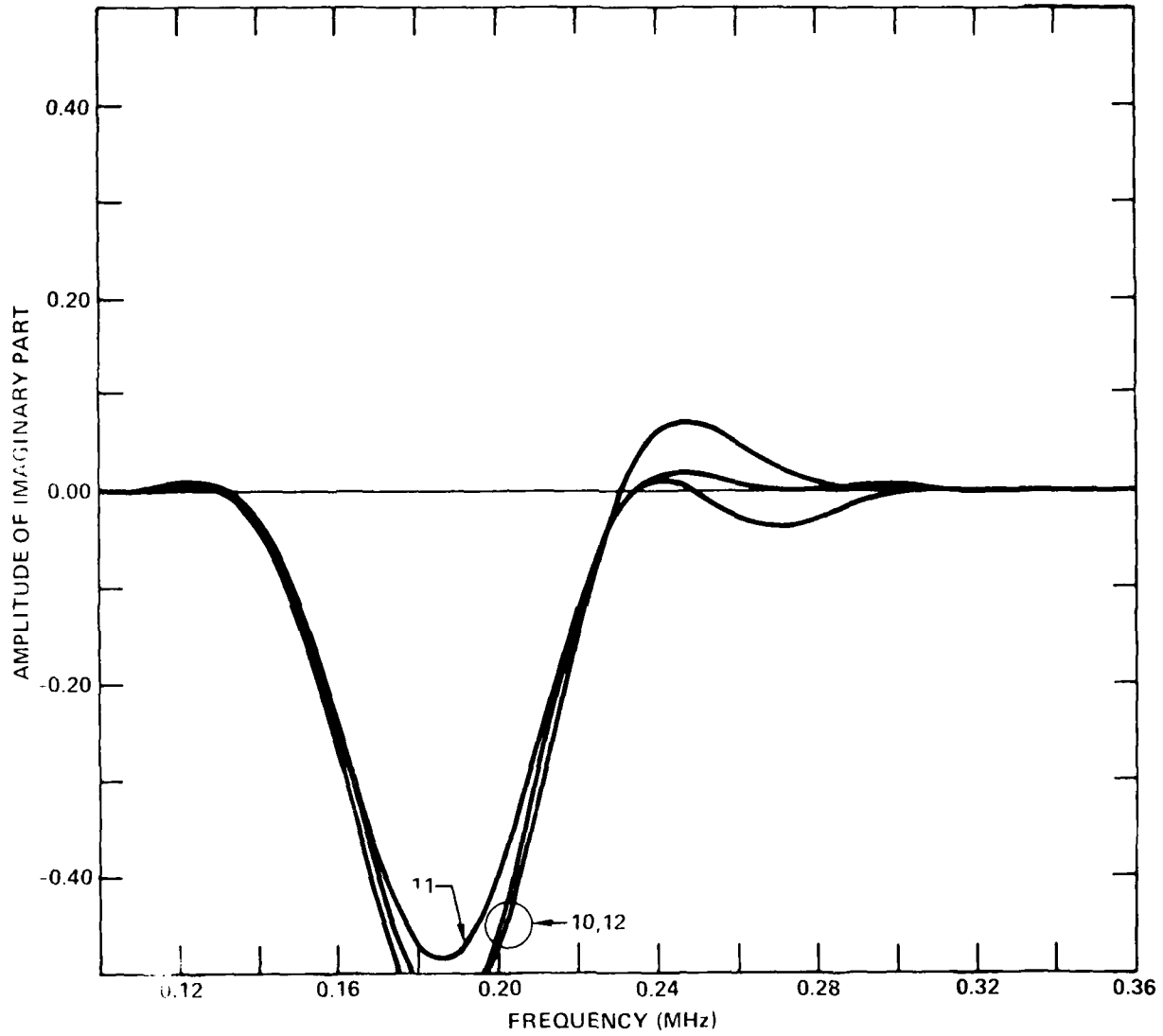
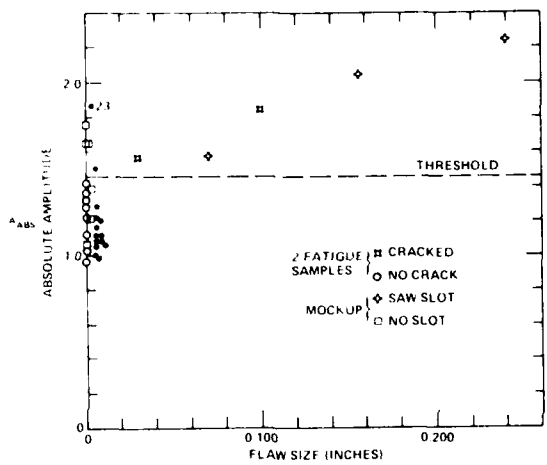


Fig. 30 Actual Wing Section, Holes 10, 11, 12, 18, 19, 20, Transducer Configuration 5b, $\beta = 50^\circ$. Real or Imaginary Part versus Frequency. (d) Imaginary Part of 10, 11, 12.

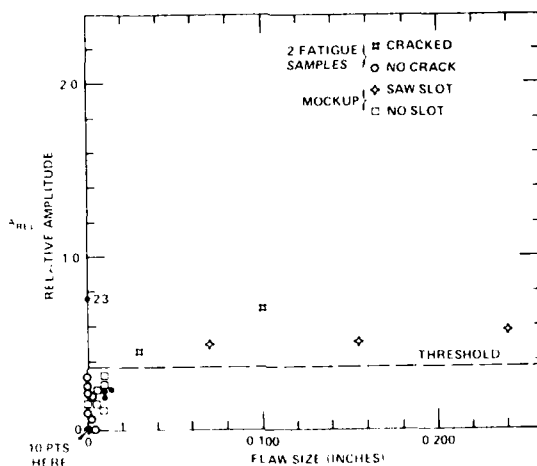
Thus, using only the amplitude information and dividing by the uncracked holes, there would be a false acceptance of the 0.030 mil corner notch and a 0.100 mil saw slot and a false rejection of one hole in addition to the correct rejection of a 0.100 in. corner EDM notch and the correct acceptance of 12 holes.

The performance of this technique on all four samples is summarized in Figs. 31a, b, and c. All points plotted within 0.02 inches (using the horizontal scale) are actually un-marred holes and belong on the vertical axis within flaw size of 0.0. Fig. 31a includes the absolute amplitudes of all holes in Figs. 26 through 29. Fig. 31b includes the absolute amplitudes of only the symmetric peaks. Note that the 0.030 inch crack, the 0.030 in. EDM notch, and the 0.100 in. saw slot in the wing section do not make it to this plot and hence would be false accepts if true flaw indications were required to be fully symmetric. Fig. 31c presents the relative amplitude of each peak in Fig. 26 through 29. This was defined as the distance from the peak down to the highest shoulder 20 kHz away from the peak.

The three plots in Fig. 31 represent the three different parameters which were used here to identify flaws. The dashed lines in each of the plots indicate where one might set thresholds for the accept/reject decision for that parameter. The plots are all in rough agreement, but there are some differences worth discussing. In the discussion below, flaws of all sizes have been lumped together in quoting statistics on the accept/reject decision. It is important to notice that the actual performance evinced in Fig. 31 is flaw-size dependent: larger flaws are definitely more accurately distinguished.



ABSOLUTE AMPLITUDE OF HIGH PEAK NEAR 200 kHz FOR ALL HOLES



RELATIVE AMPLITUDE OF PEAK NEAR 200 kHz FOR ALL HOLES

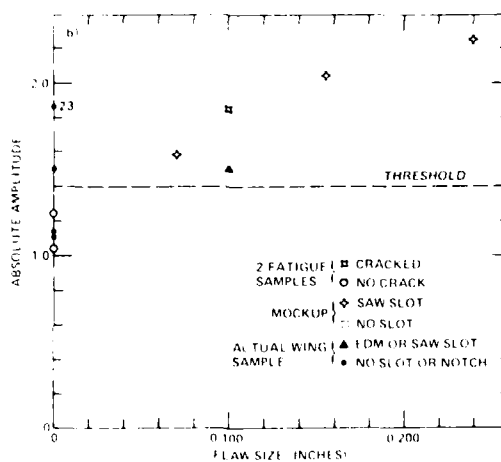


Fig. 31 Three Measurements of the Peaks in Figs. 26 through 29.
 (a) Absolute Amplitude of High Peak near 200 kHz for All Holes;
 (b) Absolute Amplitude of High Peak near 200 kHz for Symmetric Peaks Only; (c) Relative Amplitude (See Text for Definition) of Peak near 200 kHz for All Holes.

Using Fig. 31a, absolute amplitude of all peaks, the ratio of false rejects to possibles is 0/8 for the two fatigued samples, 3/6 for the mock-up, and 1/13 for the actual wing section. The ratio of false accepts to possibles is 0/2 for the fatigued samples, 0/3 for the mock-up, and 2/3 for the actual wing section for the threshold shown.

Using Fig. 31b, absolute amplitude plus requiring a flaw-associated peak to be symmetric, the ratio of false rejects to possibles is 0/8 for the fatigued samples, 0/6 for the mock-up, and 1/13 for the actual wing sample. The ratio of false accepts to possibles is 1/2 for the 2 fatigued samples, 0/3 for the mock-up, and 2/3 for the actual wing section for the threshold shown.

Using Fig. 31c, relative amplitude of all peaks, the ratio of false rejects to possibles is 0/8 for the fatigued samples, 0/6 for the mockup, and 0/13 for the actual wing sample. The ratio of false accepts to possibles is 0/2 for the fatigued samples, 0/3 for the mockup, and 3/3 for the actual wing section for the threshold shown.

Finally, it is important to notice that the statistics quoted above for the actual wing section would improve greatly if the threshold were dropped (Fig. 31a, 31c). This means the threshold for detecting cracks with this configuration is probably a function of geometry and would have to be measured.

The performance of transducer configuration 5a (Fig. 5a) is thus good for the three fixed geometry specimens, but not as good for the actual wing section with different, and varying geometry. However, remember that the Fourier

amplitude spectra can be separated out into Real and Imaginary parts. As the discussion of the plots in Fig. 30 indicates (p.33), this could yield a large improvement in the ability to identify flaws in the actual wing section. In addition, the small response from the 0.100 in. saw slot in the actual wing section (Fig. 29c) compared to the large response from a very similar flaw in the mockup (Fig. 28a) suggests that the angle β (Fig. 5a) should be a function of the geometry of the wing section.

X. ENGINEERING DRAWINGS, LAYOUTS, SKETCHES, AND SCHEMATICS

In any of the successful techniques reported above, it would be necessary in a field situation to employ a microcomputer based instrument to perform digital signal analysis and pattern recognition. For example, the procedure in Section IX above requires division of the Fourier Transform (F.T., in the rest of this discussion) of each hole by the average of the F.T.'s of its four nearest neighbors. The result must then be checked for the presence of a peak with the correct shape and magnitude. This is comparatively easy to do with a microcomputer in which data and comparison patterns can be stored, and the patterns or procedure easily changed. In an analog or even analog/digital device it would be much more difficult to allow for more than one geometry, or provide enough flexibility to modify the exact procedure or comparison patterns should extensive testing prove this advisable.

Fig. 32 shows a schematic of the hardware for a microcomputer-based instrument which we recommend to be used in the field to perform the Fourier analysis, waveform averaging and division, and graphical display tasks described in this report. A prototype of a similar version of this instrument has been built and used in another, unrelated, NDE contract performed by the Ultrasonic Applications Group here at the Science Center (6). Further design and construction of both hardware and software for this instrument is being actively carried out during FY 1980 on funds provided from Rockwell International's Independent Research and Development budget. It is to be a

DIGITAL ULTRASONIC INSTRUMENT

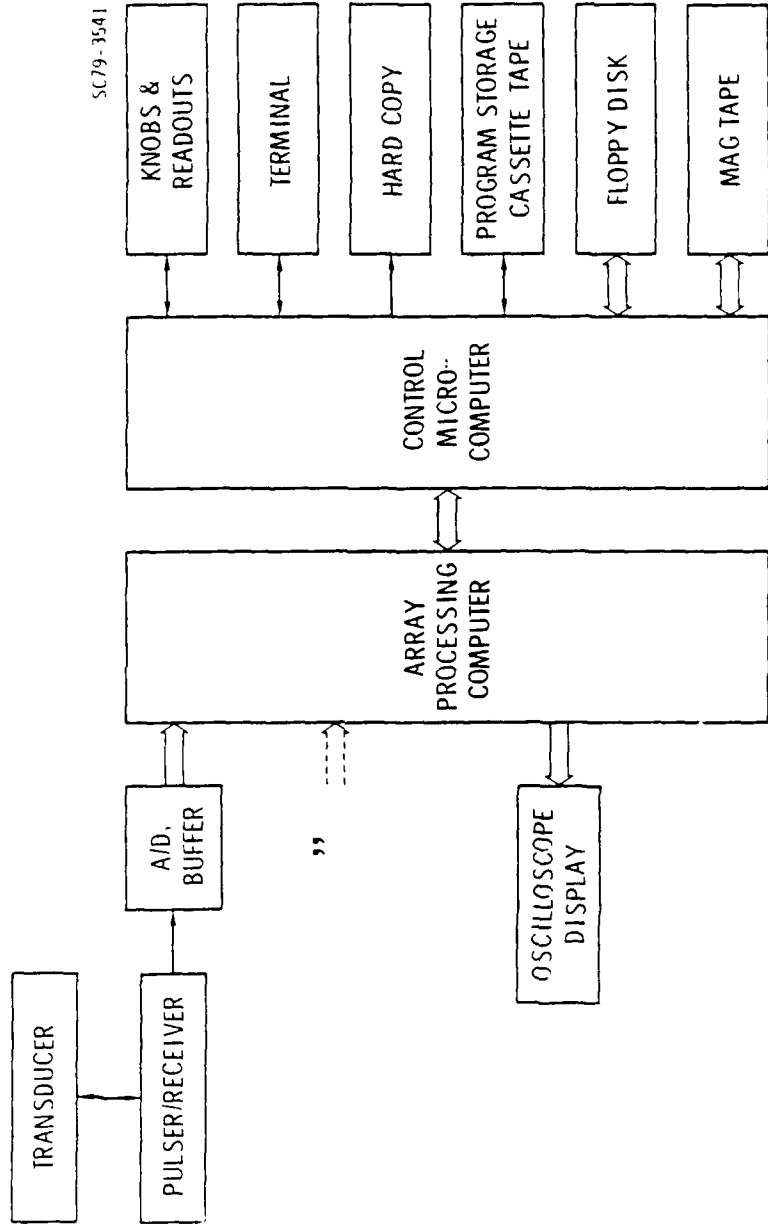


Fig. 32 Schematic of the Hardware for a Microcomputer Based Instrument Capable of Being Fielded.

general purpose, all-digital instrument for applications in the field of ultrasonic nondestructive evaluation. It will be completely programmable and modular so that portions of either software or hardware may be relatively easily updated as technology and field experience progresses.

In the schematic of Fig. 32, the ultrasonic signals are produced in the upper left-hand corner by EMAT transducers. The signals are then digitized by an analog-to-digital converter (A/D) and all subsequent processing is performed digitally. Because the waveforms contain a relatively large amount of data, the first stages of the signal processing must be performed by fast digital circuitry. The current state of the art in fast general purpose digital hardware is the array processor, which is a computer designed to perform a series of common mathematical operations on large groups of numbers as rapidly as possible. All of the signal processing will be performed within the array processor and optional display of processed waveforms on an oscilloscope will be available directly from the array processor. The array processor which is recommended based on today's technology is the Analogic AP400, which offers the best compromise of performance with size and price of any array processor on the market today.

In order that the array processor not be burdened with such "housekeeping" tasks as communicating with the operator and with peripheral devices, there will be a microcomputer for this purpose. In addition, the microcomputer will manage programs for itself and the array processor and receive the results of flaw decisions made by the array processor and route them to the operator or to a storage device. The minicomputer can have any of

a wide variety of peripheral devices attached, some of which are shown at the right of Fig. 32 for illustration. "Knobs and Readouts" refers to a set of analog controls which would allow the operator the same kind manual control that is available with a conventional ultrasonic instrument. The terminal and hard copy are for operator communication and the other three peripherals are for data and program storage.

Because of the modular nature of this design, there are many possible variations on the configuration. Alternate A/D's and peripherals have already been mentioned. For applications with modest computational needs, it is possible to leave out the array processor altogether and do the computations in the microcomputer. Furthermore, the modular construction allows one to constantly upgrade the instrument capability in step with the rapid improvements in available digital hardware.

This instrument is completely programmable. Therefore, it will be able to perform any kind of signal processing and to switch between one function and another in a fraction of a second by changing software. Thus, as improvements in flaw detection and characterization techniques are made, they can be immediately implemented in the instrument.

In compliance with the work statement for this contract (2), the following paragraphs describe a possible field test procedure based on the digital instrument described above, and the results of this report. The transducer configuration in Fig. 5c has not been employed below for two reasons. First, further work should be done to assess its reliability and

optimize the angle γ . Secondly, the field alignment of the signals from the two receiver transducers would require a more sophisticated goniometer and an additional piece of electronics designed to measure the difference in phase of the two signals.

The recommended transducer configurations appear schematically in Fig. 5. Figs. 4a and 5a show the configuration to be used in goniometer #1, designed to test for cracked holes or loose fasteners. Fig. 5b shows the configuration to be used in goniometer #2, which is designed to distinguish whether or not the hole in question has a loose fastener. Each goniometer has two EMAT transducers. Two cables from each goniometer are connected to the instrument shown schematically in Fig. 32. This instrument would fit into a rolling electronics rack (standard width) six feet high or smaller, depending on the amount of flexibility desired. A handheld device would be connected to the instrument by a cable and would contain a light, an audible alarm, one two-position switch, and two separate push buttons. This is the only portion of the system that would be required to be taken by the operator onto the wing during the inspection. Fig. 33 shows a sketch of how this might be configured.

The field test procedure would be:

1. Use goniometer #1. Set the angle α to 90° .
2. Set the distance from each transducer to the fastener hole center by aligning a mark on the transducer with a mark on the transducer arms of the plastic guide.
3. Tighten all screws to maintain 1 and 2 above.

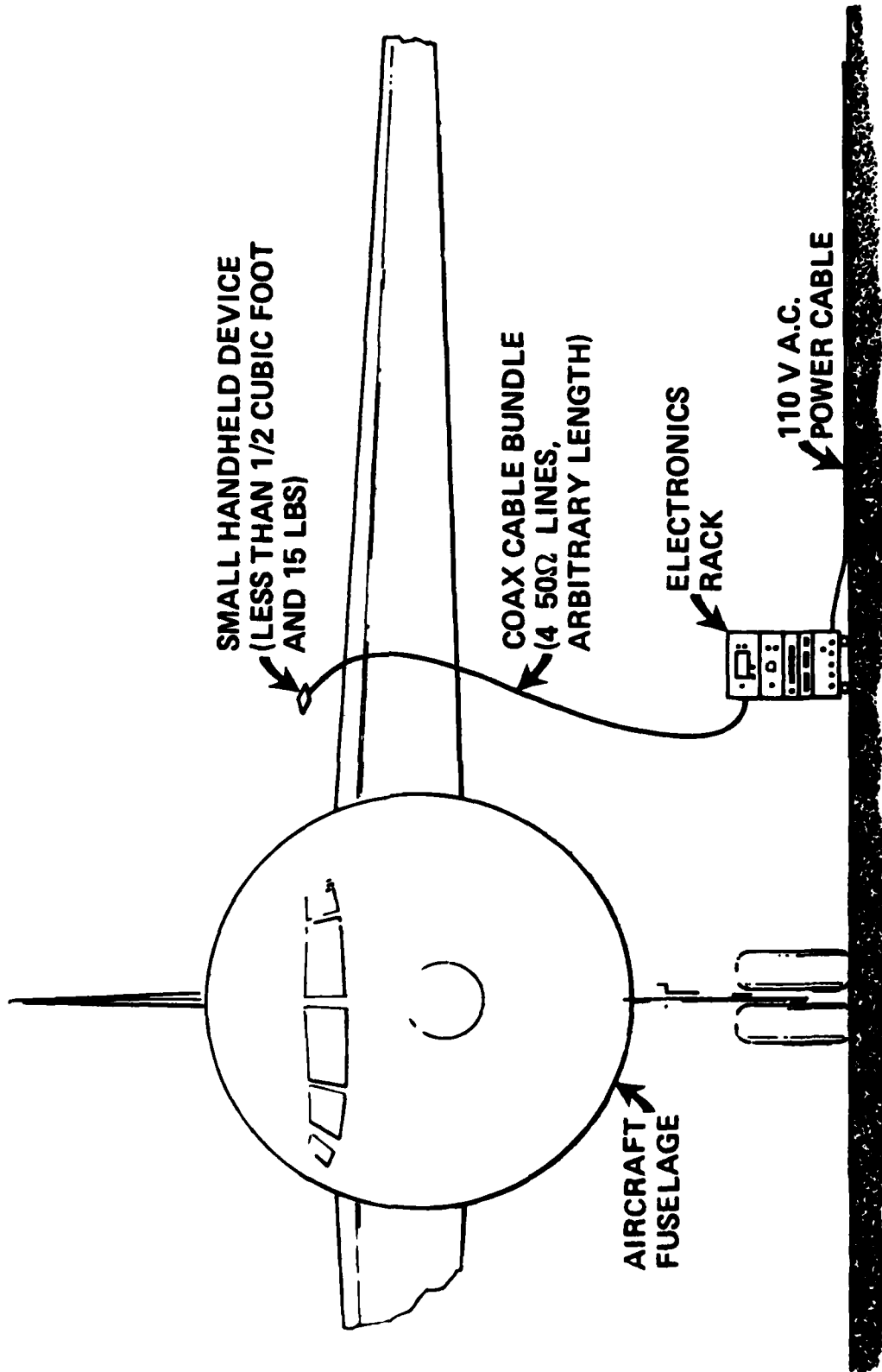


Fig. 33 Schematic of Instrumentation As It Might Appear in Use.

4. Select section of wing area to be inspected and number the fastener holes in sequential order.
5. Set the goniometer arm so that angle β is 50° .
6. Align the goniometer arm with the wing lap joint and center the vertical pin over fastener #1. (possibly using an eddy current centering device).
7. Push the "INIT" button, wait for "DG" light to go off.
8. Repeat Step 6 for fastener #2.
9. Push the "DATA" button. Wait for "DG" light to go off.
10. Perform steps 6 and 9 for subsequent holes until alarm sounds. If it does, mark the last fastener hole completed. Then proceed with Step 11, after moving goniometer #1 out of the way.
Comment: The reflection response of a fastener hole has been identified the hole as being either cracked or having a loose fastener. It is now necessary to compare the transmission properties at that hole to those of its two nearest neighbors to see if it has a loose fastener. If not, it is a candidate for being cracked. First, measure the hole in question.
11. Use Goniometer #2. Set switch labeled "1-2" to the #2 position.
12. Align goniometer centering pin over the hole which is two back from the hole marked in Step 10. That is the questionable hole.
13. Repeat Step 7. Comment: Now measure the holes on either side of the questionable hole.

14. Align goniometer centering pin over the third hole back and repeat Step 9.
15. Repeat Step 14 for the first hole back. Comment: The Fourier spectrum for the questionable hole is now divided by the average of the spectra of its nearest neighbors. If the result is 1.0 within pre-set limits, the hole is identified as a cracked one.
16. If alarm sounds, enter the hole # under "Candidate for crack."
17. If alarm does not sound and "LH" light is on, enter the hole # under "Candidate for loose fastener."
18. Return to goniometer #1. Set "1-2" switch back to #1 position. Proceed with Steps 8 and 9 for subsequent holes until alarm sounds.

XI. CONCLUSION AND RECOMMENDATIONS

In this effort, significant progress has been made in the detection of fatigue cracks under fasteners in the lower half of the C5A wing lap joint. Prior to this study, it had been shown only that the signature of holes with saw slots in an unassembled mock-up could be recognized. In this study the following new results have been obtained.

1. Fatigue cracks at fastener holes can be grown in the laboratory.
2. Fastener holes with the cracks can be found with EMAT-generated acoustic beams, even in an assembled lap joint. This was accomplished in two completely different transducer configurations, with 100% detection capability on the samples with cracks.
3. Limited success was achieved in detecting EDM notches and a saw slot in a wing section with varying geometry.
4. An achievement which was not required by the contract, but which may be significant, is the ability to detect loose fasteners.

Important questions not yet fully resolved concern the detectability of fatigue cracks of 0.030 inch size and the exact procedure for detecting fatigue cracks in other geometries, particularly those with major deviations from the one studied.

The transducers and configurations used in this study appear robust and easily fieldable. The detailed implementation of a crack-finding instrument based on the conceptual design of Section X will require future interaction with knowledgeable field personnel.

The recommendation emerging from this work, for development of a fieldable instrument based on this study, includes two phases.

Phase I Detailed Instrument Design

A. A short field study is needed to obtain feed back from testing personnel about desirable design features for a prototype instrument. This would employ more rugged transducers and goniometers, and would require a version of the digital ultrasonic instrument (described in Section X) for data collection and analysis. This would provide an early guide to how convenience and practicality would be best achieved.

B. Calibration measurements are needed to establish the angles and exact analysis procedures which will be successful for geometries which deviate in a major way from that investigated here. This would include an activity designed to measure the size of the smallest detectable crack length as carefully as is necessary.

C. A design effort would be carried out to yield a detailed plan for all of the hardware and software needed to construct a fieldable prototype. This would be submitted to the Air Force for their evaluation prior to implementation.

Phase II. Prototype Construction and Testing

This would involve construction of the instrument designed in part C of Phase I above. The resulting device would be a practical, fully operational prototype instrument for actual use by Air Force personnel. The effort should include a portion reserved for testing by a combination of Science Center and Air Force personnel, as well as some time allotted to the creation of an acceptable manual of operation/procedures.

REFERENCES

1. "Detection of Cracks in the Inaccessible Lower Half of Wing Lap Joints Using EMATS," Air Force Materials Laboratory, Contract No. F33614-74-C-5180, Rockwell International Science Center Report No. SC595-44C5A
2. Work Statement for "Reliability Evaluation and System Definition for Detection of Cracks Under Fasteners by EMATS," Air Force Materials Laboratory, Contract No. F33615-74-C-5180, Task IV.
3. The Hanning Window is defined as

$$W(t) = \cos \frac{2\pi t}{\tau} = \frac{1}{2} (1 + \cos \frac{2\pi t}{\tau}) \text{ for } |t| \leq \frac{\tau}{2}$$

= 0 elsewhere

4. B.A. Auld, Ginzton Laboratory Report 2808, (Stanford University, Palo Alto, CA).
5. B. Auld, "Acoustic Fields and Waves in Solids," (John Wiley & Sons, u.c. New York, 1973).
6. "Development of a Prototype EMAT System for Inspection of Steam Generator Tubing," Electric Power Research Institute Special Report, EPRI NP-1234-SR, p. 34-1 ff.
7. R.K. Elsley, "The Role of Digital Processing in Ultrasonic NDE," Science Center Technical Report SCTR 79-4, 1979.